ITERATIVE AND ROBUST CONTROL SCHEMES FOR INDUCTION MOTOR DRIVES

BY

MUHAMMAD MUTSAIED SHIRAZI

A Thesis Presented to the

DEANSHIP OF GRADUATE STUDIES

KING FAHD UNIVERSITY OF PETROLEUM & MINERALS

DHAHRAN, SAUDI ARABIA

In Partial Fulfillment of the
Requirements for the Degree of

MASTER OF SCIENCE

In

ELECTRICAL ENGINEERING

NOVEMBER 2017

KING FAHD UNIVERSITY OF PETROLEUM & MINERALS
DHAHRAN 31261, SAUDI ARABIA

DEANSHIP OF GRADUATE STUDIES

This thesis, written by **MUHAMMAD MUTSAIED SHIRAZI** under the direction of his thesis adviser and approved by his thesis committee, has been presented to and accepted by the Dean of Graduate Studies, in partial fulfillment of the requirements for the degree of **MASTER OF SCIENCE IN ELECTRICAL ENGINEERING**.

Thesis Committee

Dr. Salim Ibrir (Adviser)

Dr. Mohammad Ali Y. Abido (Member)

Dr. Muhammad Khalid (Member)

Dr. Ali Ahmad Al-Shaikhi
Department Chairman

Dr. Salam A. Zummo
Dean of Graduate Studies

2/11/18
Date

©Muhammad Mutsaied Shirazi
2017

I dedicate this work to my parents, wife and sister for their endless support.

ACKNOWLEDGMENTS

All praise is due to Allah and peace be upon the Prophet and his family, his companions, may Allah be pleased with them, and his followers. With immense respect, I would like to extend my deepest gratitude to my family because without their prayers, love, positive reception and affection I would not have been able to achieve my desired goal in life. I will always be thankful to them for their continuous moral and emotional support and ever-needed prayers. It has been my honor to be able to work with Dr. Salim Ibrir. I would like to admire is supervision, suggestions and guidance right from the beginning till the end of this research. His constant motivation helped me to produce quality work. I would also like to thank my committee members: Dr. Mohammad Abido and Dr. Muhammad Khalid for their useful response, advice and the time they spent reviewing this thesis. I am very obliged to King Fahd University of Petroleum & Minerals for providing me an opportunity to pursue my graduate degree. I would also like to appreciate all the support that I received from the Electrical Engineering Department in carrying out this research. I would like to thank all my friends and all the seniors at KFUPM for providing the moral support, pleasant atmosphere and unforgettable moments.

TABLE OF CONTENTS

ACKNOWLEDGEMENT **iv**

LIST OF TABLES **viii**

LIST OF FIGURES **ix**

LIST OF ABBREVIATIONS **xii**

ABSTRACT (ENGLISH) **xiii**

ABSTRACT (ARABIC) **xv**

CHAPTER 1 INTRODUCTION **1**

1.1 Problem Statement 4

1.2 Thesis Objectives 4

1.3 Contributions 5

CHAPTER 2 MATHENATICAL MODEL AND LITERATURE SURVEY **6**

2.1 Introduction 6

2.2 Dynamical Model of the Induction Motor 6

2.2.1 Preliminaries 8

2.2.2 Electric and Mechanical Equations 11

2.2.3 State Space Represntation 17

2.3 Literature Review 19

2.4 Knowledge Gap 31

CHAPTER 3 CONVENTIONAL FIELD-ORIENTED CONTROL 33

3.1 Introduction . . . 33

3.2 Conventional Field-Oriented Control . . . 34

3.2.1 Flux Control . . . 35

3.2.2 Speed Control . . . 36

3.2.3 Current Loops . . . 36

3.2.4 Numerical Simulations . . . 37

3.2.5 Experimental Results . . . 42

3.3 Summary . . . 45

CHAPTER 4 PROPOSED CONTROL SCHEMES 46

4.1 Introduction . . . 46

4.2 Inter-sample Iterative Learning Control . . . 47

4.2.1 Preliminaries and System Description . . . 48

4.2.2 Controller Design . . . 51

4.2.3 Numerical Simulations . . . 56

4.2.4 Experimental Results . . . 64

4.3 Active Disturbance Rejection Control . . . 67

4.3.1 Theory . . . 67

4.3.2 Controller Design . . . 71

4.3.3 Numerical Simulations . . . 74

4.4 Summary . . . 81

CHAPTER 5 ROBUST TRACTION CONTROL OF ELECTRIC VEHICLES 84

5.1 Introduction . . . 84

5.2 Background . . . 85

5.3 Traction Control . . . 87

5.4 Mathematical Model . . . 89

5.5 Controller Design . . . 96

5.6 Numerical Simulations . . . 106

5.7 Summary . . . 112

CHAPTER 6 CONCLUDING REMARKS **113**

6.1 Findings and Conclusion 113

6.2 Remarks on Future Research 114

APPENDIX **115**

REFERENCES **123**

LIST OF PUBLICATIONS **140**

VITAE **141**

LIST OF TABLES

3.1 Machine Parameters 37

4.1 Performance comparison of control schemes 64
4.2 Performance comparison of different control techniques in simulation . . 82
4.3 Performance comparison of different control techniques in real-time . . . 82

5.1 Parameters of the model 107

A.1 Hardware Resource Mapping 120

LIST OF FIGURES

2.1 Rotor of the squirrel cage machine 7
2.2 Clarke Transform 9
2.3 Categorization of motor control schemes 20
2.4 V/F Control of three-phase induction motor 23

3.1 Conventional FOC Scheme for Induction motor 34
3.2 Rotor speed of the machine under PI control 38
3.3 Flux magnitude of the machine under PI control 38
3.4 The d-axis stator current of the machine 39
3.5 The q-axis stator current of the machine 39
3.6 The $d-q$ axis stator voltages of the machine 40
3.7 Rotor speed with external disturbance 41
3.8 Rotor speed with internal disturbance 42
3.9 Experimental Setup 42
3.10 Real-time trajectory of the rotor speed under conventional control . . . 43
3.11 Real-time trajectory of the d-axis current 44
3.12 Real-time trajectory of the q-axis current under conventional control . . 44
3.13 Real-time d-axis control voltage generated by conventional control . . . 45
3.14 Real-time q-axis control voltage generated by conventional control . . . 45

4.1 Control Law update 52
4.2 Proposed ISILC Scheme 53
4.3 Rotor speed trajectory under ISILC control 58
4.4 Rotor flux trajectory under ILC control 58
4.5 d-axis stator current under ILC control 59

4.6 q-axis stator current under ISILC control 59
4.7 d-axis stator input voltages under ISILC control 60
4.8 q-axis stator input voltages under ISILC control 60
4.9 Rotor speed with different number of iterations 62
4.10 Rotor speed on external disturbance 62
4.11 Rotor speed on internal parameter variation 63
4.12 Real-time trajectory of rotor speed under ISILC 65
4.13 Real-time trajectory of d-axis current under (a) ISILC and (b) Conventional scheme 65
4.14 Real-time trajectory of q-axis current under (a) ISILC and (b) Conventional scheme 66
4.15 Real-time d-axis control voltage under ISILC 66
4.16 Real-time q-axis control voltage under ISILC 67
4.17 Rotor speed trajectory under ADRC control 75
4.18 Rotor flux trajectory under ADRC control 76
4.19 d-q axis stator current under ADRC control 77
4.20 d-qaxis stator voltage under ADRC control 77
4.21 Proposed time-varying structure of ADRC controller gains 78
4.22 q-axis stator with Soft-Start technique 78
4.23 q-axis stator voltage under Soft-start ADRC 79
4.24 Rotor speed under Soft-start ADRC 80
4.25 Rotor speed with external disturbance 80
4.26 Rotor speed with internal disturbance 81

5.1 Tractive force between tyre and road surface 87
5.2 $\mu - \lambda$ curve for adhesive coefficient 88
5.3 Vehicle longitudinal dynamics 90
5.4 Induction Motor coupling with the wheel 92
5.5 The LADRC control scheme 98
5.6 (a) Slip ratio trajectory (b) Rotor flux trajectory 108
5.7 (a) Estimation of λ in the case of deceleration (b) Estimation of f_b in the case deceleration 108

5.8 (a) tracking performance of λ on 50% variation of parameters (b) estimation of f_b after parameter variation 108
5.9 (a) $d-q$ axes stator currents (b) Torque of the motor 109
5.10 Trajectories of λ and ϕ_d during acceleration 110
5.11 Trajectories of stator currents and the vehicle and wheel speeds 110
5.12 Controller response upon 50% parameter variation 111
5.13 Sudden change in the road surface condition 111

A.1 TI High Voltage Motor Control Kit 116
A.2 Block diagram of hardware 117

LIST OF ABBREVIATIONS

ADRC:	Active Disturbance Rejection Control
LADRC:	Linear Active Disturbance Rejection Control
IM:	Induction Motor
2-D:	Two dimensional
1-D:	One dimentional
ISILC:	Inter-sample Iterative Learning Control
EV:	Electric Vehicle
ESO:	Extended State Observer
LESO:	Linear Extended State Observer
FL:	Feedback Linearization
SM:	Sliding Mode
STA:	Super Twisting Algorithm
ANN:	Artificial Neural Networks
V/F:	Volts per Hertz
SVM:	Space Vector Modulation
FOC:	Field Oriented Control
MRAS:	Model Reference Adaptive System
RTC:	Rotor Time Constant
PWM:	Pulse Width Modulation
ANFO:	Adaptive Nonlinear Flux Observer

Symbols are explained wherever they are used and whenever necessary.

THESIS ABSTRACT

NAME:	Muhammad Mutsaied Shirazi
TITLE OF STUDY:	Iterative and Robust Control Schemes for Induction Motor Drives
MAJOR FIELD:	Electrical Engineering
DATE OF DEGREE:	November 2017

The Induction motor is the most widely used electric motor among other types. It is prevalent due to its simple design, rugged structure, low maintenance cost and excellent reliability. However, control of an induction motor is a cumbersome task due to its high nonlinearity and multi-variable dynamics. In this work, we present the Inter-sample Iterative Learning Control (ISILC) and Active Disturbance Rejection Control (ADRC) for the speed control of 3-phase squirrel cage induction motor. The former is 2-dimensional discrete-time control algorithm designed to operate at a higher rate than the sensing and actuation rates of the system to use the excessive computational power available at the central processing unit. It has a simple control structure and uses little information about the model of the system. The numerical simulations and experimental results have shown that the ISILC performs better than the conventional technique in term of convergence. The second control technique which is presented in this work is a

linear robust control technique which is extremely robust against external and internal uncertainties. The convergence characteristics of the ADRC are comparable to that of the conventional technique. However, the numerical simulations have shown that the algorithm outperforms the conventional technique in disturbance rejection.

ملخص الرسالة

الاسم الكامل: محمد متصاعد شيرازي

عنوان الرسالة: مخططات التحكم القوية و التكرارية لمشغلات المحركات الحثية

التخصص: الهندسة الكهربائية

تاريخ الدرجة العلمية: نوفمبر ٢٠١٧

المحرك الحثي هو المحرك الكهربائي الأكثر استخداماً على نطاقٍ واسعٍ من بين أنواعٍ أخرى. يعود سبب انتشار هذا المحرك إلى: بساطة تصميمه، و قوة هيكله، و انخفاض تكاليف صيانته، و موثوقيته الممتازة. و مع ذلك، فإن التحكم في المحرك الحثي مهمةٌ مرهقةٌ بسبب عدم خطيته و ديناميكيته ذات المتغيرات المتعددة. في هذا العمل، نقدم طريقة التحكم بالتعلم التكراري للعينات البينية (ISILC) و طريقة التحكم برفض الاضطراب النشط (ADRC) للتحكم في سرعة محرك القفص السنجابي الحثي ثلاثي الطور. الطريقة الأولى هي خوارزمية تحكم، ثنائية الأبعاد، في الوقت المنفصل، مصممةٌ للعمل عند معدل أعلى من معدلات الاستشعار و التشغيل للنظام؛ لاستخدام القدرة الحسابية الزائدة و المتوفرة في وحدة المعالجة المركزية. تمتلك هذه الطريقة بنية تحكمٍ بسيطةٍ، و تستخدم قليلاً من المعلومات عن نموذج النظام. و قد أظهرت المحاكاة العددية و النتائج التجريبية أن أداء طريقة ISILC أفضل من الطريقة التقليدية من حيث التقارب. أما طريقة التحكم الثانية المقدمة في هذا العمل فهي تقنية تحكمٍ خطيةٍ و متينةٍ، و هي قويةٌ جداً تجاه المشكوكيات الخارجية و الداخلية. خصائص التقارب لطريقة ADRC مماثلةٌ للطريقة التقليدية. بالرغم من ذلك، فقد أظهرت المحاكاة العددية أن أداء هذه الخوارزمية يتفوق على أداء الطريقة التقليدية في رفض الاضطراب.

CHAPTER 1

INTRODUCTION

The field of electric drives is a continuously developing area since the mid-19th century and playing an increasingly important role in both industry and everyday applications. These drives are present in dozens of household appliances, transportation, and office equipment and even in the industry which manufactures all these equipment. Industry and transport sectors rely on these actuators for their efficient and precise operations. These drives have taken over a significant share of physical efforts that were previously undertaken by humans and also carried out tasks that were crucial and could not be performed due to physical or other limitations. Application areas of electrical drives are continuously expanding and becoming more and more sophisticated and versatile [1, 2]. Electrical drives have replaced other devices and means of doing physical work because of their numerous advantages which include energy efficiency and improvement in control over the processes, which ensures the essential quality of work that has become a necessity to fit in the modern and technologically advanced era.

Electric motors can be broadly classified into two categories: Direct current (DC) motors and Alternating Current (AC) motors. Drive systems are different for both

kinds of machines. Initially, DC motors were used for high-performance applications (such as positioning systems, rolling mills, and traction drives) due to their relative ease of control as compared to AC motors since their flux and torque are independently controlled by the field and armature current respectively. However, on the other hand, AC motors are more rugged and reliable and has lesser maintenance cost than DC motors because latter use mechanical commutator and brushes which wear out over time and need to be continuously replaced. Among AC motors, the induction motor (IM) is most popular due to its simple, rugged design, low manufacturing cost, no rotor winding in squirrel cage motors, high torque to weight ratio, smaller size, and can tolerate heavy overloading [3].

The design of control algorithms for induction motors is, however, very complex. It was used only in fixed speed applications until the 1970s when the development of power electronics and later digital signal processors paved the way for the complex algorithms to be implemented in real-time. It is a nonlinear multi-variable control problem with two inputs and two outputs to be controlled: rotor speed, and rotor flux magnitude. The electromagnetic torque which controls the rotor speed is a nonlinear function of stator currents and rotor fluxes. The linear approximation of the model cannot be used for this application because the linearization assumes that the inital conditions of the system are in the vicinity of the equilibrium point which is not true for the case of induction machine. The initial rotor speed can be far away from the desired reference speed selected for the system. The system also contains parameters such as load torque and rotor resistance which may vary during the operation; they are critical in control design and performance of the controller may be affected due to this change. A common state feedback control scheme is avoided because the measurement of rotor flux is not

available. Although it can be measured by placing the hall sensors inside the motor, this practice is now nearly abandoned by the industry because of its cost and added unreliability into the system. The aim of the control schemes is to track the desired reference signals for rotor speed and flux magnitude, despite parameter variations and external perturbations [4]. Since 1970s many control algorithms of nonlinear, adaptive and intelligent nature are proposed. A detailed discussion of existing control strategies is presented in chapter 2 and few gaps are also identified.

In this work, we have investigated the speed, flux, and torque control problems of the induction motor. For the speed and flux control, we have proposed an inter-sample iterative learning control (ISILC) and linear active disturbance rejection control (LADRC) algorithms, which were not investigated before in the literature. For the torque control, we have considered an advance application, i.e. traction control of induction motor fed electric vehicles, and have proposed the LADRC algorithm for the wheel slip ratio tracking.

This research work is organized into six chapters. Chapter 2 contains the mathematical modeling of a squirrel-cage three phase induction motor and the literature survey. In chapter 3 we present the benchmark technique for the comparison: the conventional technique which uses the cascaded PI loops. In chapter 4 we present the main contribution of this work. We propose the Inter-sample iterative learning control (ISILC) and Active Disturbance Rejection Control (ADRC) for the induction motor drives. In chapter 5 we test the ADRC technique for an advance application of the IM drive i.e., traction control of electric vehicles. Finally, we will conclude the thesis in chapter 6.

1.1 Problem Statement

Induction motors are the workhorses of the today's industry. The dynamic model of the IM is highly nonlinear and multi-variable. It is a standard issue that the sensing and actuation rates of the drive systems are limited by some external factors (such as switching frequency of power electronic devices), while the central processor tends to operate at much higher rates. There exists a need for the development of an algorithm which utilizes excessive computational power available at the processing end. Moreover, the available techniques require precise information about the parameters of the machines which are usually not available in practice. We need robust control techniques that can handle internal and external uncertainties.

1.2 Thesis Objectives

Following are the primary objectives of this work:

1. Devise the control technique that operates at a higher sampling rate than the the sensing and actuation rates of the system for Induction Motor drives

2. Prepare a test bench to test the technique in real-time.

3. Devise a robust control scheme for the rotor speed control that can compensate internal and external disturbances to the system.

4. Solve the robust traction control of IM-fed Electric Vehicles (EVs) using a robust control technique.

1.3 Contributions

Following the major contributions of this work:

1. We present the two-dimensional control algorithm, i.e., Inter-sample Iterative learning control (ISILC) for the speed control of IM Drives.

2. We proposed linear active disturbance rejection control for the speed tracking problem.

3. We solved the robust longitudinal traction control problem of IM-fed electric vehicles using ADRC.

CHAPTER 2

MATHENATICAL MODEL AND LITERATURE SURVEY

2.1 Introduction

In this chapter, a mathematical model of the three-phase squirrel cage induction motor describing its electromechanical behavior is developed. The model of the machine is highly nonlinear and time-varying, so the Clarke and Park transforms are used to reduce the complexity and convert the system to the time-invariant one. We also discuss the algorithms of IM speed control present in the literature. Furthermore, the algorithms have been categorized based on their intrinsic structure and characteristics.

2.2 Dynamical Model of the Induction Motor

An induction motor consists of two parts: stator and rotor. The stator is the static part of the motor that houses the three-phase winding inside the slots and connected to the power source. The rotor is the rotating part of the machine that delivers the mechanical

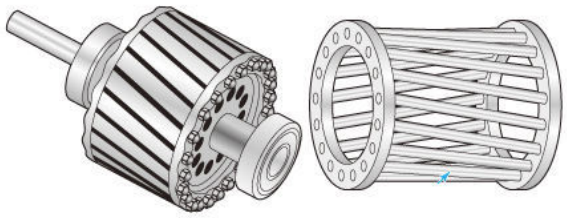

Figure 2.1: Rotor of the squirrel cage machine

energy to the system connected to it. There are two types of the rotor:

- *Coiled Rotor*: It is of a cylindrical form with multiple disks stacked on the machine shaft. The coil winding runs through the slots of the stacked disks and forms a magnetic circuit when energized. Slip rings provide the electrical connection to the winding. The motors consisting such rotors are also known as slip ring motors. Due to high-energy losses in the brushes, these machines bear a high-maintenance cost which makes them some what unfavorable for the usage.

- *Squirrel Cage Rotor*: This type of rotor does not have an external electrical connection. It is composed of conductive bars, forming a cylindrical structure, and connected to the conductive end rings. The cylinder is stacked with the metallic disks to enhance the magnetic properties. The rotor coil is in short-circuit, so the voltage across the rotor is zero. The squirrel-cage motor is the most common type of the induction motor used in the various application. Figure 2.1 shows a typical squirrel cage rotor.

This thesis is based on the analysis and control of the squirrel-cage motors. Before developing the mathematical model of the machine, we present some preliminary considerations in the following section.

2.2.1 Preliminaries

A well-known approach to study the dynamics of the AC machines is to transform the variables, i.e. voltages, currents and flux linkages, from the fixed stator frame to a rotating rotor reference frame defined by the Clark and Park transformations. These transformations reduce the complexity of the differential equations that describe the electrical and mechanical behavior of the machine. The conversion from the three-phase stationary (a, b, c) to the two-phase rotating (d, q) frame is a two stage process. First, the three-phase variables are projected to the stationary orthogonal two phases (α, β) known as *Clarke Transformation*. Then, the *Park Transformation* converts the stationary two-phase system to the rotating two-phase (d, q). Before further discussing the transformation, the following assumptions are considered:

Modeling Assumptions

- There is a uniform air gap thickness inside the machine.
- The three phases of the machine are balanced.
- The magnetic field distribution is sinusoidal inside the air gap.
- The magnetic characteristics of the machine are linear.
- Skin effect, temperature effect, eddy current losses and hysteresis phenomenon are neglected.

Clarke Transformation

The Clarke transformation is a mathematical transform used to simplify the analysis of three-phase electrical circuits. The three phase vectors are projected to two orthogonal

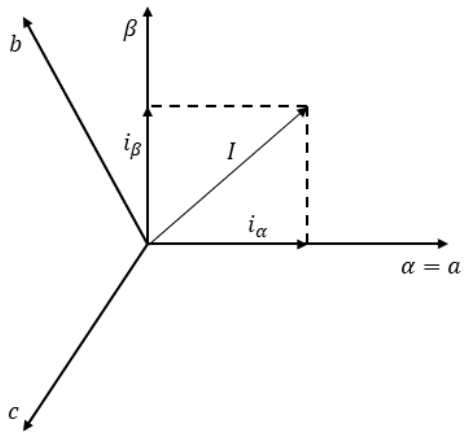

Figure 2.2: Clarke Transform

vectors called α and β. Figure 2.2 shows the comparison between the clarke orthogonal axes, i.e., $\alpha-\beta$ and the three-phase reference frame, where i_α and i_β are the transformed equivalent orthogonal current vectors. The balanced three-phase to quadrature two-phase transformation is given as,

$$\begin{bmatrix} I_\alpha \\ I_\beta \\ I_0 \end{bmatrix} = C \begin{bmatrix} I_a \\ I_b \\ I_c \end{bmatrix} \tag{2.1}$$

where

$$C = \sqrt{\frac{2}{3}} \begin{bmatrix} 1 & -\frac{1}{2} & -\frac{1}{2} \\ 0 & \frac{\sqrt{3}}{2} & -\frac{\sqrt{3}}{2} \\ \frac{1}{\sqrt{2}} & \frac{1}{\sqrt{2}} & \frac{1}{\sqrt{2}} \end{bmatrix}$$

Since we are considering the balanced three-phase system, so the current in the homopolar axis, I_0 is null. Therefore, the transformation matrix C can be rewritten as

$$\begin{bmatrix} I_\alpha \\ \\ I_\beta \end{bmatrix} = C_l \begin{bmatrix} I_a \\ \\ I_b \\ \\ I_c \end{bmatrix} \tag{2.2}$$

where

$$C_l = \sqrt{\frac{2}{3}} \begin{bmatrix} 1 & -\frac{1}{2} & -\frac{1}{2} \\ \\ 0 & \frac{\sqrt{3}}{2} & -\frac{\sqrt{3}}{2} \end{bmatrix}.$$

Park Transformation

The Park transformation, $P(\theta)$, transforms the AC variable from the $\alpha - \beta$ frame to a rotating $d-q$ reference frame where θ_s is the angle of rotation of the frame. It transforms the AC variables to the two DC variables thus converting a time-varying system to its time-invariant equivalent. The transformation is given as

$$\begin{bmatrix} I_d \\ \\ I_q \end{bmatrix} = P(\theta_s) \begin{bmatrix} I_\alpha \\ \\ I_\beta \end{bmatrix} \tag{2.3}$$

where

$$P(\theta_s) = \begin{bmatrix} cos\theta_s & sin\theta_s \\ \\ -sin\theta_s & cos\theta_s \end{bmatrix}$$

and θ_s is the angle between between the axis$-\alpha$ of the stationary frame and the axis$-d$ of the rotating frame. Figure 2.2 shows the comparison among the reference frames.

2.2.2 Electric and Mechanical Equations

The mathematical model of the three-phase squirrel cage induction motor is derived from the electromagnetic and mechanical principles. The three phase stator and rotor voltages equations in the stationary (a, b, c) frame are expressed as matrix equations as

$$V^s_{abc} = R_s I^s_{abc} + \frac{d}{dt}\Phi^s_{abc} \tag{2.4}$$

$$V^r_{abc} = R_r I^r_{abc} + \frac{d}{dt}\Phi^r_{abc} \tag{2.5}$$

where

$$V^s_{abc} = \begin{bmatrix} v^s_a \\ v^s_b \\ v^s_c \end{bmatrix}, \quad V^r_{abc} = \begin{bmatrix} v^r_a \\ v^r_b \\ v^r_c \end{bmatrix}, \quad I^s_{abc} = \begin{bmatrix} i^s_a \\ i^s_b \\ i^s_c \end{bmatrix}, \quad I^r_{abc} = \begin{bmatrix} i^r_a \\ i^r_b \\ i^r_c \end{bmatrix},$$

$$\Phi^s_{abc} = \begin{bmatrix} \phi^s_a \\ \phi^s_b \\ \phi^s_c \end{bmatrix} \text{ and } \Phi^r_{abc} = \begin{bmatrix} \phi^r_a \\ \phi^r_b \\ \phi^r_c \end{bmatrix}.$$

The vectors V^s_{abc} and V^r_{abc} represent the three-phase stator and the rotor voltages, I^s_{abc} and I^r_{abc} represents the three phase currents of the stator and the rotor respectively and Φ^s_{abc} and Φ^r_{abc} denotes the three phase stator and rotor flux linkages. The notation R_s and R_r denotes the stator and the rotor resistance respectively.

The magnetic flux linkages of the machine are given as

$$\Phi^s_{abc} = L^s I^s_{abc} + M^{sr}_o I^r_{abc} \tag{2.6}$$

$$\Phi^r_{abc} = L^r I^r_{abc} + M^{sr}_o I^s_{abc} \tag{2.7}$$

where

$$L^s = \begin{bmatrix} l^s & M^s & M^s \\ M^s & l^s & M^s \\ M^s & M^s & l^s \end{bmatrix}, \qquad L^r = \begin{bmatrix} l^r & M^r & M^r \\ M^r & l^r & M^r \\ M^r & M^r & l^r \end{bmatrix},$$

$$M_o^{sr} = M \begin{bmatrix} cos(p\theta_m) & cos(p\theta_m + \frac{2\pi}{3}) & cos(p\theta_m - \frac{2\pi}{3}) \\ cos(p\theta_m - \frac{2\pi}{3}) & cos(p\theta_m) & cos(p\theta_m + \frac{2\pi}{3}) \\ cos(p\theta_m + \frac{2\pi}{3}) & cos(p\theta_m - \frac{2\pi}{3}) & cos(p\theta_m) \end{bmatrix}.$$

The superscript s and r denotes the stator and rotor side of the quantity, l^r is the rotor self-induction, l^s is the stator self-induction, M^r is the mutual induction between two rotor phases, M^s is the mutual induction between two stator phases, p is the pole pairs of the motor and θ_m represents the mechanical angle of the rotor. The electrical angle θ_e is given as $\theta_e = p\theta_m$. Applying the Clarke and Park transformation, (2.2) and (2.3), to the voltage equations, (2.4) and (2.5), where θ_s is the angular position of the $d-q$ frame will transform the electrical equation to the rotating $d-q$ frame as

$$V_{dq}^s = R_s I_{dq}^s + \frac{d}{dt}\Phi_{dq}^s - \frac{d\theta_s}{dt}\urcorner\Phi_{dq}^s \tag{2.8}$$

$$V_{dq}^r = 0 = R_r I_{dq}^r + \frac{d}{dt}\Phi_{dq}^r - \frac{d\theta_r}{dt}\urcorner\Phi_{dq}^r \tag{2.9}$$

where

$$V_{dq}^s = \begin{bmatrix} v_d^s \\ v_q^s \end{bmatrix}, \quad V_{dq}^r = \begin{bmatrix} v_d^r \\ v_q^r \end{bmatrix}, \quad I_{dq}^s = \begin{bmatrix} i_d^s \\ i_q^s \end{bmatrix}, \quad I_{dq}^r = \begin{bmatrix} i_d^r \\ i_q^r \end{bmatrix},$$

$$\Phi_{dq}^s = \begin{bmatrix} \phi_d^s \\ \phi_q^s \end{bmatrix}, \quad \Phi_{dq}^r = \begin{bmatrix} \phi_d^r \\ \phi_q^r \end{bmatrix} \text{ and } \urcorner = \begin{bmatrix} 0 & 1 \\ -1 & 0 \end{bmatrix}.$$

The vector V_{dq}^{s} represents the d and q axis stator voltages, V_{dq}^{r} is the $d-q$ axis rotor voltages, I_{dq}^{s} is the $d-q$ axis stator current, I_{dq}^{r} is the $d-q$ axis rotor current, Φ_{dq}^{s} is the stator flux linkage in the $d-q$ frame, Φ_{dq}^{r} is the rotor flux linkage and θ_r is the relative rotor angular position with respect to the $d-q$ frame, also known as the slip angle, written as

$$\theta_r = \theta_s - p\,\theta_m \tag{2.10}$$

where θ_m is the mechanical angular position of the rotor and θ_s is the angle of the rotating synchronous frame. Differentiating (2.10) will yield,

$$\omega_s = \omega_r + p\Omega_m,$$

where ω_s is the synchronous speed of the rotating magnetic field inside the machine, Ω_m is the mechanical rotor speed and ω_r is the slip speed represented as,

$$\omega_r = \frac{R_r M_{sr} i_q^s}{L_r \phi_d^r}.$$

Rewriting the magnetic flux equations, (2.6) and (2.7), in the $d-q$ frame, yields

$$\Phi_{dq}^{s} = L_s I_{dq}^{s} + M_{sr} I_{dq}^{r} \tag{2.11}$$

$$\Phi_{dq}^{r} = L_r I_{dq}^{r} + M_{sr} I_{dq}^{s} \tag{2.12}$$

where L_s and L_r are the stator and rotor cyclic self-inductances and M_{sr} is the mutual cyclic inductance. From (2.8) and (2.9), the dynamics of the magnetic flux of the

machine can be written as

$$\frac{d}{dt}\Phi^s_{dq} = -R_s I^s_{dq} - \omega_s \urcorner \Phi^s_{dq} + V^s_{dq} \tag{2.13}$$

$$\frac{d}{dt}\Phi^r_{dq} = -R_r I^r_{dq} + (\omega_s - p\Omega)\urcorner \Phi^r_{dq}. \tag{2.14}$$

Substituting the relation of I^r_{dq} from (2.12) into (2.14) will yield the final dynamics of the rotor flux in $d-q$ frame as

$$\frac{d}{dt}\Phi^r_{dq} = \frac{R_r M_{sr}}{L_r} I^s_{dq} + \Big(-\frac{R_r}{L_r} I_{2\times 2} + (\omega_s - p\,\Omega)\urcorner \Big)\Phi^r_{dq}. \tag{2.15}$$

Substituting (2.11) and (2.12) into (2.13) and (2.14) will yeild

$$L_s \frac{d}{dt} I^s_{dq} + M_{sr}\frac{d}{dt} I^r_{dq} = -R_s I^s_{dq} - \omega_s \urcorner \Phi^s_{dq} + V^s_{dq} \tag{2.16}$$

$$M_{sr}\frac{d}{dt} I^s_{dq} + L_r \frac{d}{dt} I^r_{dq} = -R_r I^r_{dq} + (\omega_s - p\Omega)\urcorner \Phi^r_{dq}. \tag{2.17}$$

Then substituting the relation of $\frac{d}{dt} I^r_{dq}$ from (2.16) and the relation of Φ^s_{dq} from (2.11) into (2.16) will yield the final dynamics of the stator current, I^s_{dq}, as

$$\frac{d}{dt} I^s_{dq} = \Big(-\frac{R_s}{L_s \sigma} I_{2\times 2} + \omega_s \urcorner \Big) I^s_{dq} + \Big(\frac{R_r M_{sr}}{\sigma L_s L_r} I_{2\times 2} + \frac{M_{sr}}{\sigma L_s L_r} p\Omega \urcorner \Big)\Phi^r_{dq} + \frac{1}{L_s} V^s_{dq} \tag{2.18}$$

where ω_s is the synchronous angular speed of the motor given as

$$\omega_s = \frac{R_r M_{sr} i^s_q}{L_r \phi^r_d} + p\,\Omega \tag{2.19}$$

with Ω denoting the mechanical angular speed of the rotor of the machine. The notation

σ denotes the Blondel leakage constant given as

$$\sigma = 1 - \frac{M_{sr}^2}{L_s L_r} \tag{2.20}$$

and $I_{2\times 2}$ represents an identity matrix of dimension 2.

The electromagnetic torque of the machine is given as

$$\tau_e = \frac{pM_{sr}}{L_r}(\phi_d^r i_q^s - \phi_q^r i_d^s) \tag{2.21}$$

The torque of the machine has a nonlinear relation with the rotor fluxes and stator currents. The dynamics of the mechanical angular speed of the motor can be represented by the following mechanical equation

$$\frac{d\Omega}{dt} = \frac{\tau_e}{J_m} - \frac{f_v}{J_m}\Omega - \frac{T_l}{J_m} \tag{2.22}$$

where J_m is the motor's moment of inertia, T_l is the load torque and f_v is the viscous damping coefficient. The complete mathematical model of the three phase squirrel cage induction motor is represented by (2.15), (2.18) and (2.22). We can rewrite the model in extended form as

$$\frac{d\Omega}{dt} = m\,(\phi_d^r\, i_q^s - \phi_q^r\, i_d^s) - c\,\Omega - \frac{T_l}{J_m} \tag{2.23}$$

$$\frac{d\phi_d^r}{dt} = -a\,\phi_d^r + (\omega_s - p\,\Omega)\phi_q^r + a\,M_{sr}\,i_d^s \tag{2.24}$$

$$\frac{d\phi_q^r}{dt} = -(\omega_s - p\,\Omega)\phi_d^r - a\,\phi_q^r + a\,M_{sr}\,i_q^s \tag{2.25}$$

$$\frac{di_d^s}{dt} = -\gamma\,i_d^s + a\,b\,\phi_d^r + \omega_s\,i_q^s + b\,p\,\Omega\,\phi_q^r + m_1\,v_d^s \tag{2.26}$$

$$\frac{di_q^s}{dt} = -\gamma\,i_q^s - b\,p\,\Omega\,\phi_d^r - \omega_s\,i_d^s + a\,b\,\phi_q^r + m_1\,v_q^s \tag{2.27}$$

where the parameters a, b, c, γ, m and m_1 are defined as

$$a = R_r/L_r, \quad b = M_{sr}/\sigma L_s L_r, \quad c = f_v/J, \quad \gamma = (L_r^2 R_s + M_{sr}^2 R_r)/(\sigma L_s L_r^2),$$

$$m = pM_{sr}/JL_r, \quad m_1 = 1/\sigma L_s.$$

IM model in the Rotating frame Associated to the Rotor Flux

The mathematical model of the induction motor defined by $(2.23) - (2.27)$ is represented in an arbitrarily rotating frame. Designing a controller for the presented model is still quite difficult. We can further simplify the model by assuming the d-axis of the rotating frame is aligned with the rotor flux vector. In that case, the q-component of the rotor flux and its derivative will vanish, i.e.,

$$\frac{d\phi_q^r}{dt} \equiv \phi_q^r \equiv 0$$

Defining the synchronous angular speed as $\omega_s = \frac{d\rho}{dt}$, where ρ is the rotor flux angle. Eq. (2.19) can be rewritten as:

$$\frac{d\rho}{dt} = \omega_s = \frac{R_r M_{sr} i_q^s}{L_r \phi_d^r} + p\,\Omega \tag{2.28}$$

The nonlinear model of the induction motor expressed in the rotor field associated $d-q$ frame is obtained by replacing the synchronous angular speed, ω_s, and the dynamics of ϕ_q^r with the dynamics of the rotor flux angle, ρ. The general model $(2.23) - (2.27)$ will be transformed as:

$$\frac{d\Omega}{dt} = m\,\phi_d^r\,i_q^s - c\,\Omega - \frac{1}{J_m}\,T_l \tag{2.29}$$

$$\frac{d\phi_d^r}{dt} = -a\,\phi_d^r + a\,M_{sr}\,i_d^s \tag{2.30}$$

$$\frac{d\rho}{dt} = p\,\Omega + a\,\frac{M_{sr}}{\phi_d^r}\,i_q^s \tag{2.31}$$

$$\frac{di_d^s}{dt} = -\gamma\,i_d^s + a\,b\,\phi_d^r + p\,\Omega\,i_q^s + a\,\frac{M_{sr}}{\phi_d^r}\,(i_q^s)^2 + m_1\,v_d^s \tag{2.32}$$

$$\frac{di_q}{dt} = -\gamma\,i_q^s - b\,p\,\Omega\,\phi_d^r - p\,\Omega\,i_d^s - a\,\frac{M_{sr}}{\phi_d^r}\,i_d^s\,i_q^s + m_1\,v_q^s \tag{2.33}$$

Remark 1 *With the assumption of rotor flux alignment, the d-component of the rotor flux i.e., ϕ_d^r represents the total magnitude of the rotor flux.*

Remark 2 *The dynamics of Ω and ϕ_d^r, in* (2.23) *and* (2.24)*, are decoupled w.r.t to i_d^s and i_q^s. This decoupling will help us in the control design explained in the later chapters.*

2.2.3 State Space Represntation

For the state space representation of the model, we need to define the state x, the input u and the output y of the system. In this work, we consider the speed and the currents of the motor are measurable, so Ω, i_d^s and i_q^s are selected as the output of the system. Usually, the flux of the machine is not available for the measurement, because of the hall sensors, which measures the flux inside the motor, are expensive and adds unreliability to the system. The stator input voltages, v_d^s and v_q^s, are taken as the input. The load torque is considered as the bounded unknown input disturbance to the system. One can also consider T_l as a system state and consider designing an observer for its estimation, but we employed the former technique. The state vector of the system consists of the speed, the d and q axis current and the d and q axis flux. The dynamics (2.23)$-$(2.27)

are represented in an arbitrary rotating (d, q) frame. One can also consider the dynamics with the rotor flux aligned $d-q$ where $\phi_q^s = 0$.

Defining the state vector x, the input u, the output y and the external disturbance w as

$$x = \begin{bmatrix} \Omega \\ \phi_d^s \\ \rho \\ i_d^s \\ i_q^s \end{bmatrix}, \quad u = \begin{bmatrix} v_d^s \\ v_q^s \end{bmatrix}, \quad y = \begin{bmatrix} \Omega \\ i_d^s \\ i_q^s \end{bmatrix}, \quad w = T_l.$$

where $x \in \mathbb{R}^5$, $u \in \mathbb{R}^2$, $y \in \mathbb{R}^3$ and $w \in \mathbb{R}$. Then, the state space representation of the IM model (2.23)-(2.27), in an arbitrary rotating $d-q$ frame, is given as

$$\begin{aligned} \dot{x} &= f(x) + B_1 u + B_2 w \\ y &= Cx \end{aligned} \tag{2.34}$$

where

$$f(x) = \begin{bmatrix} m\,\phi_d^r\, i_q^s - c\,\Omega \\ -a\,\phi_d^r + a\,M_{sr}\, i_d^s \\ p\,\Omega + a\,\frac{M_{sr}}{\phi_d^r}\, i_q^s \\ -\gamma\, i_d^s + a\,b\,\phi_d^r + p\,\Omega\, i_q^s + a\,\frac{M_{sr}}{\phi_d^r}\,(i_q^s)^2 \\ -\gamma\, i_q^s - b\,p\,\Omega\,\phi_d^r - p\,\Omega\, i_d^s - a\,\frac{M_{sr}}{\phi_d^r}\, i_d^s\, i_q^s \end{bmatrix}, \quad B_1 = \begin{bmatrix} 0 & 0 \\ 0 & 0 \\ 0 & 0 \\ m_1 & 0 \\ 0 & m_1 \end{bmatrix}, \quad B_2 = \begin{bmatrix} -\frac{1}{J_m} \\ 0 \\ 0 \\ 0 \\ 0 \end{bmatrix}$$

$$C = \begin{bmatrix} 1 & 0 & 0 & 0 & 0 \\ 0 & 1 & 0 & 0 & 0 \\ 0 & 0 & 1 & 0 & 0 \end{bmatrix}.$$

The vector function, $f(x) \in \mathbb{R}^5$, is smooth, nonlinear and locally lipschitz. The matrices $B_1 \in \mathbb{R}^{5\times 2}$, $B_2 \in \mathbb{R}^5$ and $C \in \mathbb{R}^{3\times 5}$ are constant and known. The model representation (2.34) is used throughout the thesis.

2.3 Literature Review

The three phase induction motor is a nonlinear system with parameter variations and external perturbations. Traditionally, induction motors were used in the applications where variable speed control was not required (such as pumps, compressors, and blowers). There was virtually no possibility of controlling the motor within a wide range of speed operations with high energy efficiency up until the 1970s. The advent of power electronic devices made the high frequency switching possible with low energy losses, thus removing the major barricade in the development. Since then, the control problem of the induction motor attracted much attention from researchers and engineers. More than 80,000 patents and 4000 journal papers have been published and still growing [4]. This section briefly summarizes the broad categorization of motor control schemes and discusses the recent developments in the field.

We can broadly classify the motor control schemes of IM into two categories, i.e. Scalar methods and Vector methods. Scalar control methods are the techniques in which the control algorithm alters the magnitude of the control variable. These are the simplest and earliest methods devised to control the rotor speed of the machine.

On the other hand, the vector control schemes are more advanced and computationally intensive and require a certain amount of processing power. They are based on the vector representation of the model, described in section 2.2, and controls both the direction and the magnitude of the machine's current and voltages. Figure 2.3 shows the broad classification of the speed control algorithms.

2.3.1 Scalar Control Methods

As discussed earlier, the scalar control techniques only control the magnitude of the control variable. These are the simplest and earliest devised techniques based on the characteristic equations of the IM. In this section, we discuss the speed control techniques which fall under the category of scalar control.

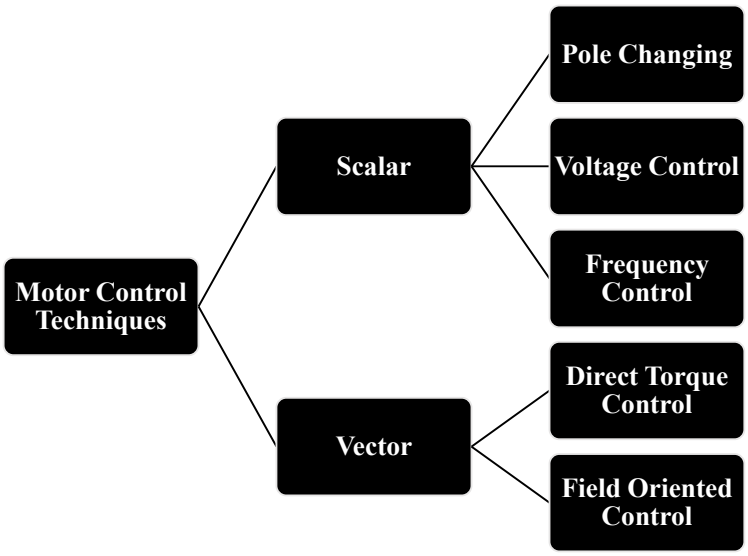

Figure 2.3: Categorization of motor control schemes

The characteristic equation for the mechanical rotor speed of the IM in given as [5]

$$N_m = N_s(1 - s) \tag{2.35}$$

$$\text{where} \qquad N_s = \frac{60 f_s}{p}. \tag{2.36}$$

The notation N_m represents the mechanical rotor speed in revolutions per minute (rpm), N_s for the synchronous speed of the rotating magnetic field in rpm, f_s is the supply frequency, p is the number of pole pairs in the motor and s is the rotor slip between 0 and 1. 0 means the rotor is rotating at the synchronous speed and 1 represents a stationary rotor. From (2.35) and (2.36) it can seen that the mechanical speed can be influenced by: 1) number of poles (p); 2) slip of the motor (s) and 3) the supply frequency (f_s). The slip control is only used for the wound rotor induction motors (also known as slip ring induction motors) because their rotor winding is externally accessible via slip rings. A series resistance is added to increase the rotor resistance which changes the slip of the motor. This method is highly inefficient due to power dissipation and is not practiced in the industry.

Pole Changing

The pole changing technique provides a discrete set of operating speeds of the motor. It is achieved by employing multiple stator windings with different number of pole pairs and energizing one set at a time. For instance, a motor can be wound with two pole and four pole configuration, so its synchronous speed could be switched from 3600 rpm to 1800 rpm, at 60 Hz supply frequency, by simply supplying power to the other set of winding. Such kind of motors are used in cranes and industrial hoists with two operating

speeds - a slower approach speed and a higher transit speed.

The major drawback of this technique is that one can only achieve the specific set of speeds, multiple of the supply frequency. At 60 Hz frequency, for successive number of pole pairs, i.e. $p = 1, 2, 3, 4...$ the corresponding synchronous speeds N_s according to (2.36) will be 3600 r/min, 1800 r/min, 1200 r/min, 900 r/min and so on. This change in synchronous speed will change the mechanical rotor speed. Moreover, the additional set of stator winding increases the complexity and cost of the motor.

Voltage Control

The speed of the induction motor can also be changed by changing the stator voltage. At steady state, the torque produced by the induction motor can be expressed as [6]:

$$T_{ind} = \frac{1.5p}{\pi f} \frac{R_r/s}{(R_s + R_r/s)^2 + X_l^2} V_s^2 \tag{2.37}$$

where V_s is the stator voltage, X_l is the total leakage reactance, R_r and R_s is the rotor and stator resistance of the motor respectively. The induced torque is directly proportional to the square of the applied voltage. If we decrease the stator voltage, at a constant load, the induced torque will also decrease, therefore resulting in the reduced rotor speed. One major disadvantage arises from the quadratic relation between the applied voltage and induced torque. A Large change in supply voltage is required for a relatively small change in speed. A Large change in applied voltage will result in substantial change in flux density. Thus it will affect the magnetic conditions of the motor.

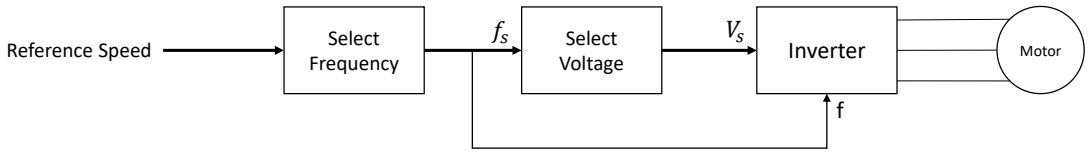

Figure 2.4: V/F Control of three-phase induction motor

Frequency Control (V/F)

Frequency control which is also known as Volts per Hertz (V/F) control is the most widely used scalar control strategy for induction motors. Initially it was designed and implemented in open loop structure but later closed loop designs were also proposed [7, 8]. This control scheme utilizes the characteristic relation described by (2.35) and (2.36). The decrease in supply frequency will decrease in mechanical speed. However on the other hand, decrease in frequency causes the increase in flux because of the following characteristic relation [9]:

$$\phi = \frac{V_s}{4.44\,K\,T\,f_s}. \tag{2.38}$$

where T is the number of turns per phase, K is the winding constant and ϕ is the flux. From equation (2.38) it can be seen that the produced flux inside the machine is inversely proportional to the applied frequency. So if we decrease the frequency to decrease the speed, the flux will increase and saturate the stator and the rotor cores causing the increase in no-load current. We need to maintain the flux at a constant value. The flux of the machine depends on the ratio of applied voltage and frequency from eq. (2.38). While decreasing the frequency, we also need to decrease the voltage to maintain the same V/F ratio. The control scheme is represented in figure 2.4.

This control technique is simple and easy to implement using power electronic based inverters, but it also has some severe disadvantages. First and the foremost, since it

is an open loop design, so the steady state error is indispensable [10] especially when load torque is applied to the machine. The slip compensation is used in the closed loop V/F schemes for steady state error cancellation. However, due to the slip-torque characteristic of the machine, it works only between a small speed range. Its overall stability is also not guaranteed so the system may start oscillating under small load or while tracking a very low reference speed [11, 12]. This happens because the control algorithm does not compensate the nonlinear and coupling behavior of the machine. Another drawback of this control technique is that it only controls the steady state response of the motor. The dynamic response cannot be controlled with this V/F method [13–17].

Over the past years, researchers have addressed these problems and proposed numerous modifications in the algorithm for better performance. In [18], the author suggested that the motors with small rotor inertia are more prone to the instability. Inverter dead-time and DC link filters also affect the stability of the motor [19]. Influence of magnetic saturation is studied in [20]. To improve the stability, [13] and [21] proposed a dynamic current compensation and current regulation schemes. The researchers also studied the characteristics of the stator currents during the oscillations to improve the stability of the system [22, 23].

Several closed loop designs for V/F control scheme were proposed to improve the transient response and steady state error. Fuzzy logic based technique is used in [10] and a fuzzy-tuned PID control scheme is proposed in [14]. The authors in [24] devised a new modulation scheme for the inverter and compared with the space vector modulation (SVM) to mitigate the torque ripple of the machine. Stator voltage and slip compensation technique was proposed in [17].

Despite having limited performance, V/F control is still used in the applications which do not require high-performance and tighter control on speed trajectories and small steady state error is also tolerable like in pumps, conveyor belts, HVAC systems, etc. However, for more sophisticated and advanced applications like electric vehicles which require a wide speed range of operation and a tighter control on torque/speed of the machine, this technique is not suitable.

2.3.2 Field Oriented Control

Unlike the scalar control techniques, the vector control schemes are complex and require computational power for their implementation. As the name suggests, this class of techniques uses the vector representation of the dynamics of the IM, (2.23)−(2.27). The performance of the vector schemes is superior to that of scalar methods. The scalar methods offer the speed control only in a limited range of operation. On the other hand, the vector methods enabled the machine to be used in the applications requiring wide speed range operation, such as electric vehicles. Moreover, they also reduced the operational losses. The technique of field-orientation is used for the vector control and the overall control structure is named as Field-Oriented Control (FOC).

In 1972 Blaschke introduced the FOC using which it became possible to mimic a three-phase induction motor as a separately excited DC motor. In DC motors the flux and the torque can be independently controlled. The current through the field winding sets the value of the flux, and the current through the rotor winding establishes the torque of the machine. In this method, the three phase system *(a,b,c)* is projected to a rotating orthogonal two phase system *(d,q)*, as explained in section 2.2. After the transformation, the d-component of the stator current (i_d^s) controls the flux and its

q-component (i_q^s) controls the torque of the motor. In FOC the control algorithm is designed in d-q frame and applied in a-b-c stationary frame using the inverse transforms. This strategy ensures the orthogonal relation between the rotor flux and the torque, which DC motor achieves through a commutator, thus ensuring maximum torque produced by the motor [2, 25].

Field-oriented control is a complex control strategy and needs fast switching power electronic devices and high computational power. It remained in the books and theoretical papers until the 1990s. The development of microcontrollers and microprocessor based embedded systems paved the way for the realization of these algorithms. Since then, many modifications and extensions to this basic algorithm have been proposed to enhance its performance and to test its applicability in various applications.

The field oriented control algorithm needs the precise information of the machine parameters (such as rotor/stator resistances, inductances) to work properly. Discrepancies may lead to unsatisfactory performance. It also requires the information of the rotor flux angle θ_e. In direct field oriented scheme hall sensors are placed inside the motor to measure the flux and its angle. This approach is not economically feasible and also affects the reliability of the systems, because it makes it more complicated. Instead of measuring the rotor flux angle directly from the motor, indirect FOC is used which uses the current model to estimate the rotor flux angle [26]. Measurement of the flux magnitude is also required for robust control designs. All these issues gave birth to the parameter identification and observer based control schemes for an induction motor.

Parameter Identification and Estimation Methods

Among all the parameters the most important are the rotor resistance (R_r), rotor time constant (RTC: L_r/R_r), rotor mechanical speed (for sensorless techniques) and load torque (T_l). Their impact on the control design is the most because they often change on run-time due to thermal effects [27, 28]. There are many proposed identification and estimation algorithms in the literature focusing on different parameters.

Speed and flux estimation methods can be categorized into two groups: 1) signal injection based methods; 2) model based techniques [29]. The accuracy of the estimation techniques for Ω and Φ^r_{dq} itself depend on the accuracy of the motor parameters. A model reference adaptive system (MRAS) based speed estimation technique with online rotor time constant update was proposed in [29]. This technique avoids injecting the test signals for estimation rather uses the spectrum of signal jitters already present in the current loops. The author in [30] proposed a second order sliding observer based flux estimation method to reduce the sensitivity of the control algorithm against motor parameter variation. Some other sliding mode observer based techniques for speed and flux estimation were proposed in [31–33]. In [34], the reduced order extended Kalman filter (EKF) and adaptive speed estimation based algorithm was proposed to enhance the robustness against internal and external disturbances for high and mid speed range applications. A descriptor-type EKF was suggested for estimation in [35]. In [36], three different flux observers: rotor-flux model reference adaptive system (MRAS); torque-current MRAS and adaptive nonlinear flux observer were compared on the basis of performance against load torque variation, parameter sensitivity and system stability. It was reported that the adaptive nonlinear flux observer (ANFO: proposed by [37]) demonstrates much better performance in real-time. The ANFO was combined with

signal injection method to enhance its performance at low speed in [38]. The author in [39] proposed a modification in ANFO algorithm for zero speed and 100% load applications. In [40], the author presented the theoretical conditions under which the speed and flux of induction motors and permanent magnetic synchronous motors can be estimated. He also proposed that the variance in motor parameters, such as RTC, can not be tracked while estimating the speed at steady state when flux is constant.

Several works have been proposed in the domain of parameter identification for induction motors especially for rotor time constant, rotor resistance and load torque. Most of the RTC identification algorithms can be superimposed on the model based speed estimation algorithms. In [41], a model reference adaptive controller has been proposed for correcting RTC using the third harmonic of d-component of stator phase voltage. A method of obtaining a recursive RTC equation by injecting a small low-frequency AC component to the flux command is also proposed in literature [42]. However, the signal injection schemes produce torque ripples which are undesirable in some applications [27], so small signal jitters which are inherently present in the system can also be used [29, 43] for this purpose. An offline strategy, based on least square method, for the identification of the RTC, the stator resistance, the stator self-inductance and the stator transient inductance with the assumption of known rotor speed was proposed in [44, 45]. A reactive power approach was introduced by [46] to estimate the rotor resistance. An approach based on Luenberger-sliding mode observer and Lyapunov's stability theory adaptive to the stator and rotor resistance was also proposed [47, 48].

Adaptive and Robust Control Methods

Due to unknown and time varying nature of the motor parameters many adaptive and robust control schemes have been proposed in the past. Among the most famous algorithms are adaptive I/O feedback linearization [49], adaptive backstepping and sliding-mode algorithms. Many variations of these techniques have been proposed and tested in the literature. In [50], a higher-order twisting sliding mode algorithm for speed and flux tracking was proposed. A robust adaptive backstepping control approach was proposed in [51]. It used function approximation technique for uncertain load torque, friction and moment of inertia. The inner current loops of IM control also play a major role in overall performance of the control design. Authors in [52] designed an adaptive control scheme for the inner current loops and [53] proposed an adaptive nonlinear controller based on the zero dynamics of the system.

In general, the identification process is complex because the parameters of interest depend on other parameters (for instance RTC depends on rotor's self-inductance and resistance). They also require online identification and update process because of their time-varying nature. These issues increase the complexity of identification and adaptive techniques, thus making them difficult to implement in real-time applications [54]. The other approach is to design robust controllers capable of dealing with these uncertain parameters with the ability to reject the internal and external disturbances without any online update mechanism. Despite parameter variations, the controller should be able to give high-performance results. A robust backstepping approach was proposed in [55].The Nonlinear Active disturbance rejection controllers (ADRC) [56] were also investigated for this control problem. In [57], two second-order ADRCs were used for flux and speed control of an induction motor. The authors in [58] investigated a hybrid

scheme of conventional PID and second-order ADRC. To reduce the complexity of the ADRCs, [54] proposed a robust first order ADRC technique for robust speed tracking.

Intelligent and Hybrid Methods

In parallel to the techniques inspired from the control theory, intelligent techniques like artificial neural networks (ANN) [59, 60], Fuzzy logic [61] and optimization algorithms [62] has also been explored. Especially, hybrid techniques [63] are quite trending nowadays because they have the ability to overcome the shortcomings of the theoretically inspired techniques (sliding-mode and backstepping) and has an exceptional ability to handle the system nonlinearities and uncertainties. Like the problem of chattering in sliding-mode control has been addressed by [64] using adaptive fuzzy approach while ensuring the high system performance. Fuzzy control design uses a linguistic rule base which is designed through expert knowledge, they are less model dependant, robust and easier to understand and implement [65]. Fuzzy Sliding mode techniques use expert knowledge and handle uncertainties very well [66]. However, it has a major drawback that it lacks methodical design techniques for the fuzzy rules and its membership functions [67]. To overcome this shortcoming, adaptive fuzzy sliding-mode control was proposed [68]. Adaptive fuzzy sliding mode control schemes for induction motor control were also explored [69–71]. Similar to the issue of chattering in sliding-mode control; the issue of 'explosion of terms' in backstepping technique was also addressed using intelligent techniques [72, 73].

Similar to fuzzy based techniques, ANNs are also very popular in this domain due to their parallelism and learning characteristics [74]. It is able to approximate wide range of nonlinear functions. ANNs are used in both estimation and control algorithms. ANN

based hybrid techniques are also explored in the literature. The authors in [75] proposed a robust backstepping controller which uses two, two layer ANNs. One for designing the fictitious controller, and other for robustly realizing the ANN signals. A wavelet neural network based strategy with adaptive learning rates was proposed in [76]. Learning algorithm used for the training of ANNs also affect their performance. A comparison of the performance of ANNs trained using different training algorithms was presented in [77, 78]. A self-tuning neuro-fuzzy technique was proposed in [79] for robust rotor speed tracking.

2.4 Knowledge Gap

In the previous section, we have skimmed through the available control techniques, which came under the scope of field oriented control, which are present in the literature. Robust, adaptive, intelligent and hybrid techniques have been presented for the speed tracking problem. However, none of these techniques address the issue of the limited sampling rate of the sensing/actuation of the system. In real-time, the control laws are implemented in discrete time using microcontrollers operating at a specific sampling rate. For the case of IM drives, the motor is operated by a voltage source inverter (VSI) controlled through the PWM signal. The maximum frequency of the PWM signal must not exceed the maximum switching frequency of the MOSFETs/IGBTs present in the VSI. Typically, the switching frequency of the power devices is $< 50KHz$. In such scenario, the control law can only be executed at a rate up to $50KHz$ while the microcontroller running the system tends to operate at the much higher frequency, i.e., at the order of 10^6Hz. All the techniques present in the literature can be executed only at the sampling rate synchronized with the sensing and actuation. Due to external

limitation, a lot of processing power is being wasted. We require a control technique that utilizes this addition computational power available at the processing end to improve the system response.

The induction machine is an uncertain system. The machine parameters are not accurately known in practice. To perform the robust tracking of the rotor speed, intelligent and adaptive control schemes have been proposed in the literature. But the schemes are heavily dependant on the structure of the model and are also complicated and much theoretically involved which is not appreciated in the industry. That is why PID control scheme is still prevalent in the industry. For these reasons it is believed that there is still a lot of room available for contribution in robust control schemes with the simple control structure.

CHAPTER 3

CONVENTIONAL FIELD-ORIENTED CONTROL

3.1 Introduction

In this chapter, we present the conventional FOC control technique. The traditional technique of control uses cascaded PI control loops for the speed and flux tracking. It is the earliest technique used to control the induction motor. However, this linear and simple method has some shortcomings. Moreover, we also present the experimental test bench prepared for the real-time testing of the results. The conventional scheme simulated as well as testing in the real-time. This scheme will be compared with the proposed scheme presented in the next chapters.

Control Objectives

The following are the control objectives for the controller design:

1. The rotor speed of the induction motor model, defined in (2.29) − (2.33), should

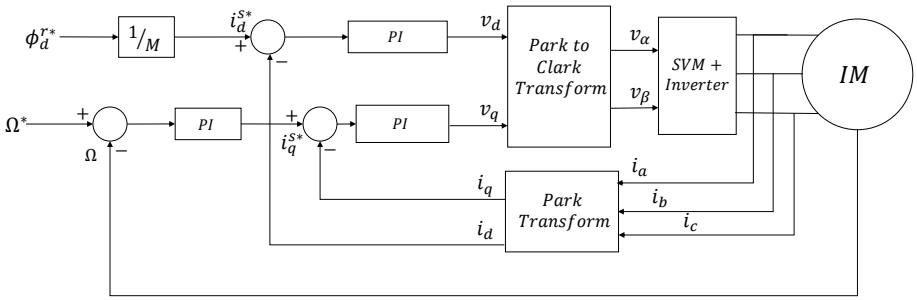

Figure 3.1: Conventional FOC Scheme for Induction motor

track a smooth and bounded reference trajectory, $\Omega^*(t)$.

2. The rotor flux magnitude of the machine, $\phi_d^r(t)$, should track a smooth and bounded reference i.e., $\phi_d^{r*}(t)$.

3.2 Conventional Field-Oriented Control

The conventional FOC uses the cascaded PI loop structure. It handles the system nonlinearities by forcing the system to the current command mode. Inner loops, known as the current loops, control the direct and the quadrature axis currents of the stator, forcing them to track their respective references generated by the outer control loops. The outer control loops control the actual speed and the flux of the machine. The overall control scheme is depicted in Figure. 3.1.

To design the flux and speed loop control, we assume the machine in the current command mode as:

$$\frac{d\Omega}{dt} = m\,\phi_d^r\,i_q^{s*} - c\,\Omega - \frac{1}{J_m}\,T_l, \tag{3.1}$$

$$\frac{d\phi_d^r}{dt} = -a\,\phi_d^r + a\,M_{sr}\,i_d^{s*}, \tag{3.2}$$

while considering i_d^{s*} and i_q^{s*} as the input to the sub system (3.1) and (3.2).

3.2.1 Flux Control

The dynamics of the flux of the motor are represented by (3.2). It can be noted that the dynamics are *linear* and *stable*, as $a > 0$. Considering i_d^{s*} as the input to the dynamics, the objective of the flux control is to find an appropriate i_d^{s*} that ensures the convergence of ϕ_d^r to some reference ϕ_d^{r*} at steady state. The error of the flux, e_ϕ, is defined as

$$e_\phi = \phi_d^r - \phi_d^{r*} \tag{3.3}$$

and its dynamics as,

$$\dot{e}_\phi = \dot{\phi^r}_d - \dot{\phi}_d^{r*}. \tag{3.4}$$

In general, the reference flux is the rated flux of the machine, and therefore its value is constant i.e., $\dot{\phi}_d^* = 0$. Substituting (3.2) into (3.4) will yield

$$\dot{e}_\phi = -a\,\phi_d + a\,M_{sr}\,i_d^{s*}. \tag{3.5}$$

Performing the steady state analysis on (3.5), where $\dot{e}_\phi = 0$. The flux magnitude will converge to its reference, ϕ_d^{r*}, if we choose i_d^{s*} as,

$$i_d^{s*} = \frac{\phi_d^{r*}}{M_{sr}}. \tag{3.6}$$

The i_d^{s*} will serve as the reference to the $d-$axis inner current loop of the scheme to make to actual i_d^s of the machine converge to the i_d^{s*}.

3.2.2 Speed Control

The dynamics of the mechanical rotor speed, (3.1), are nonlinear. The i_q^{s*} is considered as the input to the system. If control input is chosen as

$$i_q^{s*} = K_{p\Omega}(\Omega^* - \Omega) + K_{i\Omega}\int_0^t (\Omega^* - \Omega)dt, \tag{3.7}$$

then with the appropriate choice of $K_{p\Omega}$ and $K_{i\Omega}$, Ω will converge to Ω^*, for a constant T_l, as the time goes to infity. The author in [80] has shown that, the dynamics of the current-fed induction motor, (3.2) and (3.2), with the control input (3.7) are *globally asymtotically stable*.

3.2.3 Current Loops

The current loop control forces the true direct and quadrature axes currents of the machine to their respective references generated by the outer loop control, i.e., (3.6) and (3.7). The dynamics of the inner loops represented by (2.32) and (2.33) are highly nonlinear and time-varying. One way to deal with these is to use nonlinear compensation to eliminate the nonlinear terms from the equation. But this technique requires exact information about the machine parameters. Even a slight error can result in an unsatisfactory response. However, it is shown experimentally that the effect of nonlinearities can be eliminated by forcing the system into current command mode [81]. It can be achieved by using high gain PI feedback loops,

$$v_d^s = K_{dp}(i_d^{s*} - i_d^s) + K_{di}\int_0^t (i_d^{s*} - i_d^s)dt \tag{3.8}$$

$$v_d^s = K_{qp}(i_q^{s*} - i_q^s) + K_{qi}\int_0^t (i_q^{s*} - i_q^s)dt \tag{3.9}$$

Table 3.1: Machine Parameters

Induction Motor Parameters		
P_N	$180W$	Nominal Power
V_N	$220V$	Nominal Voltage
I	$1.3A$	Rated Current
n	1740 rpm	Rated Speed
R_s	11.05Ω	Stator Resistance
R_r	6.11Ω	Rotor Resistance
L_s	$316.4mH$	Stator Inductance
L_r	$316.4mH$	Rotor Inductance
J_m	$11 \times 10^{-5} Kg.m^2$	Rotor Inertia
f_v	$14 \times 10^{-5} N.m.rad^{-1}.s^{-1}$	Viscous friction
L_m	$293.9mH$	Mutual Inductance

K_{dp}, K_{di}, K_{qp} and K_{qi} are the positive number which should be tuned in a manner that the quantities i_d^s and i_q^s rapidly converge to their respective references i.e., i_d^{s*} and i_q^{s*} respectively [25, 82].

3.2.4 Numerical Simulations

To investigate the performance of the conventional FOC, the system (2.29)−(2.33) is simulated in MATLAB/Simulink using the S-Function. We used Fixed Step solver with the time step of 10^{-5} in the simulation settings. The machine parameters are taken from the documentation provided by TI for the machine used for the real-time experiment. The parameters are summarized in Table 3.1. The machine is tested for the medium speed range operation. The speed reference, Ω^*, is set to 500 RPM and ϕ_d^{r*} is set to 0.263 Wb i.e., the rated flux of the machine. The gain of the PI controllers for the outer and inner loops were tuned based on the procedure provided by the TI [83] which is similar to the Ziegler Nichols method. The gains are tuned using the method provided

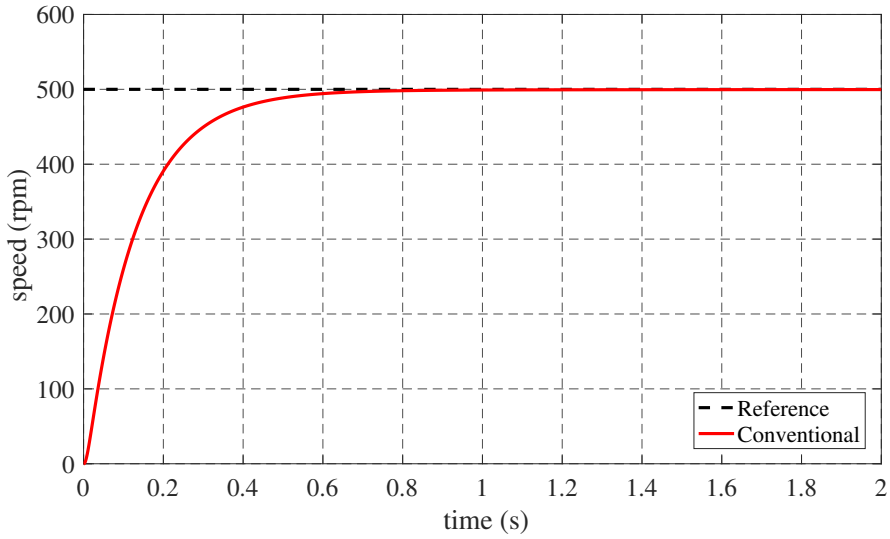

Figure 3.2: Rotor speed of the machine under PI control

by Texas Instruments [83]:

$$K_{p\Omega} = 0.009, \qquad K_{I\Omega} = 0.009,$$

$$K_{dp} = K_{qp} = 6.4 \qquad K_{di} = K_{qi} = 740.$$

Figure 3.2 shows the trajectory of the rotor speed. The settling time of the speed

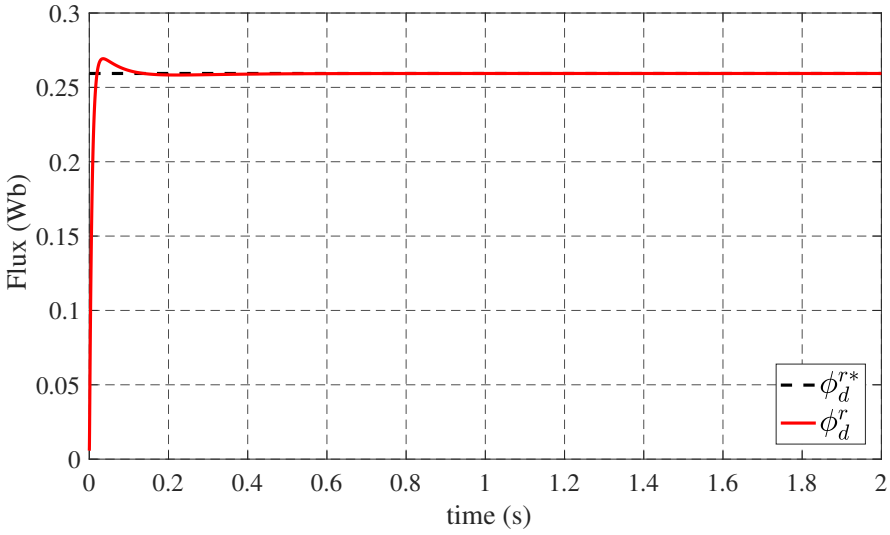

Figure 3.3: Flux magnitude of the machine under PI control

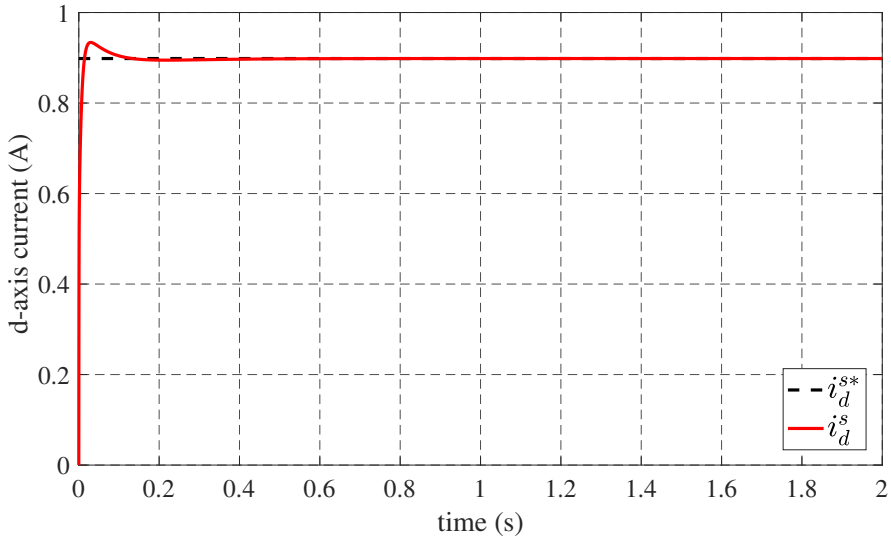

Figure 3.4: The d-axis stator current of the machine

is $630ms$ when Ω enters the 1% bound of Ω^*. No overshoot or steady state error is observed. Figure 3.3 shows the trajectory of ϕ_d^r. The settling time of the flux is $93ms$ with 3.8% overshoot. No steady state error is observed in the flux as well. The control laws (3.6) and (3.7) ensures the convergence of Ω and ϕ_d^r to their respective references.

Figs. 3.4 and 3.5 show response of the inner current loops of the system i.e., i_d^s and i_q^s. The reference for the d-axis and q-axis inner current loop is generated by (3.6)

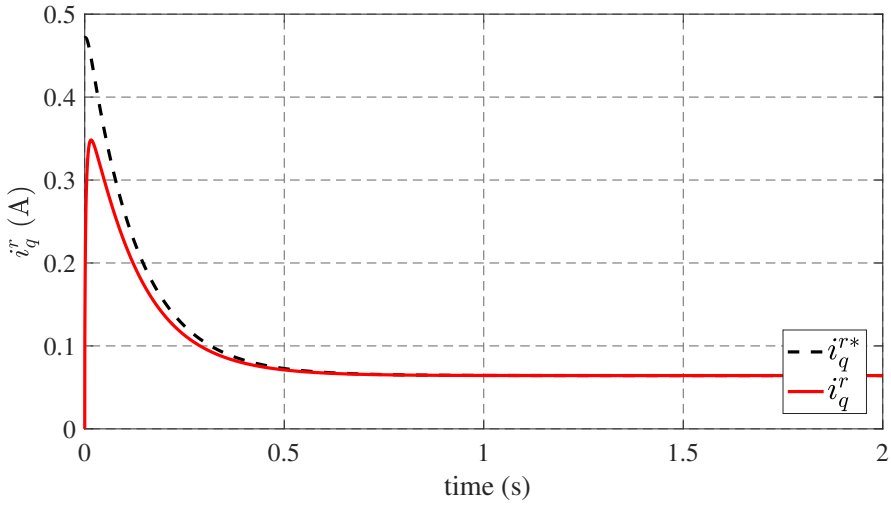

Figure 3.5: The q-axis stator current of the machine

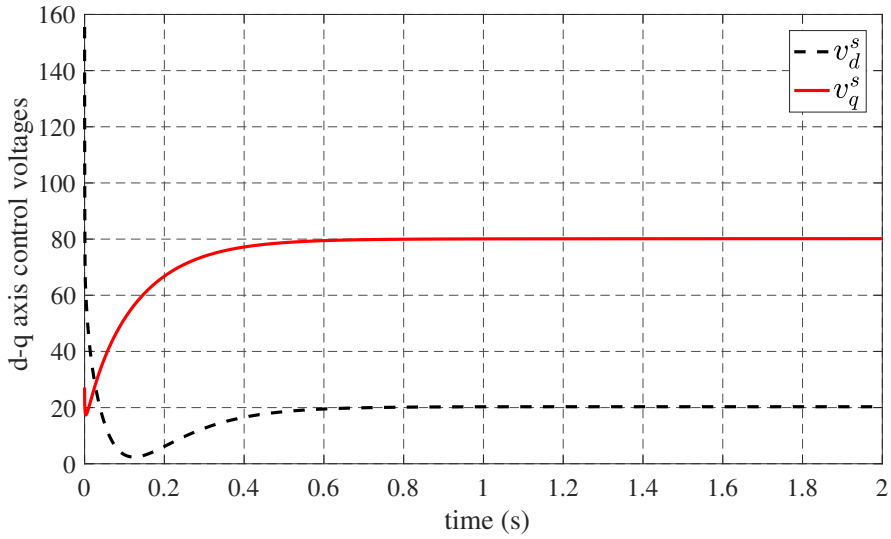

Figure 3.6: The $d-q$ axis stator voltages of the machine

and (3.7) respectively. The high gain PI loops, (3.8) and (3.9), compensates for the system nonlinearities and forces the true direct and quadrature currents of the machine to track their respective references. Both the responses are free from the steady-state errors. Moreover, both i_d^s and i_q^s are bounded and within limits. Figs. 3.6 shows the control inputs, i.e., d-axis and q-axis voltages generated by the inner control loops. The control inputs are smooth and bounded without any chattering.

External Disturbance

The load torque, T_l, is modelled as an external disturbance to the system. The external perturbation is simulated for a medium speed range operation. Once the machine reached its reference speed i.e., 500 RPM, at $t = 3s$ a load torque of 500 mN.m, i.e., half the rated torque of the machine, is applied on the machine. Figure 3.7 shows the response of the conventional FOC algorithm under the influence of external disturbance. The rotor speed drops to 156 RPM in 300ms before it starts recovering. It re-enters the 1% bound of the reference at $t = 7.7s$. The algorithm takes 4.4s to recover from the

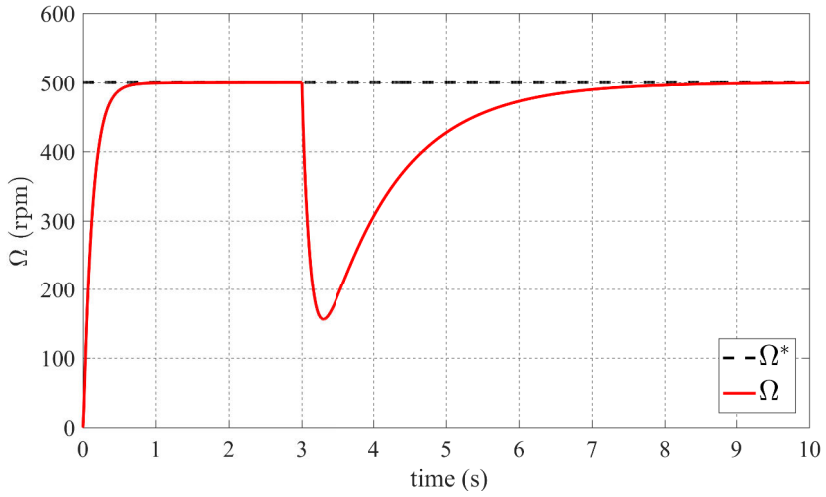

Figure 3.7: Rotor speed with external disturbance

external disturbance.

Internal Disturbances

The robustness of the conventional FOC is also investigated for the internal model uncertainties. Practically, it is a common issue that the parameters of the machine are not exactly known. The system is simulated with the same set of gains for variation of rotor resistance, i.e., R_r. The value of R_r, was perturbed to 100% of the base value. Figure 3.8 shows the trajectory of the rotor speed when the rotor resistance was changed 50%, 100%. The overshoot of 2.2% and 4.4% was observed. The settling of the response was heavily affected. The rotor speed takes $1.95s$ and $2.7s$ to settle upon 50% and 100% variation. In conclusion, the conventional FOC posses unsatisfactory robustness against both external and internal disturbances. The gains of the control law should be re-tuned to compensate for the uncertainties. The conventional FOC also lacks the mathematical conditions for system stability, especially for the inner loops of the control scheme.

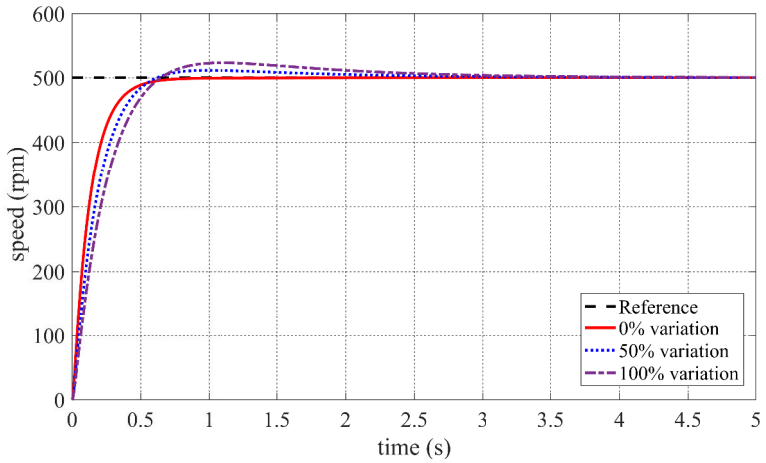

Figure 3.8: Rotor speed with internal disturbance

3.2.5 Experimental Results

In this section, we present the experimental results of the conventional FOC scheme. The Texas Instruments High Voltage Motor Control Kit is used for the realtime implementation. Figure 3.9 shows the experimental setup. The hardware consists of four functional groups: power supply, inverter, instrumentation and digital signal processor. The key aspects of this experimental setup is its low cost, compact design, and high computation power which can be used to implement even complex nonlinear control and

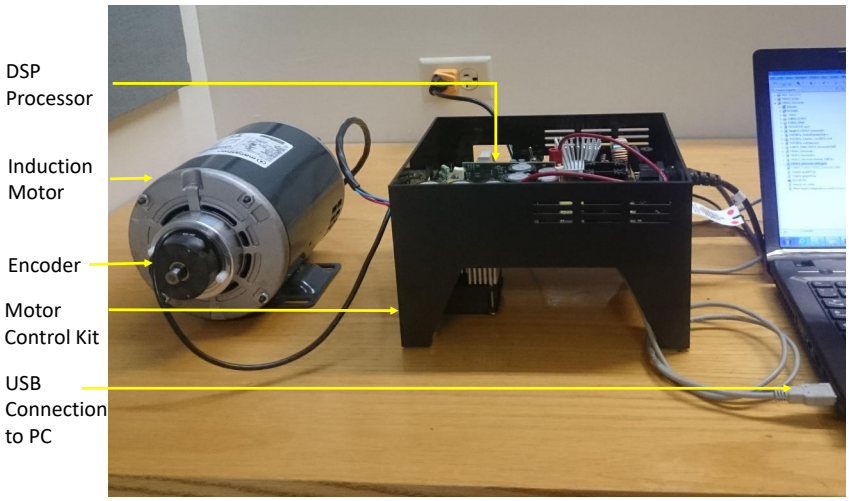

Figure 3.9: Experimental Setup

identification algorithms. Due to it's compact and plug and play nature it can be easily disassembled and moved to different places, as it is one of the major concerns of experimental setups in an academic environment. On the other hand, the downside of this experimental setup is that it provides insufficient support with the Matlab Simulink. The user needs to implement the algorithms in C-language which is quite complicated in its very nature. The details of the kit are given in the appendix.

The conventional FOC scheme was implemented on the hardware using the C-language and Code Composer Studio and digital motor control library provided by TI. The reference for the speed was set to $600rpm$. The PI gains were tuned using the procedure defined by the TI [83] as:

$$K_{dp} = K_{qp} = 2.0, \qquad K_{di} = K_{qi} = 0.003$$

$$K_{p\Omega} = 1.7, \qquad K_{I\Omega} = 0.0002$$

The PWM frequency and ADC sampling frequency both are set to $10KHz$. Figure 3.10 shows the trajectory of the rotor speed of the machine. The speed settles in $657ms$

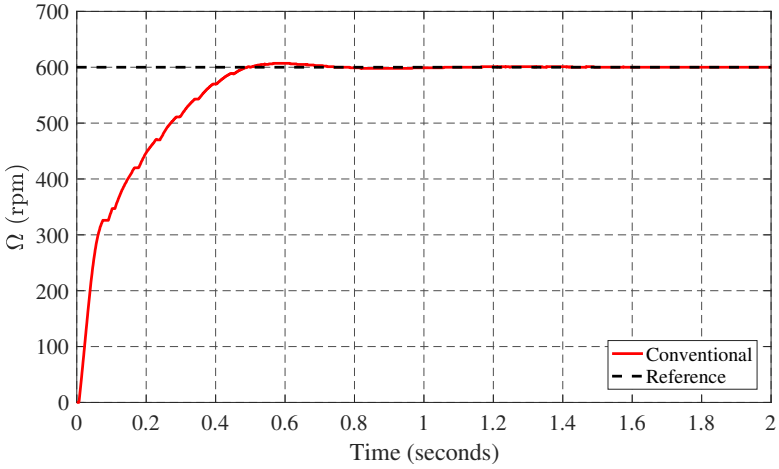

Figure 3.10: Real-time trajectory of the rotor speed under conventional control

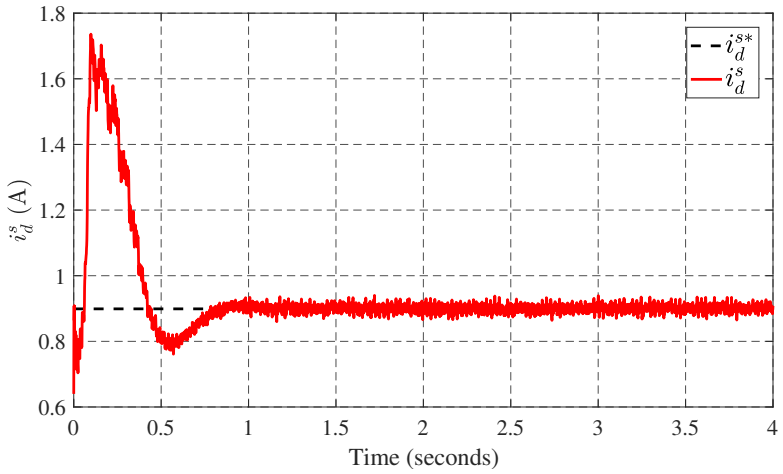

Figure 3.11: Real-time trajectory of the d-axis current

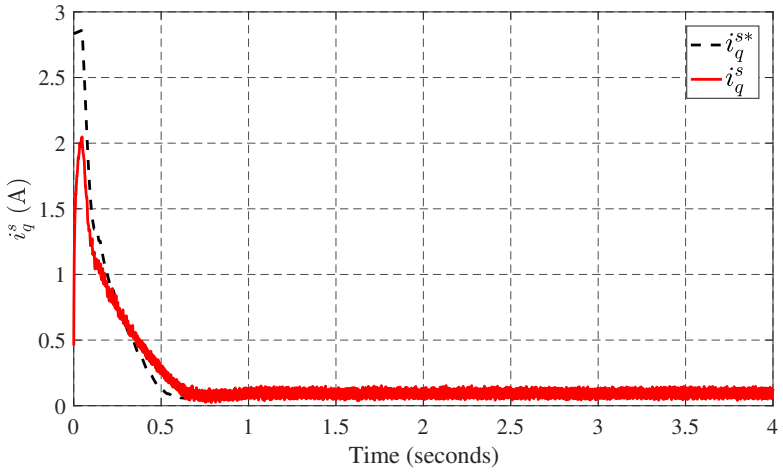

Figure 3.12: Real-time trajectory of the q-axis current under conventional control

which it enters the 1% bound for the reference. Moreover, 1.16% overshoot was also observed. Figures 3.11 and 3.12 show the real-time $d-q$ axis currents of the motor. It can be seen that the inner loops successfully make the i_d^s and i_q^s of the machine converge to i_d^{s*} and i_q^{s*} generated by the outer control loops. The vector currents are within the physical limits of the machine. Figures 3.13 and 3.14 show the control inputs generated by control scheme. The control inputs are within the physical limits of the machine.

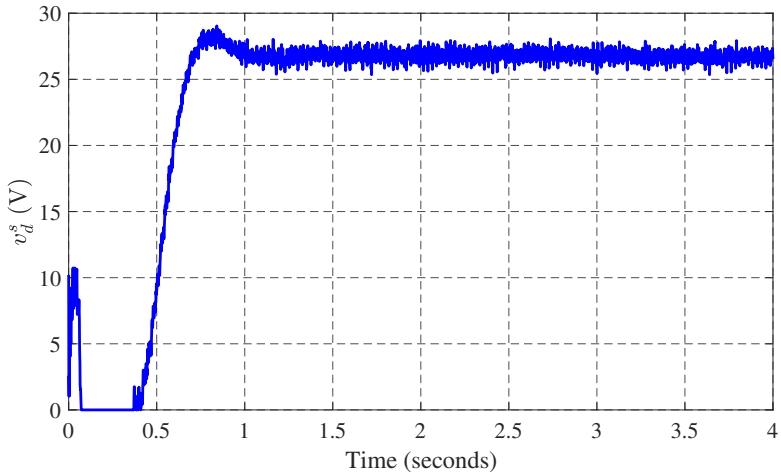

Figure 3.13: Real-time d-axis control voltage generated by conventional control

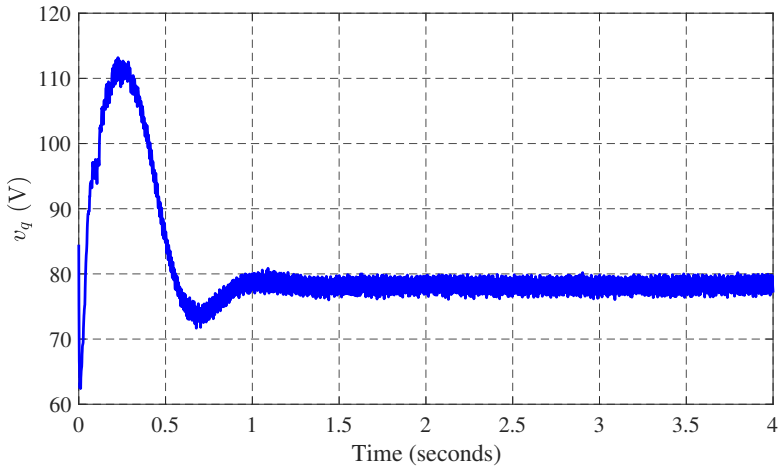

Figure 3.14: Real-time q-axis control voltage generated by conventional control

3.3 Summary

In this chapter, we presented the conventional FOC scheme. It is simple and the oldest methods for speed control of the induction motor. Its performance is adequate regarding convergence and settling time, although no overshoot and steady-steady errors were observed. The internal and external disturbance rejection qualities are average. The rotor speed successfully re-converges to the references after 4.4s. The internal disturbance profoundly affects the settling time of the system. The technique was also implemented in real-time. The real-time performance is comparable with the simulations.

CHAPTER 4

PROPOSED CONTROL SCHEMES

4.1 Introduction

In this chapter, we present the main contribution of the thesis. We propose two control schemes for the rotor speed control of the three-phase squirrel cage Induction motor, namely 1) Inter-sample Iterative Learning Control (ISILC) and 2) Active Disturbance Rejection Control (ADRC). The ISILC is a $2-D$ control technique which uses an iterative process between two-time samples to enhance the performance of the system. It is an especially useful technique for the systems where the sampling rate of the sensing and actuation devices is constrained due to some external factor while the central processor still possessing a higher rate for the control law execution. The ADRC is based on an active linearization of the system using an Extended State Observer (ESO). The ADRC is exceptionally robust against uncertainties. In literature, the nonlinear ADRC with a nonlinear ESO has been used for the IM drives [57,58], but the nonlinear ADRC

has discontinuous control law and experiences chattering at steady state. Moreover, the stability criterion for the nonlinear ADRC is still an open problem. Later, Gao has introduced a linear ADRC (LADRC), and its stability characteristics was studied by [84, 85]. LADRC is more simple than its nonlinear counter part. Moreover, the stability criterion is also established for this technique. Previously, LADRC is not been investigated for this control problem. Both ISILC and ADRC are tested for their effectiveness through numerical simulations while ISILC is also implemented in real-time using the experimental setup explained in chapter 3.

4.2 Inter-sample Iterative Learning Control

Iterative learning control (ILC) is a simple technique devised to take advantage of the repetitive nature of the system and improves the response on trial by trial basis by adding the information of the previous control input [86]. ILC was born in the field of robotics but has been very popular in other areas of engineering as well, multi agent control, motor control, stochastic systems, mechatronics and more [87–90]. Specifically, in motor control, ILC has been used to mitigate the speed ripple of permanent magnet synchronous motor operated at low speeds [88]. The idea was also proposed for the speed tracking problem of DC motor with nonlinear friction [91]. For more references, the reader can refer the survey papers [92, 93].

In this work, we propose a new scheme of implementation of ILC, which we call as ISILC. The proposed scheme enables the conventional ILC to be investigated for non-repetitive control problems as well. The main contribution of this work is to propose a new control scheme inspired from the conventional ILC to use the excess computational power available at the central processor. The stability of the algorithm is mathematically

studied and validated through numerical simulations.

4.2.1 Preliminaries and System Description

Throughout this work, the notation $\mathbb{R}$, $\mathbb{Z}^+$ and $\mathbb{N}$ represents the set of real numbers, positive integers, and natural numbers respectively. The notation $M > 0$ ($M < 0$), where M being a Hermitian matrix, denotes a matrix M being positive definite (negative definite) and M' denotes the matrix transpose of M. The notation I and $\mathbf{0}$ represent an identity matrix and a null matrix of appropriate dimension, respectively.

The ISILC is a discrete-time control technique. We use the forward Euler discretized dynamics of a three-phase squirrel-cage induction motor i.e., (2.29)-(2.33) in, rotor flux aligned, d-q frame. The discretized dynamcis are given by the following structure [25,94]:

$$x(k+1) = f\Big(x(k)\Big) + B\,u(k) \tag{4.1}$$

where,

$$x(k) = \begin{pmatrix} \omega_m(k) \\ \phi_d(k) \\ \rho(k) \\ i_d(k) \\ i_q(k) \end{pmatrix}, \quad B = \begin{pmatrix} Tm_1 & 0 \\ 0 & Tm_1 \\ 0 & 0 \\ 0 & 0 \\ 0 & 0 \end{pmatrix}, \quad u(k) = \begin{pmatrix} u_d(k) \\ u_q(k) \end{pmatrix}$$

$$f\big(x(k)\big) = \begin{pmatrix} (1 - Tm)\,\phi_d(k)\,i_q(k) - T\,c\,\omega_m(k) \\ (1 - Ta)\,\phi_d(k) + a\,M\,T\,i_d(k) \\ T\,\rho(k) + Tp\,\omega_m + Ta\,\frac{M}{\phi_d}\,i_q \\ (1 - T\,\gamma)\,i_d(k) + Ta\,b\,\phi_d(k) + Tp\,\omega_m(k)\,i_q(k) + Ta\,\frac{M}{\phi_d(k)}\,i_q^2(k) \\ (1 - T\gamma)\,i_q(k) - b\,p\,T\,\omega_m(k)\,\phi_d(k) - p\,T\,\omega_m(k)\,i_d(k) - T\,a\,\frac{M}{\phi_d(k)}\,i_d(k)\,i_q(k) \end{pmatrix}.$$

The state vector is denoted by $x(k) \in \mathbb{R}^5$, $u(k) \in \mathbb{R}^2$ is the control input and $f(.) : \mathbb{R}^5 \to \mathbb{R}^5$ is a locally lipschitz nonlinear function vector. The time index is denoted by $k \in \mathbb{N}$. In the system dynamics, $\omega_m(k)$ and $\rho(k)$ are the rotor mechanical angular speed and the rotor flux angle respectively. $\phi_d(k)$ denotes the rotor flux magnitude and $i_d(k)$, $i_q(k)$, $u_d(k)$ and $u_q(k)$ are the stator currents and the control voltages along d-axis and q-axis of the rotating frames respectively. p and T denotes the number of pole pairs and the sampling period of the model. All the state variables and the control inputs are assumed to be bounded with their maximum values be $x^{\max}(k)$ and $u^{\max}(k)$ respectively. The parameters a, b, c, γ, m and m_1 are defined as:

$$a = \frac{R_r}{L_r}, \quad b = \frac{M}{\sigma L_s L_r}, \quad c = \frac{f_v}{J}, \quad m = \frac{pM}{JL_r},$$
$$\gamma = \frac{L_r^2 R_s + M^2 R_r}{\sigma L_s L_r^2}, \quad \sigma = 1 - \frac{M^2}{L_s L_r}, \quad m_1 = \frac{1}{\sigma L_s},$$

where R_r is the rotor resistance, R_s is the stator resistance, L_r is the rotor self-inductance, L_s is the stator self-inductance and M is the mutual inductance of the motor. f_v and J represent the viscous coulomb friction and the load inertia. Moreover, it is assumed that the machine is symmetric and all the resistances and self-inductances are equal among all the three phases.

It is assumed that the system dynamics (4.1) also satisfies the following assumption

$\forall\, k \in \mathbb{N}$.

Assumption 1 *For the reference output trajectory $y^{ref}(k)$, for the given system* (4.1)*, there exists a bounded controller; $u^{ref}(k) \forall\, k \in \mathbb{N}$ such that the desired state space trajectory, $x^{ref}(k) \in \mathbb{R}^5$, is the solution of the following dynamics:*

$$x^{ref}(k+1) = f\big(x^{ref}(k)\big) + B\, u^{ref}(k),$$

$$y^{ref}(k) = C\, x^{ref}(k),$$

where $C = \begin{bmatrix} I & \boldsymbol{0} \end{bmatrix}$ is a constant matrix of appropriate dimension.

Assumption 2 *The load torque on the machine in zero and all the parameters of the machine are constant and known.*

Before presenting the main results, we recall the following Lemmas.

Lemma 4.1 *[95] A linear discrete time system of the form,*

$$z(k+1) = Uz(k) + Vv(k). \tag{4.2}$$

where $z(k) \in \mathbb{R}^n$ is the state vector, $v(k) \in \mathbb{R}^m$ is the control input, $k \in \mathbb{N}$ is the time index and U, V are the system matrices of appropriate dimensions. The system (4.2) *is stable if and only if there exists a positive definite matrix $P \in \mathbb{R}^{n \times n}$ such that,*

$$U'PU - P < 0. \tag{4.3}$$

Lemma 4.2 *[96] A 2-dimensional discrete-time dynamics represented in Röesser form,*

$$\begin{bmatrix} z_1(k+1,l) \\ z_2(k,l+1) \end{bmatrix} = U \begin{bmatrix} z_1(k,l) \\ z_2(k,l) \end{bmatrix} + Vu(k,l), \tag{4.4}$$

where U, V are some real matrices of appropriate dimensions, $z_1(k,l) \in \mathbb{R}^p$ and $z_2(k,l) \in \mathbb{R}^q$ are the state dynamics along k and l axis respectively, are stable if there exists matrices $W_1 \in \mathbb{R}^{n\times n}$, $W_2 \in \mathbb{R}^{m\times m}$, $W = diag(W_1, W_2)$ and Q symmetric positive definite matrices such that

$$U'WU - W = -Q. \tag{4.5}$$

4.2.2 Controller Design

In this section, we present an inter-sample iterative control algorithm for the rotor speed control of an induction motor. The control objective is to force $\omega_m(k)$ to track a certain reference $\omega_m^{ref}(k)$ with better convergence rate and overshoot. For simplicity, the rotor flux, $\phi_d(k)$, is controlled by a feedforward compensator to track its corresponding reference, $\phi_d^{ref}(k)$, as explained in section 3.2.1. The overall idea is to update the control law at a higher rate than the sampling period, T, of the system. The control input is calculated using an iterative process which modifies the control input, N times, before sending it to the actuator. After each iteration, the calculated control input is applied to the system model to calculate a virtual output error. This virtual output error is used to modify the control input again in the next iteration and so on. This iterative process is repeated for N times, and the final control input is sent to the actuator, as shown in Figure 4.1. The implementation structure of the proposed techniques is similar to that of the basic FOC scheme, see Figure 4.2, which uses cascaded control loops.

Let us represent the system (4.1) with two discrete indices:

$$x(k+1,i) = f\big(x(k,i)\big) + B\,u(k,i),$$
$$y(k,i) = C\,x(k,i) \tag{4.6}$$

where $k \in \mathbb{N}$ is the time index and $i \in \{1, 2, 3 \cdots N\}$ is the iteration index between k and $k+1$. The overall proposed scheme is depicted in Figure 4.2.

Speed Control

Before presenting the proposed control law, let's assume the machine is operating in current command mode. Rewriting the dynamics of $\omega_m(k)$, with respect to time and iteration index i.e., k and i as,

$$\omega_m(k+1,i) = (1 - T_s\,c)\,\omega_m(k,i) + T_s\,m\,\phi_d\,i_q(k,i), \tag{4.7}$$

where T_s is the sampling time of the speed loop. From assumption 1, we can write the desired dynamics for $\omega_d^{ref}(k)$ as,

$$\omega_m^{ref}(k+1) = (1 - T_s\,c)\,\omega_m^{ref}(k) + T_s\,m\,\phi_d^{ref}\,i_q^{ref}(k). \tag{4.8}$$

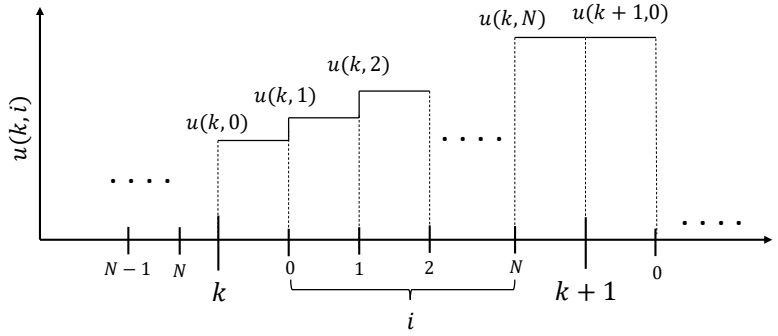

Figure 4.1: Control Law update

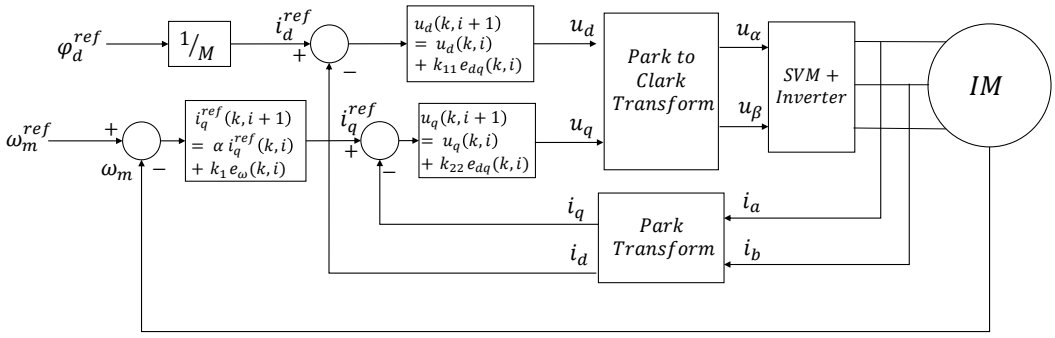

Figure 4.2: Proposed ISILC Scheme

The solution of (4.8) is the desired trajectory of the rotor speed which we also call as the reference trajectory for the system. It can be a constant or time-varying. The proposed iterative control input for (4.7) is:

$$i_q(k, i+1) = i_q(k, i) + k_1 e_\omega(k, i) \tag{4.9}$$

where,

$$e_\omega(k, i) = \omega_m(k, i) - \omega_m^{ref}(k). \tag{4.10}$$

The dynamics of the error, $e_\omega(k+1, i)$ will be

$$e_\omega(k+1, i) = \omega_m(k+1, i) - \omega_m^{ref}(k+1). \tag{4.11}$$

From (4.7) and (4.8):

$$e_\omega(k+1, i) = (1 - T_s\, c)\, \omega_m(k, i) - (1 - T_s\, c)\, \omega_m^{ref}(k) + T_s\, m\, \phi_d^{ref}\, i_q(k, i) - T_s\, m\, \phi_d^{ref}\, i_q^{ref}(k)$$

$$e_\omega(k+1,i) = (1 - T_s\, c)\big(\omega_m(k,i) - \omega_m^{ref}(k)\big) T_s\, m\, \phi_d^{ref}\big(i_q(k,i) - i_q^{ref}(k)\big)$$

$$e_\omega(k+1,i) = (1 - T_s\, c) e_\omega(k,i) + T_s\, m\, \phi_d^{ref} \delta i_q(k,i), \tag{4.12}$$

where $\delta i_q(k,i) = i_q(k,i) - i_q^{ref}(k)$. Subtracting $i_q^{ref}(k)$ from both sides of (4.9) yields:

$$\delta i_q(k,i+1) = \delta i_q(k,i) + k_1 e_\omega(k,i). \tag{4.13}$$

We can write (4.12) and (4.13) in 2-dimensional Röesser form as:

$$\begin{bmatrix} e_\omega(k+1,i) \\ \\ \delta i_q(k,i+1) \end{bmatrix} = \begin{bmatrix} 1 - T_s\, c & T_s\, m\, \phi_d^{ref} \\ \\ k_1 & 1 \end{bmatrix} \begin{bmatrix} e_\omega(k,i) \\ \\ \delta i_q(k,i) \end{bmatrix}. \tag{4.14}$$

The convergence of errors i.e. $\delta i_q(k,i) \to 0$ and $e_\omega \to 0$ will depend on the value of $k_1 \in \mathbb{R}$ which can be selected according to the following criteria.

Proposition 4.1 *The errors $\delta i_q(k,i) \to 0$ and $e_\omega \to 0$ as $i \to \infty$ and $k \to \infty$ of 2-D discrete-time system* (4.14) *if and only if for the given positive constant $k_1 \in \mathbb{R}$, there exists a positive definite matrix $P = diag(p_1, p_2) \in \mathbb{R}^{2\times 2}$ such that,*

$$A_\omega' P A_\omega - P < 0 \tag{4.15}$$

where

$$A_\omega = \begin{pmatrix} 1 - T_s\, c & T_s\, m\, \phi_d^{ref} \\ \\ k_1 & 1 \end{pmatrix}$$

holds true.

Proof. Using Lemma 4.1 on (4.14), will give the condition, (4.15), of the proposition.

∎

Remark 3 *The control law* (4.9) *successfully ensures the convergence of* $\omega_m(k)$ *to* $\omega_m^{ref}(k)$. *However, the system experiences a large overshoot. To eliminate the overshoot, we introduce a forgetting factor* α *where* $0 < \alpha < 1$. *The system performs at its best when* α *is close to* 1. *The final control law for the speed loop with a forgetting factor is proposed as*

$$i_q(k, i+1) = \alpha\, i_q(k, i) + k_1 e_\omega(k, i). \tag{4.16}$$

The Proposition 4.1 also holds for the control law (4.16) with

$$A_\omega = \begin{pmatrix} 1 - T_s\, c & T_s\, m\, \phi_d^{ref} \\ k_1 & \alpha \end{pmatrix}.$$

The $i_q(k)$ will converge to i_q^{ref} which is fed as a reference to the $q - axis$ current loop control.

Current Loops

The purpose of the current loop control is to ensure that the true $i_q(k)$ and $i_d(k)$ of the machine converges to $i_q^{ref}(k)$ and $i_d^{ref}(k)$ generated by the outer flux and speed loops. Considering system (4.6), we propose the control law for the inner current loops as,

$$u(k, i+1) = u(k, i) + K_2\, e_{dq}(k, i) \tag{4.17}$$

where,

$$e_{dq}(k, i) = y(k, i) - y^{ref}(k, i), \quad K_2 = \begin{pmatrix} k_{11} & 0 \\ 0 & k_{22} \end{pmatrix} \tag{4.18}$$

and

$$y(k,i) = Cx(k,i); \quad y^{ref}(k,i) = Cx^{ref}(k,i) \quad C = \begin{pmatrix} \mathbf{0}_{2\times 2} & I_{2\times 2} \end{pmatrix}. \tag{4.19}$$

The control input is $u(k,i) = [u_d(k,i) \;\; u_q(k,i)]'$ and the output is $y = [i_d(k,i) \;\; i_q(k,i)]'$.

The control law (4.17) ensures the convergence of the $i_d(k)$ and $i_q(k)$ to their respective references i.e. $i_d^{ref}(k)$ and $i_q^{ref}(k)$. The simulation results are discussed in the next section.

Remark 4 *In practical applications often the sensing and actuation rate depends on the hardware devices independent from the processor on which the control algorithm is running. In that case, the 2D iterative control utilizes the maximum capacity of processing power available to improve the overall performance.*

4.2.3 Numerical Simulations

To investigate the performance of the ISILC algorithm, the system (4.1) is simulated in MATLAB/Simulink using the user-defined Fcn block. We used Fixed Step discrete solver with the time step of 10^{-4} in the simulation settings. The sampling time, T, of the model is taken as 10^{-4}s. The machine parameters used are presented in Table 3.1. The speed and flux references are taken as, $\Omega^* = 500$ and $\phi_d^{r*} = 0.261$. By fixing the discrete step size of the simulation we are ensuring that the control algorithm interacts with the system model only at $10^{-4}s$. However, between to samples the control law iterates multiple times to improve the control input thus operating at a higher frequency than the system. The parameters of the ISILC are tuned by trial and error and satisfying the Proposition 4.1, to get the best response as:

$$\alpha = 0.99 \quad k_1 = 0.01, \quad K_2 = \begin{bmatrix} 0.09 & 0 \\ 0 & 0.09 \end{bmatrix}, \tag{4.20}$$

$$N_o = 22, \qquad N_i = 1$$

where N_o is the number of outer loop iterations i.e., speed loop iterations and N_i is the number of current loop iterations. The speed loop gains, (4.20), for the control law (4.16) satisfies the Proposition 4.1 for

$$P = \begin{bmatrix} 104.8104 & 0 \\ 0 & 88.1786 \end{bmatrix}.$$

The maximum number of iterations which can be executed between two time-sample depends on the operating clock frequency of the microcontroller on this control law will execute. The embedded processor which we are using for the real-time experiment is TMS320F28035 which operates at 60MHz and has a cycle time of 16.67ns. The time required to perform one iteration can be calculated by the following relation [97],

$$T_i = N_c \times T_c \tag{4.21}$$

where T_i is the time required for one iteration, N_c is the number of clock cycles required to execute the control law, and T_c is the cycle time of the processor which in our case is 16.67ns. The control laws (4.16) and (4.17) has three arithmetic operations: one multiplication, one addition and one assignment. Multiplication requires two clock cycles to execute and both addition and assignment requires one clock cycle each. The ISILC control law requires 4 clocks cycles to perform one iteration. According to (4.21),

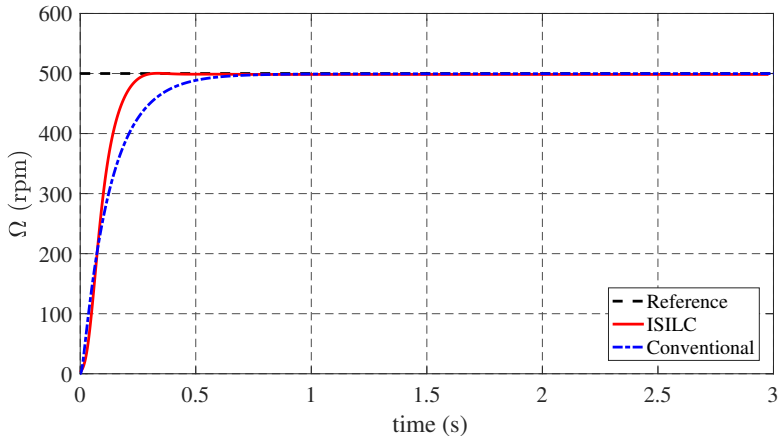

Figure 4.3: Rotor speed trajectory under ISILC control

the time required to perform one iteration is 66.68ns. TMS320F28035 can carry out maximum 900 iterations between two 10KHz time-samples.

Figure 4.3 shows the trajectory of the rotor speed. The settling time of the rotor speed trajectory is $268ms$ when the Ω enters the 1% bound of Ω^*. The settling time of the ISILC algorithm is 57.2% less than that of the conventional algorithm. No overshoot or steady state error is observed. Figure 4.4 shows the trajectory of ϕ_d^r. The settling time of the flux is $34ms$ with 10% overshoot. The settling time for the flux is 63% better that its conventional counterpart however it possess larger overshoot. No steady

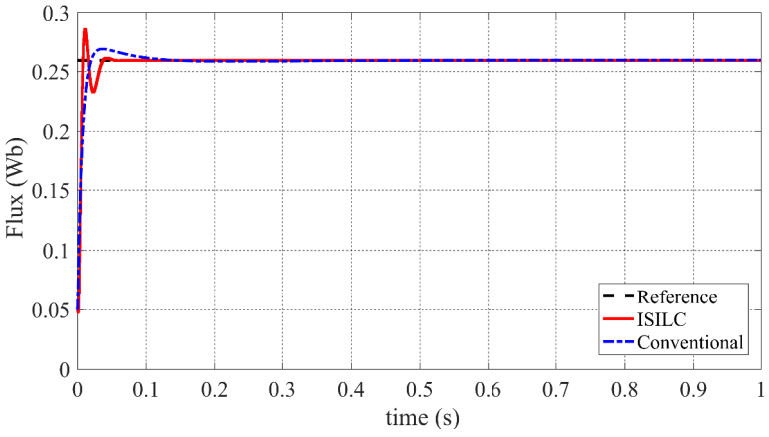

Figure 4.4: Rotor flux trajectory under ILC control

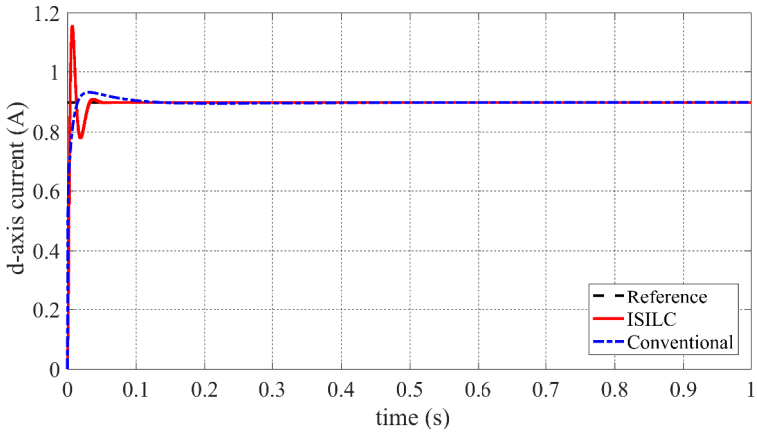

Figure 4.5: d-axis stator current under ILC control

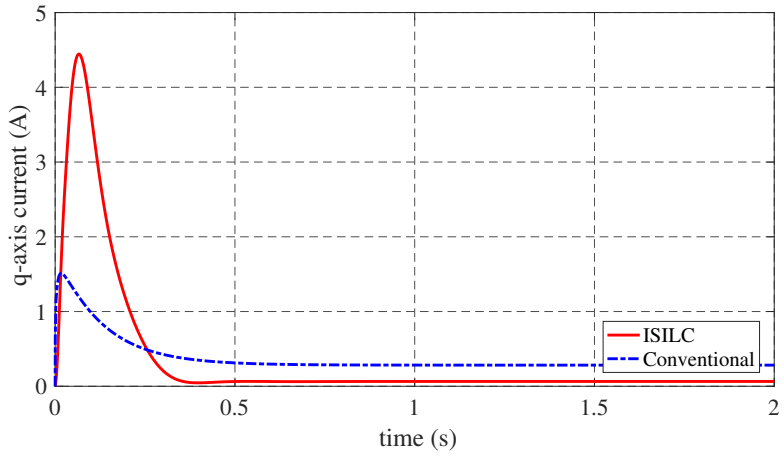

Figure 4.6: q-axis stator current under ISILC control

state error is observed in the flux as well. The control laws (4.16) and (4.17) ensures the convergence of Ω and ϕ_d^r to their respective references.

Figures 4.5 and 4.6 shows response of the inner current loops of the system i.e., i_d^s and i_q^s. The reference for the $d$axis and q-axis inner current loop is generated by (4.16) and $\frac{\phi_d^{r*}}{M}$ respectively. The $2-D$ control law (4.17), compensates for the system nonlinearities and forces the true direct and quadrature currents of the machine to track their respective references. In Figure 4.6, it can be seen that the starting current for the ISILC is higher than the conventional scheme. It is because the settling time of

the ISILC is smaller than the conventional, so the proposed requires higher amount of starting current to push the rotor speed to its reference in a short period of time. On the other hands, the steady state value for the ISILC is smaller than the conventional. It is because the the ISILC does not use an integrator to eliminate the steady-state error, like the conventional scheme. The integrator raises the steady-state of the control input to eliminate the steady-state error. Figure 4.7 and 4.8 show the generated control voltages by the $2-D$ control scheme in the rotating $d-q$ frame. The control voltages are within the physical limits of the machine, bounded and free from chattering. The initial v_d^s for the ISILC is lower than its conventional counter part. However, the transient v_q^s for the

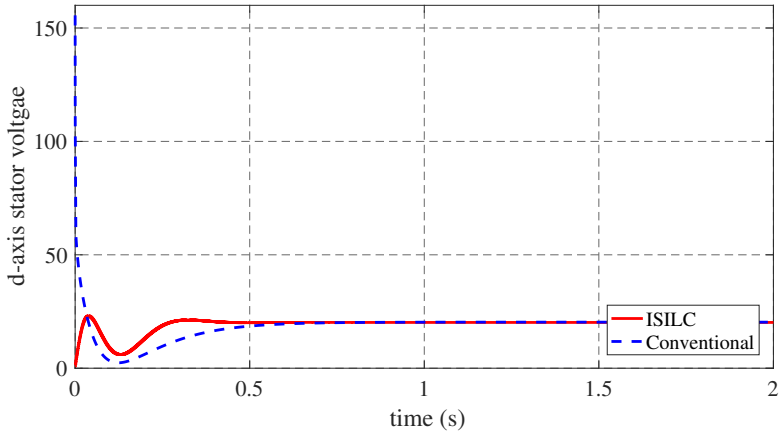

Figure 4.7: d-axis stator input voltages under ISILC control

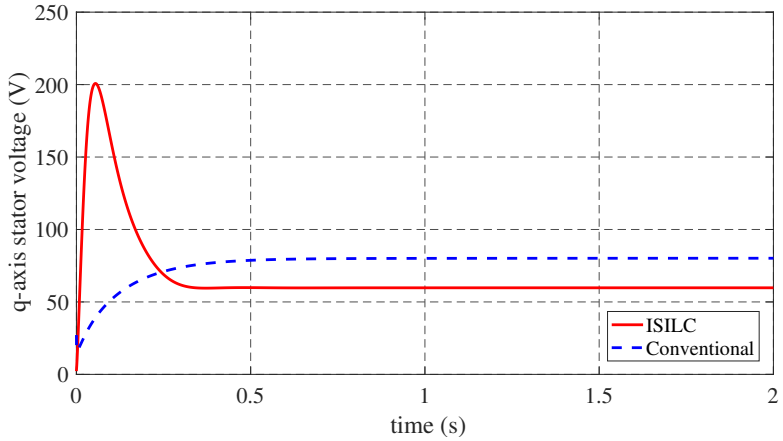

Figure 4.8: q-axis stator input voltages under ISILC control

ISILC is higher. On the other hand, the steady-state value of q-axis control voltage is lower than the conventional scheme because the ISILC doesn't use the integrator.

The sampling time of the system is taken $10^{-4}s$ and the speed control law, (4.16), is updated for 21 times using the system dynamics before sending the final signal to the actuator. Similarly, the sampling rate of the current and voltages sensors are also 10KHzs. Since we are updating the control law multiple times between two-time samples, therefore the control law is executed at a higher rate than the sampling time of the system. In our case, the execution rate of the control law is 210KHz because we are updating the control input 21 times between two consecutive time samples. This scheme is particularly useful for those applications where there are physical constraints on the actuation and sensing rate of the devices. In our particular case, the actuation signal is the PWM signal operating the silicon-based power devices. The frequency of the PWM is limited by the maximum switching frequency of the IGBTs or MOSFETs. Similarly, for the case for sensing, it is a common practice to synchronize the ADC sampling of the current with the PWM signal to reduce the switching noise in the sensing. However, the control algorithms are implemented at microcontrollers and microprocessors capable of executing a task at a rate in the order of 10^{-6}.In our particle case, given that both PWN and ADC are operating at 10KHz, i.e., the sampling time of the system, the control law is being executed at 210 KHz. In this way, we are using the excessive computational power available to improve the response of the system.

Figure 4.9 shows the response of the system at different number of iterations per sample. It can be seen that as we decrease the number of iterations for a given value of k_1, the rise time of the system decrease resulting in the fast response. However, the system experiences an overshoot and undershoot resulting in a higher settling time. On

the other hand, if we increase the iterations per sample, the overshoot and undershoot are eliminated but settling time of the system also increase. The iteration value is selected by trial and error to get the best response.

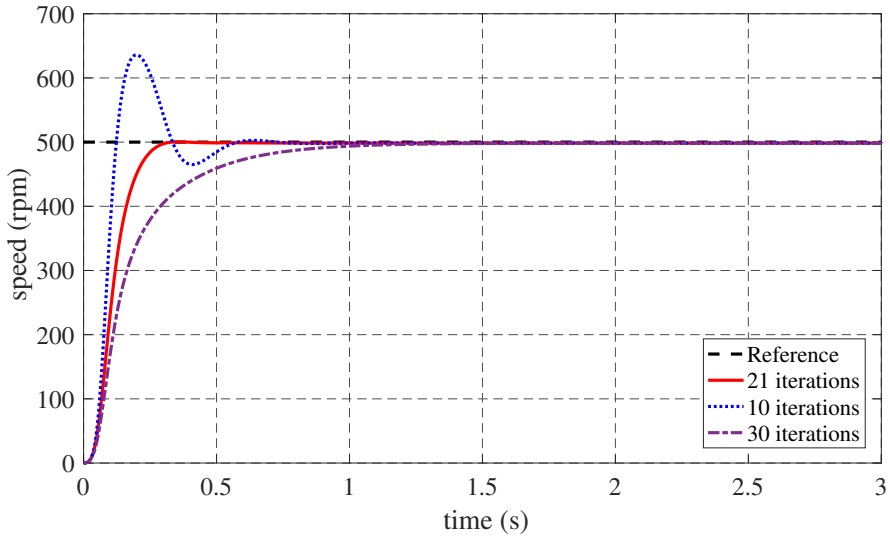

Figure 4.9: Rotor speed with different number of iterations

External Disturbance

The load torque, T_l, is modelled as an external disturbance to the system. The external perturbation is simulated for a medium speed range operation. Once the machine

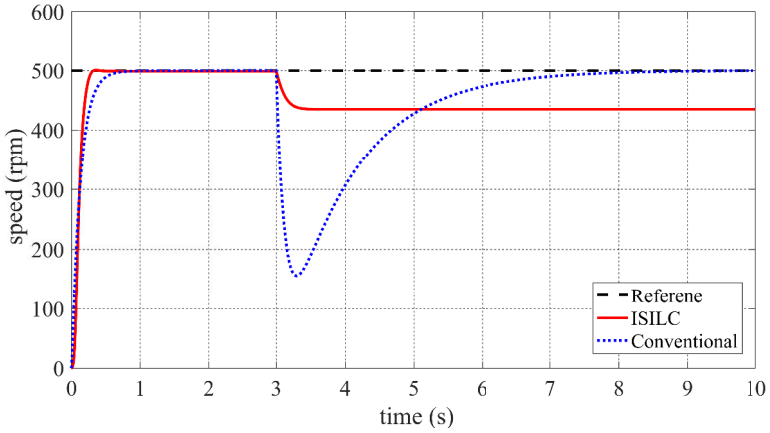

Figure 4.10: Rotor speed on external disturbance

reached its reference speed i.e., 500 RPM, at $t = 3s$ a load torque of 500 mN.m is applied on the machine. Figure 4.10 shows the response of the ISILC algorithm under the influence of an external disturbance. The rotor speed drops to 436 RPM resulting in a steady state error of 12.8%. The control scheme lacks the mechanism to compensate the external disturbances to the system. The robustness to the external uncertainties can be investigated in future.

Internal Disturbance

The robustness of the ISILC is also investigated for the internal model uncertainties. The system is simulated with the same set of gains for the parameter variation of the rotor resistance, i.e., R_r. The value of R_r was perturbed to 100% of this base value. Figure 4.11 shows the trajectory of the rotor speed on the variation of the parameter. The overall system remains stable, and no steady state error was observed. However, the response shows an overshoots of 36.8% and 48% on 50% and 100% variation. The settling time was also increased to $1.5s$ and $2.1s$ respective. The ISILC experiences

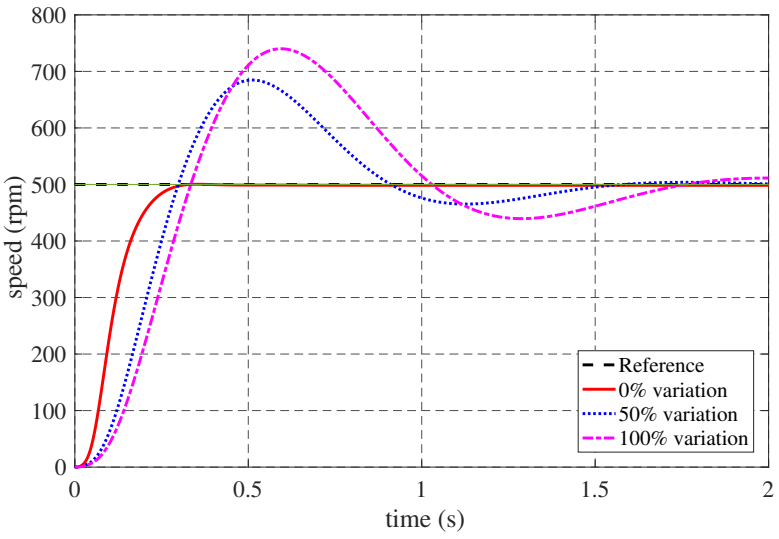

Figure 4.11: Rotor speed on internal parameter variation

34.6% and 43.6% larger overshoots, but the deterioration of the settling time is 23.4% and 22% lesser the conventional one.

4.2.4 Experimental Results

The ISILC was implemented in real-time using the experimental setup explained in section 3.2.5. The algorithm was coded in C-language using the Code Composer Studio and the digital motor control (DMC) library provided by TI. The DMC uses a specialized IQ math format for floating point calculations. The overall implementation scheme is depicted in figure 4.2. The reference speed was chosen as $600rpm$ and the $\phi_d^{r*} = 0.261$ Wb. The ISILC gains where chosen by trial and error and satisfying the Proposition 4.1, to get the best response, as:

$$\begin{aligned} &\alpha = 0.96 \quad k_1 = 0.9, \quad K_2 = \begin{bmatrix} 0.5 & 0 \\ 0 & 0.5 \end{bmatrix}, \\ &N_o = 15, \qquad N_i = 1. \end{aligned} \tag{4.22}$$

The chosen gains satisfies the Proposition 4.1 for,

$$P = \begin{bmatrix} 600.818 & 0 \\ 0 & 0.045 \end{bmatrix}.$$

The gains where chosen to achieve the best performance of the system. Figure 4.12

Table 4.1: Performance comparison of control schemes

Parameters	**Conventional**	**ISILC**	**Improvement**
Settling time	$657ms$	$319ms$	+51.4%
Overshoot	1.16%	zero	+100%
Steady state error	negligible	negligible	-

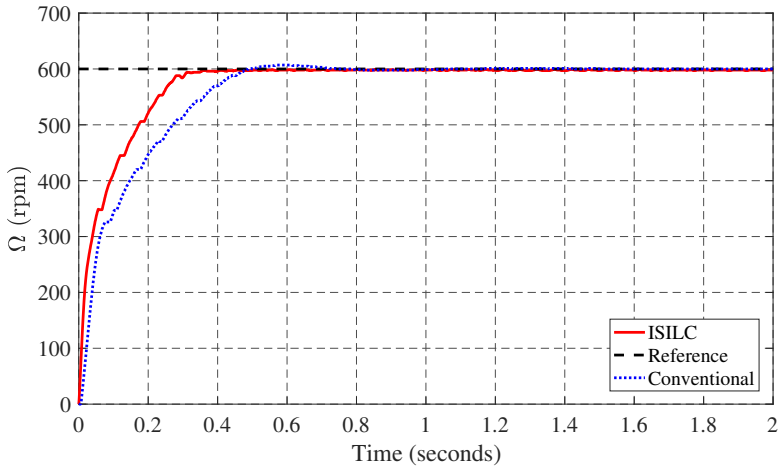

Figure 4.12: Real-time trajectory of rotor speed under ISILC

shows the response of the rotor speed. The settling time of the proposed scheme is $319ms$ when the rotor speed enters the 1% bound of the reference and stays inside. The scheme converges faster than the PI control which takes $657ms$ resulting in 51.4% improvement in the settling time. The PI control also experiences an overshoot of 1.16% while no overshoot is observed for the proposed scheme. The scheme converges directly in the neighborhood of the reference. The results of the performance parameters are summarized in Table 4.1.

Figure 4.13 and 4.14 shows the real-time trajectory of the d-axis and q-axis currents

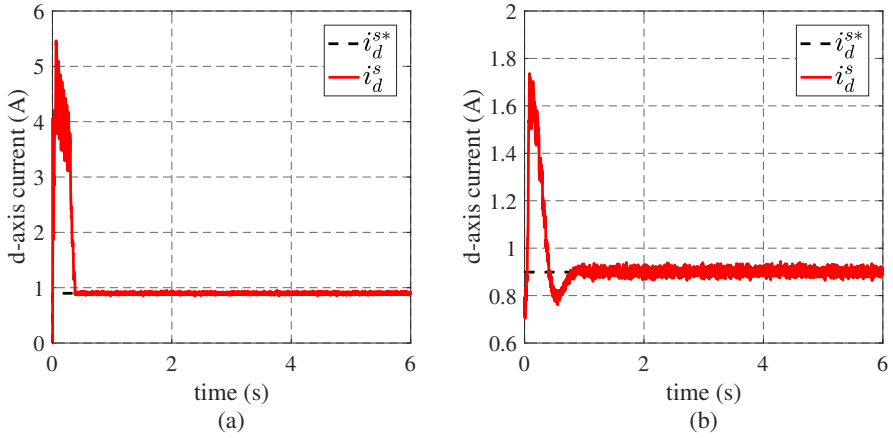

Figure 4.13: Real-time trajectory of d-axis current under (a) ISILC and (b) Conventional scheme

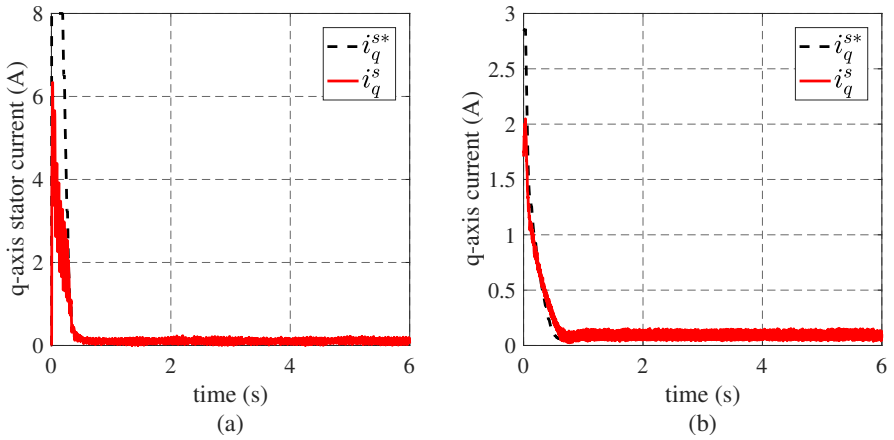

Figure 4.14: Real-time trajectory of q-axis current under (a) ISILC and (b) Conventional scheme

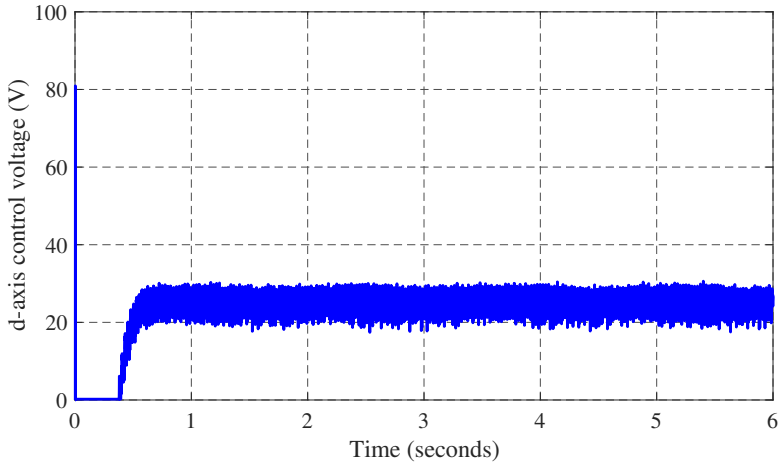

Figure 4.15: Real-time d-axis control voltage under ISILC

of the machine. The inner loops the ISILC make the currents converge to their respective references without any noticeable chattering. Moreover, the currents are bounded and within the physical limits of the machine.

Figure 4.15 and 4.16 shows the real-time trajectory of the control inputs generated by the algorithm. A hard saturation of $187V$ was imposed on the q-axis voltage to prevent any damage to the system.

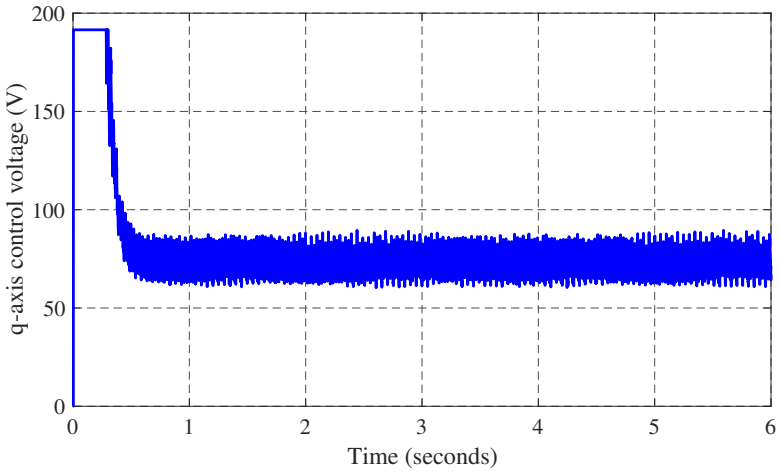

Figure 4.16: Real-time q-axis control voltage under ISILC

4.3 Active Disturbance Rejection Control

In this section, we present the ADRC technique for robust speed control of the Induction motor. The ADRC can be considered as an advanced form of feedback linearization (FL) technique which compensates the nonlinearities of the model actively through as an Extended State Observer (ESO). Unlike the FL, which requires precise information about the structure of nonlinearities and the parameters of the system. Even a small about of uncertainty in the structure or the system parameter would result in deteriorated performance of FL. In the next subsection, we will discuss the theory of ADRC followed by the application on Induction motor control and the numerical simulation results.

4.3.1 Theory

The ADRC was proposed by Han in the year 1995 to deal with the plants having a large amount of uncertainties both in dynamics and external disturbances [56]. Initially, the technique proposed by Han was nonlinear and contained discontinuous terms. It was further simplified by Gao to linear ADRC (LADRC) using a linear ESO (ESO) [84]

making it extremely simple and practical. LADRC achieves asymptotic tracking for the case when the plant dynamics are accurately known, and for the case of largely unknown plant the tracking error is bounded, and its upper bound monotonously decreases with the controller and observer bandwidths [85].

Consider a general nonlinear and time-varying system with single input u and single output y as:

$$y^{(n)}(t) = f(y^{(n-1)}(t), \cdots, y(t), w(t)) + bu(t). \tag{4.23}$$

where b is the given constant and w is the external disturbance. The function $f(.)$ represents the nonlinear and time-varying dynamics that are unknown. Only the order n and b are known for this case. The ADRC technique is centered around the estimation and compensation of $f(.)$ actively. Assuming f is differentiable and let $h = \dot{f}$, (4.23) can be rewritten in an augmented state space form as:

$$\begin{aligned}
\dot{x}_1 &= x_2 \\
&\vdots \\
\dot{x}_{n-1} &= x_n \\
\dot{x}_n &= z + bu \\
\dot{z} &= h(x, w) \\
y &= x_1
\end{aligned} \tag{4.24}$$

where $x = [x_1, x_2, \cdots, z] \in \mathbb{R}^{n+1}$ is the states, $u \in \mathbb{R}$ is the control input and $y \in \mathbb{R}$ is the system output. Any state observer of (4.24) will estimate the derivative of y and f. Because $z = f$ is the now the state of the system. Such observers are known as Extended state Observers (ESO). For an unknown f, the LESO for the system (4.24)

is of the form [98, 99],

$$\begin{aligned}
\dot{\hat{x}}_1 &= \hat{x}_2 + l_1(x_1 - \hat{x}_1) \\
&\vdots \\
\dot{\hat{x}}_{n-1} &= \hat{x}_n + l_{n-1}(x_1 - \hat{x}_1) \\
\dot{\hat{x}}_n &= \hat{z} + l_n(x_1 - \hat{x}_1) + bu \\
\dot{\hat{z}} &= l_{n+1}(x_1 - \hat{x}_1)
\end{aligned} \tag{4.25}$$

where $l_j, j = 1, 2, \cdots, n+1$ are the observer gains to be chosen. We consider a case where the gains are chosen as

$$[l_1, l_2, \cdots, l_{n+1}] = [\gamma\beta_1, \gamma^2\beta_2, \cdots, \gamma^{n+1}\beta_{n+1}] \tag{4.26}$$

with $\gamma > 0$. Here $\beta_j, j = 1, 2, \cdots, n+1$ needs to be selected such that the characteristic polynomial

$$\lambda(s) = s^{n+1} + \beta_1 s^n + \cdots + \beta_n s + \beta_{n+1} \tag{4.27}$$

is Hurwitz. The observer error can be defined as $\eta_j = x_j - \hat{x}_j, j = 1, 2, \cdots, n+1$. Using (4.24) and (4.25), the error dynamics of the LESO can be written as

$$\begin{aligned}
\dot{\eta}_1 &= \eta_2 - \gamma\beta_1\eta_1 \\
&\vdots \\
\dot{\eta}_{n-1} &= \eta_n - \gamma^{n-1}\beta_{n-1}\eta_1 \\
\dot{\eta}_n &= \eta_z - \gamma^n\beta_n\eta_1 \\
\dot{\eta}_z &= h(x, w) - \gamma^{n+1}\beta_{n+1}\eta_1.
\end{aligned} \tag{4.28}$$

Let $\epsilon_j = \frac{\eta_j}{\gamma^{j-1}}$ for $j = 1, 2, \cdots, n, z$. Then (4.28) can be rewritten as

$$\dot{\epsilon} = \gamma A\epsilon + B\frac{h(x,w)}{\gamma^n} \tag{4.29}$$

where

$$A = \begin{pmatrix} -\beta_1 & 1 & 0 & \cdots & 0 \\ -\beta_2 & 0 & 1 & \cdots & 0 \\ \vdots & \vdots & \ddots & \vdots & \vdots \\ -\beta_n & 0 & \cdots & 0 & 1 \\ -\beta_{n+1} & 0 & \cdots & 0 & 0 \end{pmatrix} \text{ and } B = \begin{pmatrix} 0 \\ 0 \\ \vdots \\ 0 \\ 1 \end{pmatrix}.$$

The matrix A is Hurwitz if β_j are chosen according to the above mentioned criteria. The stability of (4.29) implies the convergence of $\hat{f} \to f$. The following theorem was proposed by [85] on the boundedness of η_j.

Theorem 4.1 *Assuming $h(x,w)$ bounded, there exists a finite time $T > 0$, such that $|\eta_j(t)| \leq O(\frac{1}{\gamma^k}), j = 1, 2, \cdots, n, z, \forall t \geq T > 0$ with $\gamma, k > 0$*

Proof. The proof is given in [85]. ∎

The Theorem 4.1 states that the η_j will converge to a ball, centered around the origin, with a radius proportional to $\frac{1}{\gamma^k}$ where γ is the observer bandwidth. So we can conclude, the higher observer bandwidth will result in better convergence of the LESO.

The control objective here is to make the output of the system (4.23) follow a given and bounded reference y_r, and its derivative $\dot{y}_r, \ddot{y}_r, \cdots, y_r^{(n)}$ are also bounded. Employing the LESO (4.25) to the system (4.24), the ADRC control law is given as

$$u = \frac{k_1(y_r - \hat{x}_1) + k_2(\dot{y}_r - \hat{x}_2) + \cdots + k_n(y_r^{(n-1)} - \hat{x}_n) - \hat{z} + y_r^{(n)}}{b} \tag{4.30}$$

where $k_j, j = 1, 2, \cdots, n$ are the controller gain parameters selected such that the characteristic polynomial

$$\Delta(\lambda) = \lambda^n + k_n\lambda^{n-1} + \cdots + k_1$$

is Hurwitz. The closed loop dynamics of the system will become

$$y^n(t) = (f - \hat{z}) + k_1(y_r - \hat{x}_1) + k_2(\dot{y}_r - \hat{x}_2) + \cdots + k_n(y_r^{(n-1)} - \hat{x}_n) + y_r^{(n)}. \quad (4.31)$$

From (4.31) it can be seen that a properly designed LESO will eliminate the the first time in the RHS and the rest of the terms constitute a generalized PD control structure with a feedforward term. It has been shown in [85] that with the ADRC control law (4.30) and LESO (4.25) the closed loop system is stable. Furthermore the tracking error is bounded and converges to the ball centered at the origin.

4.3.2 Controller Design

For the ADRC control design, we need to represent the system in the extended state space form of $n + 1$ order where n is order of the original system. The additional state variable represents the total disturbance of the system consisting both intrinsic and extrinsic uncertainties and nonlinearities. The second step is to design a LESO to estimate the extended state. Finally a control is determined which consists of two components, first compensates for the total disturbance of the system, and second assigns the desired behaviour. Before presenting the control design, we assume the following set assumptions to be true for the given system:

Assumptions:

- The rotor speed, Ω, and rotor flux, ϕ_d^r of the machine are accurately measurable.

- The references Ω^* and ϕ_d^{r*} are bounded.

For the Flux control, we used feedforward compensation with PI inner loop as explained in section 3.2.1. The ADRC is used for the speed loop dynamics, (2.29) and (2.33). We recall the rotor speed dynamics of the machine,

$$\frac{d\Omega}{dt} = m\,\phi_d^r\,i_q^s - c\,\Omega - \frac{1}{J_m}\,T_l \tag{4.32}$$

$$\frac{di_q}{dt} = -\gamma\,i_q^s - b\,p\,\Omega\,\phi_d^r - p\,\Omega\,i_d^s - a\,\frac{M_{sr}}{\phi_d^r}\,i_d^s\,i_q^s + m_1\,v_q^s + \xi \tag{4.33}$$

where T_l and ξ are the external disturbances to the dynamics. For the extended state representation, we define the variables $x_1 = \Omega$ and $x_2 = \dot{\Omega}$. The speed dynamics can be rewritten in terms of x_1 and x_2 as:

$$\dot{x}_1 = x_2 \tag{4.34}$$

$$\dot{x}_2 = f + bu, \tag{4.35}$$

where

$$f = m\,\phi_d^r\Big(-\gamma\,i_q^s - b\,p\,x_1\,\phi_d^r - p\,x_1\,i_d^s - a\,\frac{M_{sr}}{\phi_d^r}\,i_d^s\,i_q^s + \xi\Big) + m\,\big(-a\,\phi_d^r + a\,M_{sr}\,i_d^s\big)\,i_q^s - c\,x_2 - \frac{1}{J_m}\,T_l, \tag{4.36}$$

$$b = mm_1\phi_d^r, \qquad u = v_q^s.$$

It can be seen that the function f contains all the nonlinearities and external disturbances of the system. This f is considered as *total disturbance* of the system and will be

estimated and compensated. It is worthy to note that, both the external uncertainties i.e., T_l and ξ are consolidated in the total disturbance. The function f is also differentiable over the domain expect $\phi_d^r = 0$. Finally, defining a new state variable $x_3 = f$, the extended state space model of the rotor speed dynamics of the machine are

$$\begin{aligned} \dot{x}_1 &= x_2 \\ \dot{x}_2 &= x_3 + bu, \\ \dot{x}_3 &= h, \end{aligned} \tag{4.37}$$

where $h = \dot{f}$. According to ADRC, we need to design an LESO to estimate the *total disturbance* i.e., x_3. The following LESO is presented for the estimation:

$$\begin{aligned} \dot{\hat{x}}_1 &= \hat{x}_2 + l_1(x_1 - \hat{x}_1) \\ \dot{\hat{x}}_2 &= \hat{x}_3 + l_2(x_1 - \hat{x}_1) + bu \\ \dot{\hat{x}}_3 &= l_3(x_1 - \hat{x}_1) \end{aligned} \tag{4.38}$$

where $\hat{x}_1$, $\hat{x}_2$ and $\hat{x}_3$ are the estimated states of the system (4.37) and $l_j, j = 1, 2, 3$ are the observer gains. Considering the observer gains as;

$$[l_1, l_2, l_3] = [\gamma\beta_1, \gamma^2\beta_2, \gamma^3\beta_3].$$

With $\gamma > 0$ is the observer bandwidth, we need to choose $\beta_j, j = 1, 2, 3$ such that the characteristic polynomial

$$\Delta(\lambda) = \lambda^3 + \beta_1\lambda^2 + \beta_2\lambda + \beta_3 \tag{4.39}$$

is Hurwitz. With appropriate selection of the observer gains the $\hat{x}_3 \to x_3$ i.e., $\hat{x}_3 \to f$. An appropriately designed LESO will give the estimation of the total disturbance of the system. Assuming Ω^* be the reference and using the estimation of the total disturbance, the ADRC control law is written as,

$$u = \frac{1}{b}\Big[k_1(\Omega^* - \hat{x}_1) + k_2(\dot{\Omega}^* - \hat{x}_2) - \hat{x}_3 + \ddot{\Omega}^*\Big], \tag{4.40}$$

where k_1 and k_2 are the controller gain parameters chosen such that the characteristic polynomial

$$\Delta(\lambda) = \lambda^2 + k_1\lambda + k_2 \tag{4.41}$$

is Hurwitz. The control law (4.40) makes the rotor speed, Ω, converge to Ω^*. Moreover, according to [85] the tracking errors are bounded.

Remark 5 *Note that, both LESO and ADRC control,* (4.38) *and* (4.40)*, are linear and does not depend on the nonlinear structure of the original system. This characteristic suggests the robustness of the control technique toward unmodeled dynamics of the system.*

4.3.3 Numerical Simulations

To investigate the performance of the ADRC technique, the system (2.29)−(2.33) is simulated in MATLAB/Simulink using the user-defined S-Function. We used Fixed Step solver with the time step of 10^{-5} in the simulation settings. The machine parameters of Table 3.1 are used. The speed and flux references are taken as, $\Omega^* = 500$ and $\phi_d^{r*} = 0.261$. The parameters of the LESO and ADRC control law are selected by trial and error, and satisfying the hurwitz condition of (4.39) and (4.41), to get the best

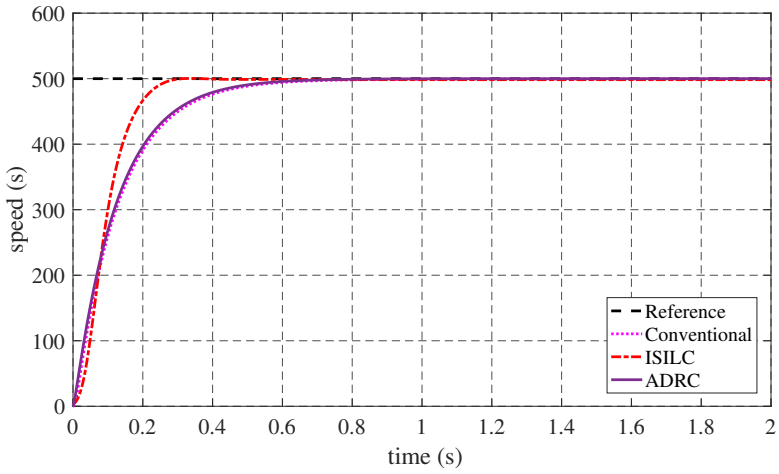

Figure 4.17: Rotor speed trajectory under ADRC control

response as:

$$\gamma = 1000, \quad \beta_1 = \beta_2 = 3, \quad \beta_3 = 1,$$
$$k_1 = 150000, \quad k_2 = 17000. \tag{4.42}$$

The roots of the characteristic polynomial (4.39) for the chosen values of $\beta_j, j = 1, 2, 3$ are places at -1. For the chosen set of parameters, the poles of the LESO are placed at -1000. The chosen values of k_1 and k_2 satisfies the condition on the characteristic polynomial (4.41). The roots of the controller are placed at -150000 and -0.1133. The gains of the LESO and ADRC are chosen by trail and error to get the best response of the system. Here it should be noted that the ADRC requires high gains for a good performance.

Figure 4.17 shows the trajectory of the rotor speed in comparison with other control techniques investigated in this work. No overshoot and steady state errors are observed in the response. The settling time of the speed is $579ms$ which is 8% better than that of Conventional technique. On the other hand, the response is 216% greater than that of ISILC respectively. Figure 4.18 shows the response of the flux loop. ϕ_d^r settles in $91ms$. An overshoot of 3.3% is also observed. We kept the flux loop control same as

the conventional one for simplicity.

Figure 4.19 shows the trajectory of the $d-q$ stator current. The q-axis current controls the speed of the machine is bounded and free from chattering. However, a large initial current can be seen at the q-axis. The speed loop in ADRC scheme is a signal loop technique unlike the conventional scheme which uses a cascaded loop structure. In ADRC we do not need the measurement of the current, however the measurement of control voltage is required by the LESO to estimate the total disturbance of the system. Figure 4.20 shows the $d-q$ axis control voltages generated by the scheme. It can be noted that the ADRC generated a large amount of control input during transient state which is well beyond the physical limits of the machine. It is due to the high values of k_1 and k_2 needed to eliminate the steady state error, as explained in section 4.3.1. The high value of the control input i.e., $1300V$ exceeds the maximum input voltage, $220V$. To take care of this problem, we proposed a modification in gain selection to a give soft-start to the algorithm.

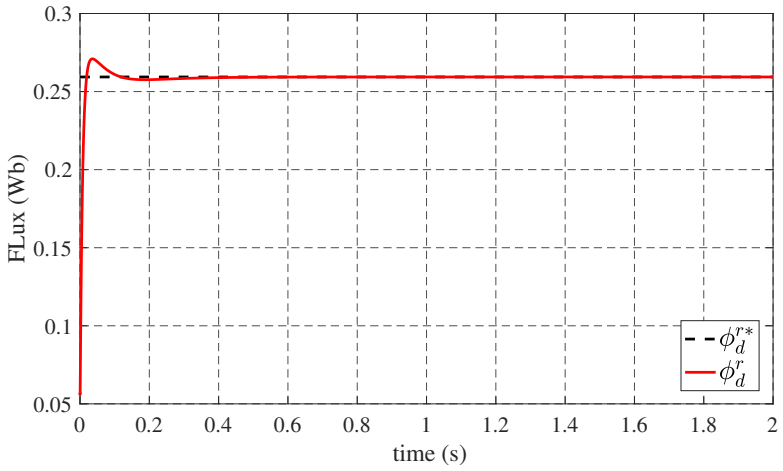

Figure 4.18: Rotor flux trajectory under ADRC control

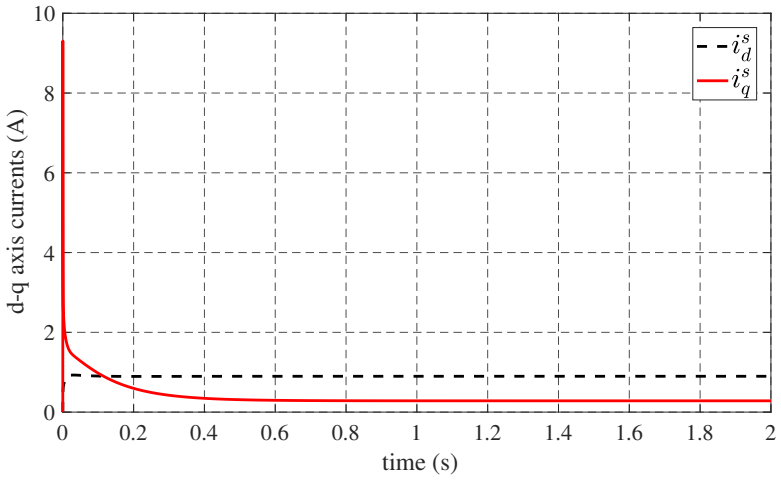

Figure 4.19: d-q axis stator current under ADRC control

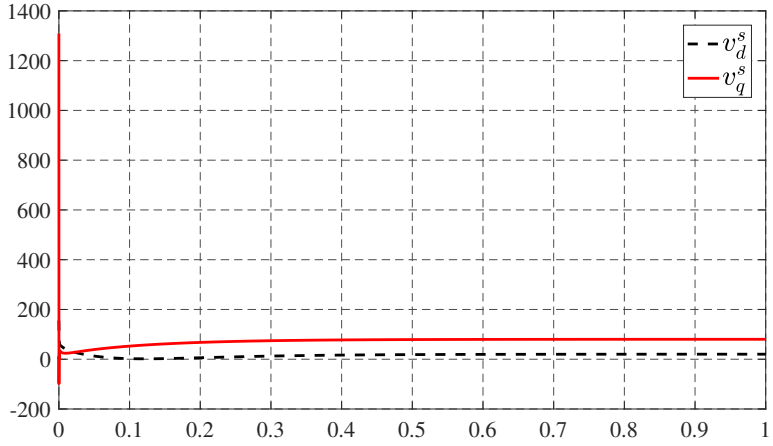

Figure 4.20: d-qaxis stator voltage under ADRC control

Soft-start Scheme

To eliminate the issue of high control input during the transient state we propose the following time-varying structure of the control gains:

$$k_j(t) = \begin{cases} \alpha_j t, & \text{if } k_j(t) < \alpha_j^{max} \\ \alpha_j^{max}, & \text{if } \alpha_j(t) \geq \alpha_j^{max}, \end{cases} \tag{4.43}$$

where $j = 1, 2$, α_j is some positive constant and α_j^{max} is the minimum value of the gain

required to eliminate the steady state error. The soft-start gain parameters are selected by trial and error, satisfying the hurwitz condition for $s + \alpha_j t$ and $s + \alpha_j^{max}$, to get the best response as:

$$\begin{aligned} \alpha_1 &= 2600000, \quad \alpha_1^{max} = 260000, \\ \alpha_2 &= 250000, \quad \alpha_2^{max} = 25000. \end{aligned} \tag{4.44}$$

Figure 4.21 shows the $k_1(t)$ and $k_2(t)$. It can be noted that the gains have a lower value during the transient state. Figures 4.22 and 4.23 show the new i_q^s and v_q respectively generated by the control law (4.30) with control gains selected as 4.43. The

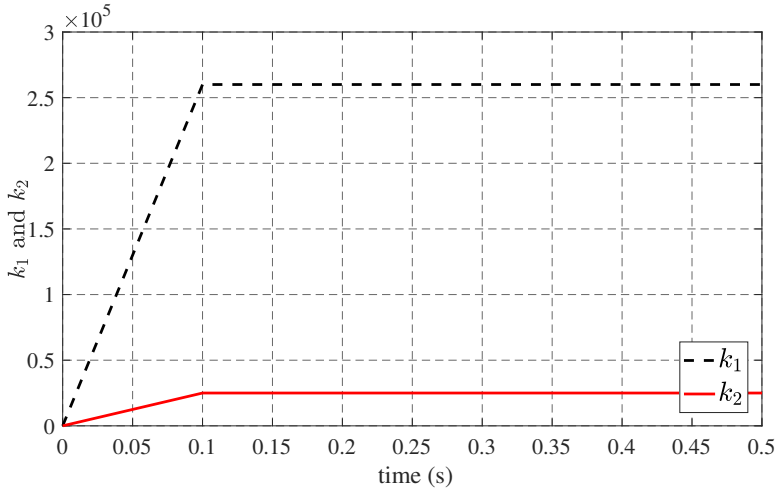

Figure 4.21: Proposed time-varying structure of ADRC controller gains

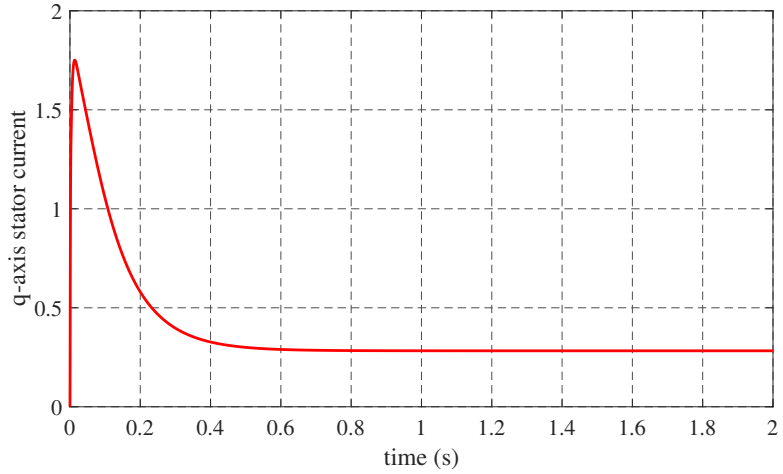

Figure 4.22: q-axis stator with Soft-Start technique

proposed soft-start scheme effectively suppressed the initial voltage spike. Figure 4.24 shows the new system response. Moreover, the settling time of the system is also improved to 497ms from 579ms.

External Disturbance

The load torque, T_l, is modelled as an external disturbance to the system. The external perturbation is simulated for a medium speed range operation. Once the machine reached its reference speed i.e., 500 RPM, at $t = 3s$ a load torque of 500 mN.m is applied on the machine. Figure 4.25 shows the response of the ADRC scheme in comparison with other techniques presented in this thesis. The rotor speed drops to 467 RPM, and recovers to the reference value in 73ms. The recovery time is 98% less than the that of the conventional scheme. The ADRC scheme shows a strong performance against external disturbance.

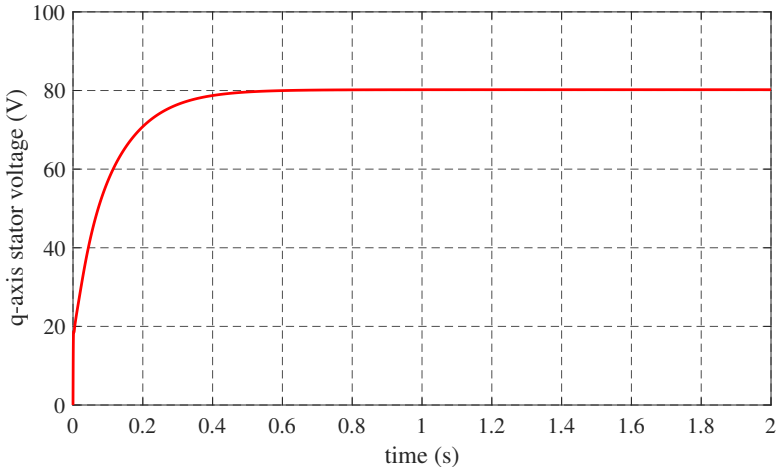

Figure 4.23: q-axis stator voltage under Soft-start ADRC

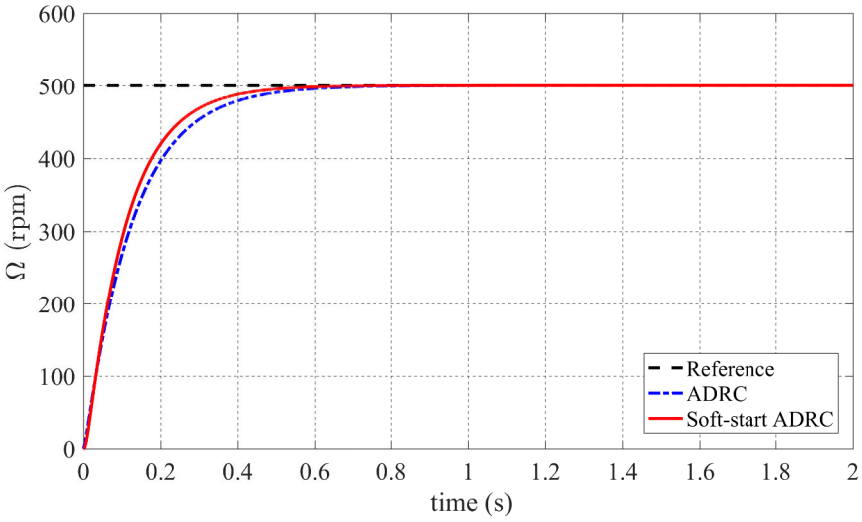

Figure 4.24: Rotor speed under Soft-start ADRC

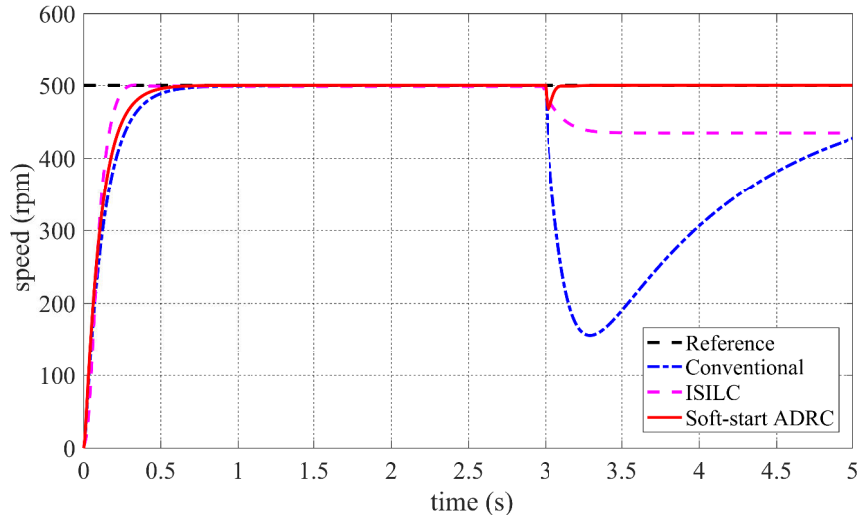

Figure 4.25: Rotor speed with external disturbance

Internal Disturbance

The robustness of the ADRC is also investigated for the internal model uncertainties. The system is simulated with the same set of gains for the parameter variation of rotor resistance, i.e., R_r. The value of R_r were perturbed upto 100% of the base value. Figure 4.26 shows the trajectory of the rotor speed when the mentioned parameter was changed. The overall system remains stable, and performance remained almost the

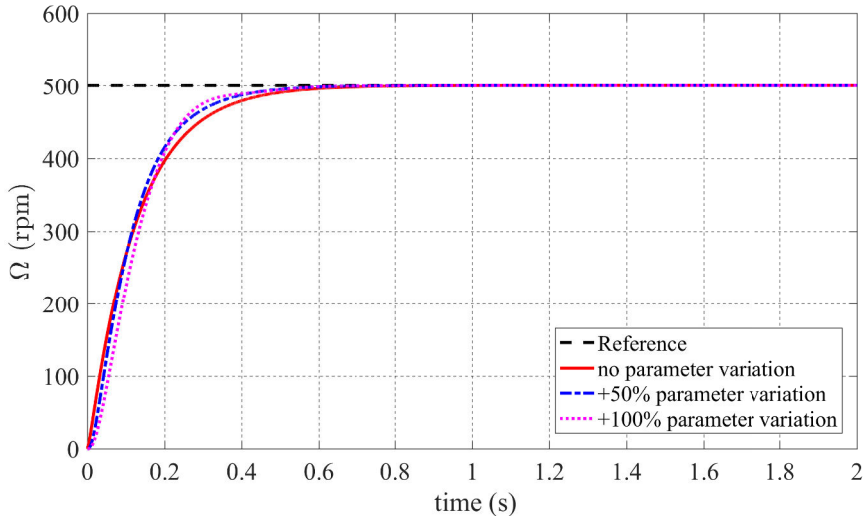

Figure 4.26: Rotor speed with internal disturbance

same. The settling time changed from 579ms to 507ms and 512ms on 50% and 100% variation. Resulting in the mere change of 12% and 11.5% respectively. The percentage change is low as compared to the conventional and ISILC scheme. This shows the superior performance of ADRC in terms of robustness against external and internal uncertainties.

4.4 Summary

This chapter consists the main contribution of this thesis. We proposed an Inter-sample Iterative control scheme, which is a $2-D$ control scheme based on an iterative process between two-time samples. It is modified version of the conventional ILC which is used for the repetitive processes. We have shown the effectiveness of this technique through numerical simulations and the experimental results. The rotor speed of the machine converges to the provided reference in a considerable short period as compared to the Conventional technique. However, the technique does not perform well against

external and internal disturbances. The second technique which we presented is Active Disturbance Rejection Control. It is a robust, linear and based on active linearization of the system. The technique is based on the Extended state Observer is extremely robust against exogenous and endogenous disturbances. The control law and the observer do not need precise information about the parameters and dynamics of the system. The original ADRC scheme requires high controller gains to remove the steady-state error, but high gains generate large control input during the initial transient state when the error is large. We proposed a soft-start scheme to resolve the issue. As a result, the performance of the system enhances while keeping the robustness properties intact. However, the settling time of the ADRC is higher than that of the ISILC.

In conclusion, we can remark that the ISILC is better regarding convergence and

Table 4.2: Performance comparison of different control techniques in simulation

Disturbance	Parameter	Conventional	ISILC	ADRC
No Disturbance	Settling time	630ms	268ms	579ms
	Overshoot	No	No	No
	Steady State Error	No	No	No
Ext. Disturbance	Settling time	4.4s	243ms	73ms
	Overshoot	No	No	No
	Steady State Error	No	12.8%	No
Int. Disturbance	Settling time	2.7s	2.1s	512ms
	Overshoot	4.4%	48%	No
	Steady State Error	No	No	No

Table 4.3: Performance comparison of different control techniques in real-time

Type	Parameter	Conventional	ISILC
Experimetal	Settling time	657ms	319ms
	Overshoot	1.16%	No
	Steady State Error	No	No
Simulation	Settling time	630ms	268ms
	Overshoot	No	No
	Steady State Error	No	No

ADRC is more robust against endogenous and exogenous disturbances.The results of the control schemes are compared in Tables 4.2 and 4.3. Both schemes can be mixed to construct a hybrid control law to address the shortcomings of each control algorithm.

CHAPTER 5

ROBUST TRACTION CONTROL OF ELECTRIC VEHICLES

5.1 Introduction

In this chapter, we are solving the traction control problem for the class of Electric Vehicles (EVs) that use induction motor for propulsion. Usage of Induction motor for such application is a very recent development. Previously, DC motors and Permanent magnet synchronous motors were used. There are two main contributions of this work: 1) We have considered the nonlinear dynamics of the actuator, i.e. induction motor, in control design which is ignored in the previous studies, 2) We have considered uncertainties in the parameters of the vehicle and friction coefficient simultaneously. We propose the Linear Active Disturbance Rejection Control (LADRC) for the slip-ratio tracking under the stated conditions.

5.2 Background

In recent times, EVs are gaining much attention because they emit zero emissions during operation. Moreover, with a charging station powered from renewable sources can be a promising and a viable solution to many environmental problems. Technological advancements in electric propulsion and battery management systems offered numerous advantages over the internal combustion engine (ICE), and this advancement paved the way for the market growth of this technology. Similar to the ICE based vehicles, safety and stability are the essential factors for EVs. Thus, the active safety technologies like anti-lock braking system (ABS), traction control (TC) and yaw stabilization also have to be studied and implemented in EVs. Since EVs use an electric motor instead of ICE for propulsion, therefore the dynamics and control of both the vehicles are much different [100]. In this work, we are studying the TC problem for the class of EVs which use the induction motor as a primary actuator for propulsion. TC, by definition, is a system that prevents the skidding of wheels during driving to achieve the optimal tractive force during acceleration, braking and take-off to maintain the longitudinal stability of the vehicle [101].

The traction control for ICE based vehicles is achieved by adjusting the engine output torque, using throttle position or ignition timing, and regulating the braking torque acting on the driving wheels using friction brakes as an actuator. On the other hand, the TC for the EVs can be achieved by only adjusting the motor current. As a result, the response time for the actuator is much faster and efficient than its counterpart. The external friction brakes can also be eliminated in EVs making the implementation much simpler. Current studies on the traction control are focused on the wheel slip-ratio control. The slip-ratio (λ) controls the tractive force of the vehicle and has a nonlinear

relation with the friction coefficient. PID, fuzzy logic, sliding mode and optimal control schemes has been proposed for ICE based vehicles [102–107]. An optimal TC algorithm based on feedback linearization was presented in [108] to maintain the maximum tractive force between the tyre and the road surface. However, the algorithm requires precise information about the parameters of the system. Inherently, the parameters of an EV are uncertain and time-varying. For instance, the mass of the car will depend on the number of passengers and the amount of fuel present in the tank. These parameters can also change on the go. Similarly, the relation between the tractive force and the wheel slip ratio is nonlinear and uncertain due to uncertain road conditions. To address this uncertain nature of the model, adaptive control schemes were proposed in the literature. A tractive force estimation algorithm based on gradient descent was presented in [109] to online update $\mu - \lambda$ curve. Another estimation based algorithm for adhesive coefficient based on the real-time sensory data was proposed in [110]. A super-twisting sliding mode controller (STA-SMC) was proposed by [111] with nonlinear tractive force observer. A model predictive control based strategy was presented in [112] without considering the model uncertainties. For more references and details on different implementation architectures of traction control for electric vehicles, the reader is referred to the survey paper [101].

We are proposing LADRC for the said application. LADRC is a robust control algorithm that does not requires precise information of the system. Unlike [111], the control law we propose is continuous and does not need the exact information about the parameters of the vehicle. The STA-SMC is effective against the model uncertainties. However, the control input generated by the algorithm, for this application, posses chattering. Chattering in the control input will induce harmonics in the stator current

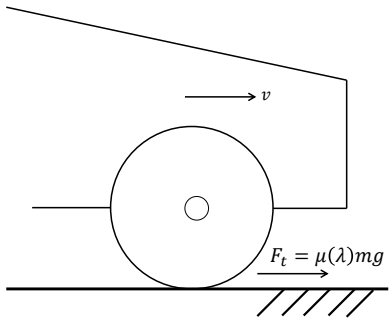

Figure 5.1: Tractive force between tyre and road surface

of the machine which will increase the losses and reduces the machine life. Studies have proposed algorithms to handle the uncertainties in road conditions [22, 109] but neglected the uncertainties of the vehicle model. In this work, we have considered uncertainties in both: vehicle parameters and the road conditions.

5.3 Traction Control

Traction control is an active vehicle safety feature designed to help vehicles make effective use of all the traction available on the road when accelerating or decelerating on low-friction road surfaces. When a vehicle without traction control attempts to accelerate/decelerate on a slippery surface like ice, snow, or wet asphalt, the wheels are liable to slip. The result of wheel slip is that the tires spin quickly on the surface of the road without gaining any actual grip, so the vehicle does not accelerate/decelerate. Traction control activates when it senses that the wheels may slip, helping drivers make the most of the traction that is available on the road surface. However, it is important to note that traction control cannot create traction where there is none. On a truly frictionless surface (e.g., ice), vehicles with traction control would perform just as poorly as vehicles without it.

The vehicle moves on the surface of the road due to a tractive force, F_t exerted by

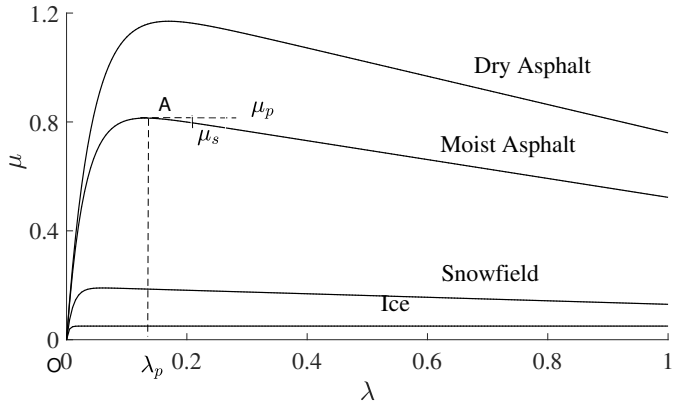

Figure 5.2: $\mu - \lambda$ curve for adhesive coefficient

the tyre on the road, shown in figure 5.1. This tractive force, or traction, depends on the surface conditions. The maximum available traction is different for different surfaces. For instance, a dry asphalt road provides higher traction than a wet asphalt or a snowfield. This means that the value for the maximum achievable acceleration/deceleration will be higher for the dry asphalt than the others. If the engine/electic motor exerts a higher tractive force than the maximum tractive force available at the surface, the wheels will slip and thus affect the stability of the vehicle. Experimental studies have shown that the tractive force of vehicle can be represented as [113]

$$F_t = \mu(\lambda) mg, \tag{5.1}$$

where m is the mass of the vehicle and g is the gravitational acceleration. The $\mu(\lambda)$ is the adhesive coefficient with represents the adhesion of the vehicle type to the road. It is a nonlinear function of the wheel slip-ratio, λ, of the wheel. Figure 5.2 shows $\mu - \lambda$ relation. The relation can be fairly approximated with a nonlinear relation [114],

$$\bar{\mu}(\lambda) = \frac{2\mu_p \lambda_p \lambda}{\lambda_p^2 + \lambda^2} \tag{5.2}$$

where μ_p is the point of maximum adhesion between the tyre and the road corresponding to the slip-ratio λ_p. The μ_s is the sliding value of coefficient. It the point when the wheel of the vehicle actually starts slipping on the road. Section OA of the plot 5.2 represents the difference between the wheel and the vehicle velocity which occurs due to the elasticity of the tyre and not the actually slipping. The actual slipping of the wheel starts from μ_p. The wheel slip-ratio λ is defined as,

$$\lambda = \frac{\omega_w - \omega_v}{\max(\omega_w, \omega_v)}$$

where ω_w and ω_v are the radial angular velocities of the wheel and the vehicle.

The objective of the traction control of the vehicle is to maintain the λ of the vehicle to λ_p, the point of maximum adhesion, during hard acceleration/deceleration of the vehicle by regulating the input torque to the wheel or friction brakes.

5.4 Mathematical Model

The control objective of this work is to ensure the convergence of the vehicle's wheel slip ratio , λ, to some reference λ^*. In this section, we present the combined uncertain mathematical model for the wheel slip ratio including the nonlinear dynamics of the induction motor. The slip ratio model is derived from the vehicle longitudinal dynamics and the dynamics of the induction motor which are presented in the subsequent subsections.

5.4.1 Vehicle Longitudinal Dynamics

Suppose an electric vehicle of an uncertain mass $\bar{m}$ is moving with a linear velocity v and its front right wheel is rotating at an angular velocity of ω_w. The wheel of the vehicle is applying a tractive force f_t on the road for the movement, and approximately known gravitational acceleration $\bar{g}$ is acting on the vehicle. Then the uncertain dynamics of the angular motion of the wheel and the linear motion of the vehicle are described as [111]:

$$\bar{m}\dot{v} = \bar{\mu}(\lambda)\bar{m}\bar{g} - \bar{f}_r\bar{m}\bar{g} - \bar{c}_a v^2 \tag{5.3}$$

$$J\dot{\omega}_w = \tau_m - r_w\bar{\mu}(\lambda)\bar{m}\bar{g}, \tag{5.4}$$

where J is the wheel moment of inertia, $\bar{f}_r$ and $\bar{c}_a$ are the uncertain coefficient of rolling resistance and aerodynamic drag respectively. τ_m represents the motor input torque to the wheel and r_w is the wheel radius. The free body diagram of the quarter vehicle while braking is presented in Figure 5.3. The term $\bar{f}_r\bar{m}\bar{g}$ represents the uncertain rolling resistance on the tyre [113]. The tyre is considered as a nonrigid body that can be deformed. The rolling resistance is caused due to asymmetric distribution of the normal reaction forces acting against the tyre of the vehicle. The pressure in the leading half of the tyre becomes greater than the trailing half, thus shifting the normal

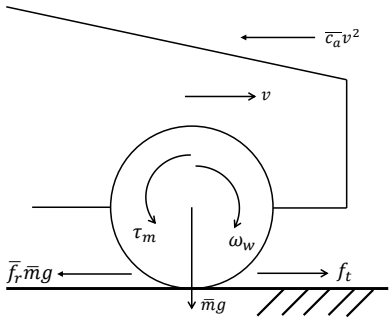

Figure 5.3: Vehicle longitudinal dynamics

reaction force from the center towards the leading half. This shift of normal reaction force produces a torque on the wheel, the force is represented as $f_r mg$. $\bar{\mu}(\lambda)$ is the uncertain adhesive coefficient which depends on the wheel and the road conditions. A typical $\mu - \lambda$ curve is shown in Figure 5.2. The curve can be fairly approximated by the nonlinear relation [114],

$$\bar{\mu}(\lambda) = \frac{2\mu_p \lambda_p \lambda}{\lambda_p^2 + \lambda^2} \tag{5.5}$$

where μ_p is the optimal adhesive coefficient and λ_p is the optimal slip ratio. We have used (5.5) in our numerical simulations. The parameters $\bar{m}$, $\bar{f}_r$, $\bar{c}_a$ and $\bar{\mu}(\lambda)$ are considered as uncertain and bounded.

5.4.2 Current-Fed Induction Motor

The wheel of the vehicle in directly driven by a three-phase induction motor via reduction gear [101]. Figure 5.4 shows the coupling of the in-wheel motor with the wheel. The torque of the induction motor in rotor flux aligned rotating $d - q$ frame is given as [25]

$$\tau_m = \frac{3p\, G_r L_m}{2L_r} \phi_d i_q, \tag{5.6}$$

where p is the number of pole pairs of the machine, G_r is the reduction gear ratio of the coupling, L_m is the mutual inductance, L_r is the rotor inductance, ϕ_d is the d axis rotor flux established inside the machine and i_d, i_q are the d and q-axis stator currents which are considered as the inputs to the motor. The dynamics of the flux of the machine are

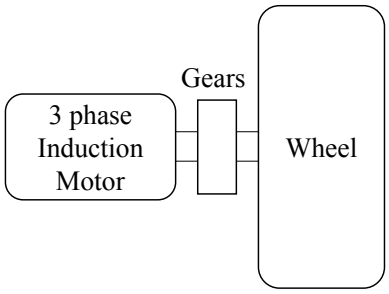

Figure 5.4: Induction Motor coupling with the wheel

given as [25]

$$\dot{\phi}_d = \frac{R_r L_m}{L_r} i_d - \frac{R_r}{L_r} \phi_d \tag{5.7}$$

$$\dot{\rho} = \frac{p\,\omega_w}{G_r} + \frac{R_r L_m}{L_r \phi_d} i_q \tag{5.8}$$

where ρ is the angle of synchronous rotating frame, and R_r is the rotor resistance. The torque of the motor depends on both: the input current, and the flux. In order to control the torque of the machine, we need to control the flux as well as the q axis current, i_q. In this work it is assumed that all the parameters of the motor are constant and known.

5.4.3 Vehicle Slip-ratio Model

The control objective of this work is to control the slip ratio λ of the vehicle using the input currents i_d and i_q of the motor. The slip ratio is defined as

$$\lambda = \frac{\omega_w - \omega_v}{\max(\omega_w, \omega_v)} \tag{5.9}$$

where ω_v is the angular velocity of the vehicle.

Remark 6 *It can be observed from* (5.9) *that a free moving wheel, where* $\omega_w = \omega_v$*, is*

described by $\lambda = 0$*, whereas a locked wheel can be described by* $\lambda = -1$ *when* $\omega_w = 0$*. The value of* λ *ranges between* -1 *and* 1*.*

The angular velocity of the vehicle is defined as

$$v = r_w \omega_v. \tag{5.10}$$

Substituting (5.10) into (5.3) will yield

$$\dot{\omega}_v = \frac{\bar{g}}{r_w}\bar{\mu}(\lambda) - \frac{\bar{f}_r \bar{g}}{r_w} - \frac{\bar{c}_a r_w}{\bar{m}}\omega_v^2. \tag{5.11}$$

Substituting (5.6) into (5.4),

$$\dot{\omega}_w = \frac{3p\, G_r L_m}{2J\, L_r}\phi_d i_q - \frac{r_w \bar{m} \bar{g}}{J}\bar{\mu}(\lambda). \tag{5.12}$$

For simplicity we will consider only 1^{st} quadrant operation of the longitudinal dynamics, (5.11) and (5.12), where both ω_w and ω_v are always positive. At lower speed, i.e. $v < 10Kmph$, the wheel slip is not of great concern. We will design the slip ratio control for speed $v > 10Kmph$ where the singularity doesn't occur.

Deceleration

For the case of deceleration where $\omega_w < \omega_v$, the slip ratio will be

$$\lambda = \frac{\omega_w - \omega_v}{\omega_v}. \tag{5.13}$$

Differentiating (5.13) with respect to time will yield

$$\dot{\lambda}\omega_v + \lambda\dot{\omega}_v = \dot{\omega}_w - \dot{\omega}_v. \tag{5.14}$$

Substituting (5.11) and (5.12) into (5.14) will give the uncertain slip ratio dynamics of the vehicle during deceleration. Therefore the complete uncertain slip ratio model of an EV, while decelerating, including the actuator dynamics is given as

$$\dot{\lambda} = f_b(\lambda, \omega_w, \omega_v) + \frac{b}{\omega_v}\phi_d i_q \tag{5.15}$$

$$\dot{\phi}_d = -\frac{R_r}{L_r}\,\phi_d + \frac{R_r L_m}{L_r}\,i_d \tag{5.16}$$

$$\dot{\rho} = \frac{p\,\omega_w}{G_r} + \frac{R_r L_m}{L_r \phi_d} i_q \tag{5.17}$$

where

$$f_b(\lambda, \omega_w, \omega_v) = \frac{1}{\omega_v}\big(k_1 - k_2 - k_2\lambda\big)\bar{\mu}(\lambda) - \Big(k_3\omega_v - \frac{k_4}{\omega_v}\Big)\lambda - k_3\omega_v - \frac{k_4}{\omega_v},$$

and

$$k_1 = -\frac{r_w}{J}\bar{m}\bar{g}; \quad k_2 = \frac{\bar{g}}{r_w}; \quad k_3 = -\frac{\bar{c}_a r_w}{\bar{m}}; \quad k_4 = -\frac{\bar{f}_r\bar{g}}{r_w};$$
$$b = \frac{3p\,G_r L_m}{2J\,L_r}.$$

$f_b(\lambda, \omega_w, \omega_v)$ is the nonlinear and uncertain part of the model.

Acceleration

For the case of acceleration when $\omega_w > \omega_v$ the slip ratio will be

$$\lambda = \frac{\omega_w - \omega_v}{\omega_w}. \tag{5.18}$$

Differentiating (5.18) with respect to time and substituting (5.11) and (5.12) in the resultant will yield the uncertain slip ratio dynamics of the vehicle for the case of acceleration. Therefore, (5.16), (5.17) and (5.19) represents the complete slip ratio model for an accelerating EV with actuator dynamics.

$$\dot{\lambda} = f_a(\lambda, \omega_w, \omega_v) + \big(1 - \lambda\big)\frac{b}{\omega_w}\phi_d i_q, \tag{5.19}$$

where

$$f_a(\lambda, \omega_w, \omega_v) = \frac{1}{\omega_w}\big(k_1 - k_2 - k_1\lambda\big)\mu(\lambda) - \frac{k_3\omega_v^2}{\omega_w} - \frac{k_4}{\omega_w}.$$

$f_a(\lambda, \omega_w, \omega_v)$ is the nonlinear and uncertain part of the model.

Remark 7 *The d and q axis stator currents, i_d and i_q, are the control inputs of the slip ratio dynamics,* (5.15)−(5.17) *and* (5.19)*.*

Remark 8 *The slip ratio dynamics for both deceleration and acceleration,* (5.15) *and* (5.19)*, are highly nonlinear and time-varying.*

Remark 9 *In* (5.15) *and* (5.19)*, ω_w and ω_v are considered as time-varying known parameters.*

5.5 Controller Design

In this section, we present the proposed control scheme under the following assumptions.

Assumptions:

1. The stator currents of the IM are measurable, and all the machine parameters are known and constant.

2. The reference trajectory for the slip ratio, λ^*, is smooth and bounded.

3. The motor is operated under the base speed for all the time in the constant torque region.

4. The uncertain parameters of the model (5.15) and (5.19) are bounded.

Under these assumptions, the control problem is to design a robust traction controller which guarantees the convergence of the slip-ratio, λ, to a reference, λ^*, while maintaining the rotor flux, ϕ_d, to its rated value, ϕ_d^*. In the subsequent subsections, we present the details of the flux and slip ratio controller.

5.5.1 Flux Control

The dynamics of the flux of the motor are represented by (5.16). It can be noted that the dynamics are linear and stable, as $\frac{R_r}{L_r} > 0$. Considering i_d as the input to the dynamics, the objective of the flux control is to find an appropriate i_d^* that ensures the convergence of ϕ_d to some reference ϕ_d^* at steady state. The flux error, e_ϕ, is defined as

$$e_\phi = \phi_d - \phi_d^* \tag{5.20}$$

and its dynamics as,

$$\dot{e}_\phi = \dot{\phi}_d - \dot{\phi}_d^*. \tag{5.21}$$

Since we need to converge the flux to its constant rated value, therefore $\dot{\phi}_d^* = 0$. Substituting (5.16) into (5.21) will yield

$$\dot{e}_\phi = -\frac{R_r}{L_r}\,\phi_d + \frac{R_r L_m}{L_r}\,i_d. \tag{5.22}$$

Performing the steady state analysis on (5.22), where $\dot{e}_\phi = 0$. It is easy show that,

$$i_d^* = \frac{\phi_d^*}{L_m} \tag{5.23}$$

will make the tracking error, e_ϕ, zero at the steady-state. Eq. (5.23) will serve as the reference for the inner current loop of the d-axis. The inner loop control will make the true i_d of the machine converge to its reference, (5.23) to make the flux of the machine converge to its reference.

5.5.2 Linear Active Disturbance Rejection Control

For the slip ratio control, we propose the LADRC technique for robust tracking of the reference, λ^*. The LADRC approach is based on the concept of total disturbance estimation and rejection. The extended state model of $n+1$ order, where n is the order of the system to be controlled, is constructed. The extended state consists the nonlinear terms depending on the states and the parameters of the system including external disturbances and internal uncertainties present in the model. This extended state is termed as *total disturbance* of the system, and it is estimated through a LESO.

Unlike the conventional observers, LESO does not require the exact information of the mathematical model. It provides a robust estimation of the total disturbance of the system which makes it a powerful tool in the control design. Finally, a control law is determined which compensates for the *total disturbance* and assigns the desired behavior to the system. The complete control scheme is shown in Figure 5.5. We assume the flux is already established at its rated value, ϕ_d^*, which is a valid assumption because we assume the EV is already moving. This will transform (5.15) and (5.19) to

$$\dot{\lambda} = f_b(\lambda, \omega_w, \omega_v) + \frac{b}{\omega_v}\phi_d^* i_q \qquad \text{(for deceleration)} \tag{5.24}$$

$$\dot{\lambda} = f_a(\lambda, \omega_w, \omega_v) + \big(1-\lambda\big)\frac{b}{\omega_w}\phi_d^* i_q. \qquad \text{(for acceleration)} \tag{5.25}$$

The Eqs. (5.16) and (5.17) will be ignored, since the former is decoupled with (5.24) and (5.25) and latter is the electrical angle of the synchronous frame which keeps on increasing as the motor rotates. In the following subsections, we present the LADRC based design of i_q such that λ will converge to λ^* at steady state.

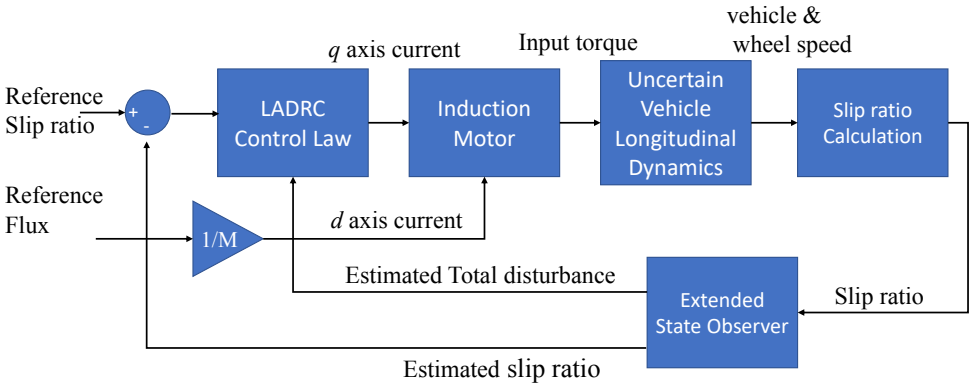

Figure 5.5: The LADRC control scheme

Deceleration

The extended state representation of (5.24) can be written as

$$\begin{aligned} \dot{\lambda} &= z_1 + \frac{b}{\omega_v}\phi_d^* i_q \\ \dot{z}_1 &= h_1(\lambda, \omega_w, \omega_v) \\ y &= \lambda, \end{aligned} \tag{5.26}$$

where $z_1 = f_b(\lambda, \omega_w, \omega_v)$ is the extended state and is considered as the total disturbance of the system. $h_1(\lambda, \omega_w, \omega_v)$ is the derivative of $f_b(\lambda, \omega_w, \omega_v)$ and y is the measurable output of the system. With i_q and y as input and output of the system, the LESO for (5.26) is given as

$$\begin{aligned} \dot{\hat{\lambda}} &= \hat{z}_1 + l_1\big(\lambda - \hat{\lambda}\big) + \frac{b}{\omega_v}\phi_d^* i_q \\ \dot{\hat{z}}_1 &= l_2\big(\lambda - \hat{\lambda}\big) \end{aligned} \tag{5.27}$$

where $\hat{\lambda}$ and $\hat{z}_1$ are the estimated states of the system (5.26) and l_1 and l_2 are the observer gains parameters to be chosen. The observer gains should be selected such that the characteristic polynomial $s^2 + l_1 s + l_2$ is Hurwitz [85]. For tuning simplicity, we assume both the observer poles are placed at $-\alpha$. It results in the characteristic polynomial of (5.27) to be

$$\lambda_{eso}\big(s\big) = s^2 + l_1 s + l_2 = \big(s + \alpha\big)^2 \tag{5.28}$$

where α is the observer bandwidth and $L = [l_1\,,\, l_2] = [2\alpha\,,\, \alpha^2]$.

Remark 10 *Generally, large observer bandwidth will lead to more accurate estimation. However, the large bandwidth will also increase the sensitivity to the noise. Therefore,*

a proper observer bandwidth should be selected in a compromise between the tracking performance and the noise tolerance.

Once the observer is designed and well tuned, it will accurately estimate $f_b(\lambda, \omega_w, \omega_v)$ which can be used to actively linearize (5.26). The LADRC control law for the system (5.26) is given as

$$i_q^* = \frac{\omega_v}{b\,\phi_d^*}\Big(\gamma_1(t)\big(\lambda^* - \hat{\lambda}\big) - \hat{z}_1 + \dot{\lambda}^*\Big) \tag{5.29}$$

where $\hat{z}_1$, i.e. $\hat{f}_b(\lambda, \omega_w, \omega_v)$, is the estimated total disturbance of the system and $\gamma_1(t)$ is the time-varying controller gain of the following structure

$$\gamma_1(t) = \begin{cases} \beta t, & \text{if } \gamma_1(t) < \gamma_1^{max} \\ \gamma_1^{max}, & \text{if } \gamma_1(t) \geq \gamma_1^{max}. \end{cases} \tag{5.30}$$

where $t \in [0, \infty[$ is the time and β is the parameter chosen such that $s + \beta t$ is Hurwitz $\forall t$. And γ_1^{max} is the maximum gain value assigned such that $s + \gamma_1^{max}$, Hurwitz. This time-varying gain strategy gives a soft start to the algorithm. Generally LADRC requires high value of gains for the best performance, but high gains exhibit *peaking phenomenon* which generates a high control input during the transient state which is not suitable in practical scenarios. A static γ_1 can also be used instead of $\gamma_1(t)$ for the deceleration case but it becomes necessary during acceleration. Performance comparison between static and dynamic gain is further discussed in Section 5.6.

The control law (5.29) will yield a closed loop system

$$\dot{\lambda} = \Big(f_b(\lambda, \omega_w, \omega_v) - \hat{f}_b(\lambda, \omega_w, \omega_v)\Big) + \gamma_1(t)\Big(\lambda^* - \hat{\lambda}\Big) + \dot{\lambda}^*. \tag{5.31}$$

Note that with a well designed LESO, the first term in the right hand side of (5.31) will be negligible and the rest of the terms constitutes a mere proportional controller with a feedforward gain. The simulation results for the presented control scheme are discussed in the upcoming section.

Acceleration

For the case of acceleration the system (5.25) can be written in the extended state representation as

$$\begin{aligned} \dot{\lambda} &= z_2 + \big(1-\lambda\big)\frac{b}{\omega_w}\phi_d^* i_q \\ \dot{z}_2 &= h_2(\lambda, \omega_w, \omega_v) \\ y &= \lambda, \end{aligned} \tag{5.32}$$

where $z_2 = f_a(\lambda, \omega_w, \omega_v)$ is the extended state and is considered as the total disturbance of the system. $h_2(\lambda, \omega_w, \omega_v)$ is the derivative of $f_a(\lambda, \omega_w, \omega_v)$. The LESO for the system (5.32) is given as

$$\begin{aligned} \dot{\hat{\lambda}} &= \hat{z}_2 + l_1\big(\lambda - \hat{\lambda}\big) + \big(1-\lambda\big)\frac{b}{\omega_w}\phi_d^* i_q \\ \dot{\hat{z}}_2 &= l_2\big(\lambda - \hat{\lambda}\big) \end{aligned} \tag{5.33}$$

where $\hat{\lambda}$ and $\hat{z}_2$ are the estimated states of the system (5.32) and l_1 and l_2 are the observer gains parameters to be chosen such that the characteristic polynomial $s^2 + l_1 s + l_2$ is Hurwitz. Let us consider the case where the gains are chosen as

$$\begin{bmatrix} l_1 & l_2 \end{bmatrix} = \begin{bmatrix} \omega_o \alpha_1 & \omega_o^2 \alpha_2 \end{bmatrix}. \tag{5.34}$$

where $\omega_o > 0$ is the observer bandwidth. Let $e_1^o = \lambda - \hat{\lambda}$ and $e_2^o = z_2 - \hat{z}_2$ be the observer errors. Then the error dynamics of the LESO (5.33) with the gains chosen as (5.34) can

be written as,

$$\begin{aligned} \dot{e}_1^o &= e_2^o - \omega_o \alpha_1 e_1^o \\ \dot{e}_2^o &= h_2(\lambda, \omega_w, \omega_v) - \omega_o^2 \alpha_2 e_1^o. \end{aligned} \tag{5.35}$$

Now let $\epsilon_1 = e_1^o$ and $\epsilon_2 = \frac{e_2^o}{\omega_o}$ and defining a vector $\epsilon = \begin{bmatrix} \epsilon_1 \\ \\ \epsilon_2 \end{bmatrix}$. The error dynamics, (5.35), can be rewritten in terms of ϵ as,

$$\epsilon = \omega_o A \epsilon + B \frac{h_2(\lambda, \omega_w, \omega_v)}{\omega_o}. \tag{5.36}$$

where

$$A = \begin{bmatrix} -\alpha_1 & 1 \\ \\ -\alpha_2 & 0 \end{bmatrix} \qquad B = \begin{bmatrix} 0 \\ \\ 1 \end{bmatrix}.$$

The parameters α_1 and α_2 need to be selected such that A is Hurwitz. In the following theorem, we will prove that the estimation error of the LESO (5.33) is bounded using the error dynamics (5.35).

Theorem 5.1 *Assuming $h_2(\lambda, \omega_w, \omega_v)$ is bounded, there exists a constant $\sigma_i > 0$ and a finite time $T > 0$ such that $|e_i^o| \leq \sigma_i$, $i = 1, 2$ $\forall t \geq T > 0$ and $\omega_0 > 0$, for the system (5.35).*

Proof. The solution of (5.36) is,

$$\epsilon(t) = e^{\omega_o A t} \epsilon(0) + \int_0^t e^{\omega_o A (t-\tau)} B \frac{h_2(\lambda(\tau), \omega_w, \omega_v)}{\omega_o} d\tau. \tag{5.37}$$

Let

$$p(t) = \int_0^t e^{\omega_o A (t-\tau)} B \frac{h_2(\lambda(\tau), \omega_w, \omega_v)}{\omega_o} d\tau,$$

since $h_2(\lambda, \omega_w, \omega_v)$ is bounded, that is $|h_2(\lambda, \omega_w, \omega_v)| < \mu$, μ is a positive constant. For $i = 1, 2$ we have

$$|p_i(t)| \leq \frac{\mu}{\omega_o^2}\big[|(A^{-1}B)_i| + |(A^{-1}e^{\omega_o At}B)_i|\big]. \tag{5.38}$$

for A and B defined in (5.36),

$$A^{-1} = \begin{bmatrix} 0 & -1/\alpha_2 \\ 1 & -\alpha_1/\alpha_2 \end{bmatrix}, \qquad |(A^{-1}B)_i| \leq \nu \tag{5.39}$$

where $\nu = \max\big\{\frac{1}{\alpha_2}, \frac{\alpha_1}{\alpha_2}\big\}$. Since A is Hurwitz, there exists a finite time $T > 0$ such that

$$\Big|\big[e^{\omega_o At}\big]_{ij}\Big| \leq \frac{1}{\omega_o^2}$$

for all $t > T$, $i, j = 1, 2$. Hence

$$\Big|\big[e^{\omega_o At}B\big]_i\Big| \leq \frac{1}{\omega_o^2}$$

for all $t > T, i = 1, 2$. Note that T depends on $\omega_o A$. Therefore,

$$|\big[A^{-1}e^{\omega_o At}B\big]_i\Big| \leq \frac{\delta}{\omega_o^2} \tag{5.40}$$

for all $t > T, i = 1, 2$, where $\delta = \max\big\{\frac{1}{\alpha_2}, \frac{\alpha_1}{\alpha_2}\big\}$. From (5.38), (5.39) and (5.40) we obtain,

$$|p_i(t)| \leq \frac{\mu\nu}{\omega_o^2} + \frac{\mu\delta}{\omega_o^4} \tag{5.41}$$

for all $t > T, i = 1, 2$. Let $\epsilon_s(0) = \epsilon_1(0) + \epsilon_2(0)$. It follows that

$$\left| \left[e^{\omega_o A t} \epsilon(0) \right]_i \right| \leq \frac{\epsilon_s(0)}{\omega_o^2}$$

for all $t > T, i = 1, 2$. From (5.37),

$$\left| \epsilon_i(t) \right| \leq \left| \left[e^{\omega_o A t} \epsilon(0) \right]_i \right| + \left| p_i(t) \right| \tag{5.42}$$

Let $e_s^o(0) = e_1^o(0) + e_2^o(0)$. According to $\epsilon_i = \frac{e_i^o}{\omega_o^{i-1}}$ and (5.40),(5.41) and (5.42), we have

$$\left| e_i^o(t) \right| \leq \left| \frac{\epsilon_s(0)}{\omega_o^2} \right| + \frac{\mu\nu}{\omega_o^2} + \frac{\mu\delta}{\omega_o^{5-i}} \tag{5.43}$$

$$= \sigma_i \tag{5.44}$$

for all $t \geq T, i = 1, 2$. Q.E.D ∎

In summary, it has been proved that the estimation error of LESO (5.33) is bounded and its upper bounded monotonously decreases with the observer bandwidth as shown in (5.43).

The control law for the case of acceleration is given as

$$i_q = \frac{\omega_w}{(1-\lambda)\, b\, \phi_d^*} \Big(\gamma_2 \big(\lambda^* - \hat{\lambda} \big) - \hat{z}_2 + \dot{\lambda}^* \Big), \tag{5.45}$$

where γ_2 is the controller gain. For convergence and stability, $s + \gamma_2$ should be Hurwitz. Similar to the case of deceleration, the LESO (5.33) will estimate $f_a(\lambda, \omega_w, \omega_v)$ and the control law (5.45) will online compensate for the uncertainties and nonlinearities of the system to the achieve the tracking objective. The control law (5.45) will yield a

closed-loop system

$$\dot{\lambda} = \Big(f_a(\lambda, \omega_w, \omega_v) - \hat{f}_a(\lambda, \omega_w, \omega_v) \Big) + \gamma_2 \Big(\lambda^* - \hat{\lambda} \Big) + \dot{\lambda}^*. \tag{5.46}$$

Note that with a well designed LESO, the first term in the right hand side of (5.46) will be negligible and the rest of the terms constitutes a mere proportional controller with a feedforward gain. The control objective is make the output of the plant (5.32) track a bounded reference λ^*, whose derivative $\dot{\lambda}^*$ is also bounded. The tracking error can be written as,

$$e_\lambda = \lambda^* - \lambda. \tag{5.47}$$

The error dynamics of the closed loop system is,

$$\dot{e}_\lambda = \dot{\lambda}^* - \Big[z_2 + \big(1 - \lambda\big) \frac{b}{\omega_w} \phi_d^* i_q \Big]. \tag{5.48}$$

We can rewrite the control input (5.45) in terms of tracking and estimation errors, i.e., e_λ, e_1^o, and e_2^o as,

$$i_q = \frac{\omega_w}{(1-\lambda)\, b\, \phi_d^*} \Big(\gamma_2 \big(e_\lambda + e_1^o \big) - \big(z_2 - e_2^o \big) + \dot{\lambda}^* \Big) \tag{5.49}$$

Substituting (5.49) into (5.48) will yield

$$\dot{e}_\lambda = -\gamma_2 e_\lambda + F e^o, \tag{5.50}$$

where $F = [-\gamma_2, -1]$ and $e^o = [e_1^o, e_2^o]'$ is the estimation error of the LESO. Is has been shown in Theorem 5.1 that the estimation errors, e_o, is bounded. Therefore, if

the γ_2, the gain of the controller, is chosen positive, then the error dynamics, (5.50), will be *stable* and *bounded*. The controller will not be able to achieve the asymptotic tracking performance. However, if the gains of the LESO and controller are chosen large enough, than the steady state error would be negligible thus achieving a practical stability. The simulation results for the presented control scheme are discussed in the upcoming section.

Remark 11 *Note that, both the LESOs,* (5.27) *and* (5.33)*, and LADRC control laws,* (5.29) *and* (5.45)*, are free from the uncertain and nonlinear terms of the model. It is a simple and linear strategy which controls a highly nonlinear and uncertain system.*

5.6 Numerical Simulations

In this section we present and discuss the numerical simulation results of the presented technique. The system is simulated in *Simulink 2016* using user-defined and s-functions. The parameters of the vehicle longitudinal dynamics, (5.3) and (5.4), are taken from [111], and the parameters of a $50\,KW$ in-wheel traction induction motor are taken from [115]. Table 5.1 summarizes all the parameters of the model used for the numerical simulations.

5.6.1 Deceleration

For the case of deceleration, the initial vehicle velocity, ω_v, and the wheel velocity, ω_w, are assumed to be $43\,rad/s$ and $42.05\,rad/s$ respectively with the initial slip ratio, λ, of -0.023. We assume the EV is moving on a wet asphalt road for which the optimum slip ratio is -0.1308 [108] which will serve as the reference, λ^*, for the control loop. The

Table 5.1: Parameters of the model

Mass of the vehicle	m	$1202\,kg$
Wheel radius	r_w	$0.32\,m$
Moment of inertia	J	$1.07kg.m^2$
Drag coefficient	c_a	0.4
Rolling friction coefficient	f_r	0.013
Gravitational acceleration	g	$9.8\,m/s$
Optimal adhesive coefficient	μ_p	0.8142
Optimal slip ratio	λ_p	0.1308
Gear ratio	G_r	9.3
Rotor Resistance	R_r	0.04Ω
Rotor Inductance	L_r	$1.5mH$
Mutual Inductance	L_m	$30\,mH$
Pole pairs	p	2

rated flux of $0.9Wb$ is maintained inside the machine. Using the concept of in-direct field orientation, the feedforward compensator (5.23) ensures the tracking of ϕ_d to ϕ_d^* during deceleration, shown in Figure 5.6b. The LADRC control law (5.29) ensures the convergence of λ to λ^*, shown in Figure 5.6a. The performance of the LESO, (5.27), is shown in Figure 5.7. It successfully estimates λ and f_b. The values for l_1, l_2 and $\gamma_1(t)$ are selected by trial and error, satisfying the hurwitz condition for (5.28) and $s+\beta$, to get the best response as:

$$\beta = 600 \times 10^3, \qquad \gamma_2^{max} = 6000, \qquad l_1 = 2000, \qquad l_2 = 1000^2.$$

The settling time of λ is $12ms$ when the solution enters within the 1% bound of the reference and stay inside. No overshoot and steady state error is observed.

To test the robustness of the control scheme, the values of $\bar{m}$, $\bar{c}_a$, $\bar{f}_r$, $\bar{g}$, and $\bar{\mu}_p$ were reduced by 50%. The results are depicted in Figure 5.8 . The proposed algorithm effectively estimates the new f_b and cancels the nonlinear and uncertain terms of the

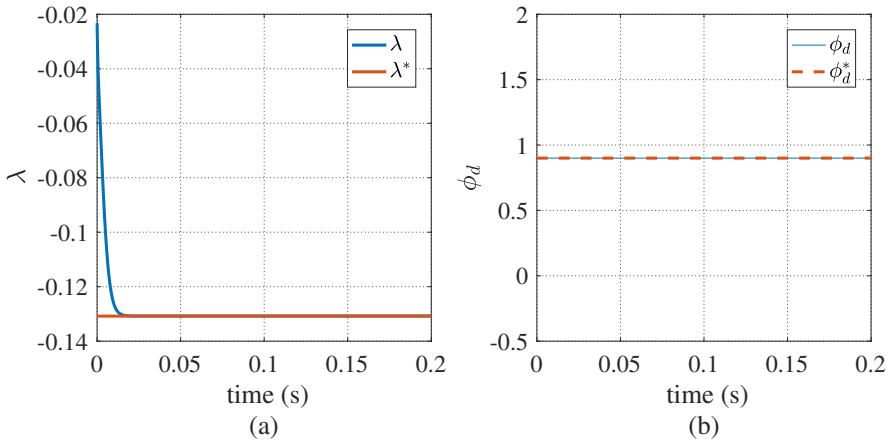

Figure 5.6: (a) Slip ratio trajectory (b) Rotor flux trajectory

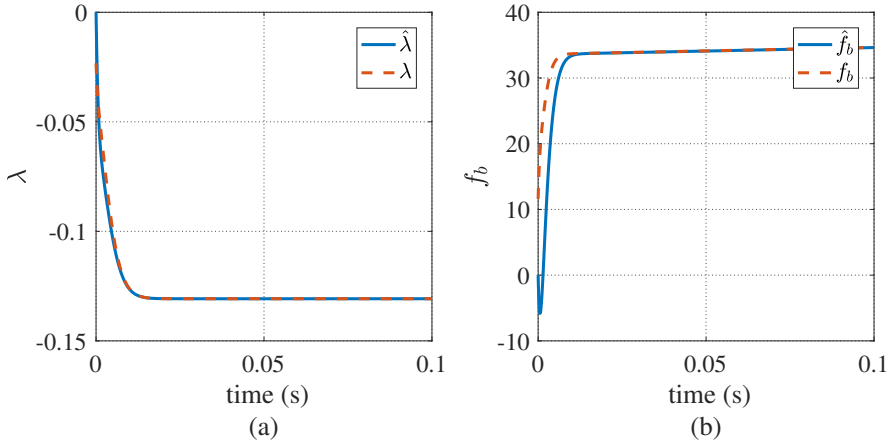

Figure 5.7: (a) Estimation of λ in the case of deceleration (b) Estimation of f_b in the case deceleration

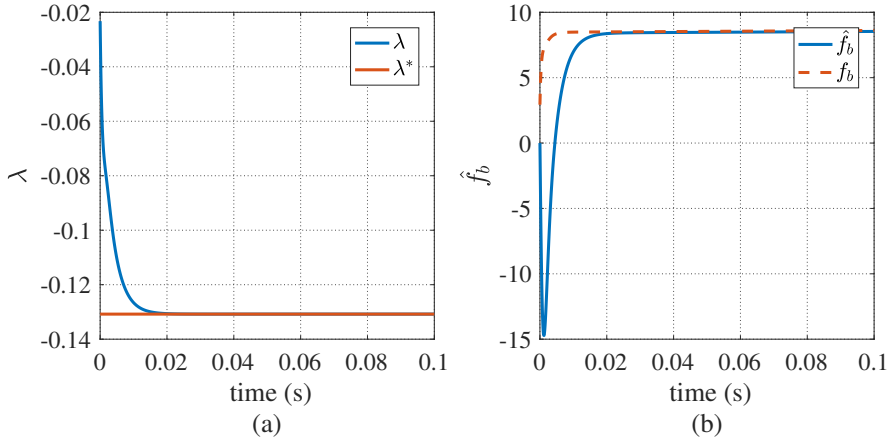

Figure 5.8: (a) tracking performance of λ on 50% variation of parameters (b) estimation of f_b after parameter variation

model. The parameter variation does not affect the tracking performance of the closed loop system. The trajectories of $d-q$ axis stator currents and vehicle and wheel speeds are shown in Figure 5.9.

5.6.2 Acceleration

For the case of acceleration, the initial vehicle velocity, ω_v, and wheel velocity, ω_w, are assumed to be $9.8\,rad/h$ and $10rad/s$ respectively with the initial slip ratio, λ, of 0.02. We assume the EV is accelerating on a wet asphalt road for which the optimum slip ratio is 0.1308 [108] which will serve as the reference, λ^*, for the control loop. Similar to the case deceleration, the initial value of ϕ_d is equal to ϕ_d^*, i.e. $0.9Wb$. The LESO, (5.33), and the control law (5.45) are used to control the closed loop dynamics. The gains are selected by trial and error, satisfying the hurwitz condition for $s+\beta$ and (5.28), to get the best response as:

$$\beta = 600 \times 10^3, \qquad \gamma_2^{max} = 6000, \qquad l_1 = 2000, \qquad l_2 = 1000^2.$$

The λ converges to λ^* in 8ms when the trajectory enters the 1% bound of the

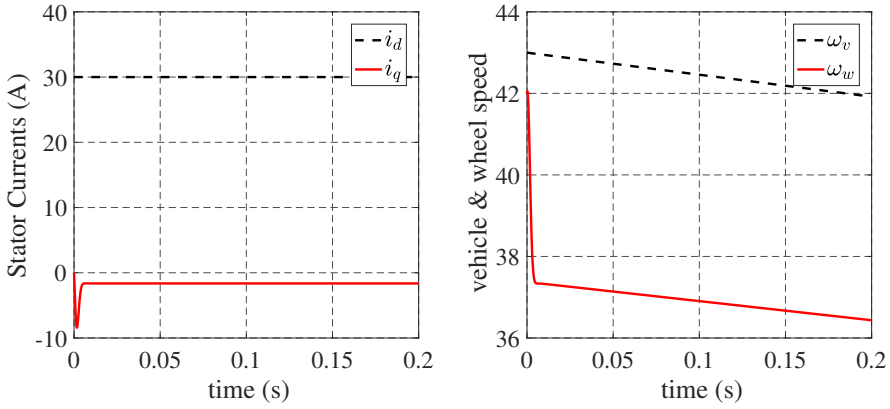

Figure 5.9: (a) $d-q$ axes stator currents (b) Torque of the motor

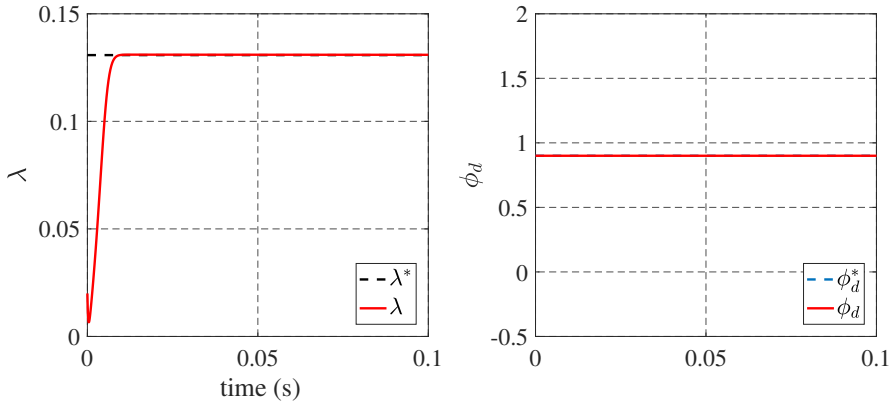

Figure 5.10: Trajectories of λ and ϕ_d during acceleration

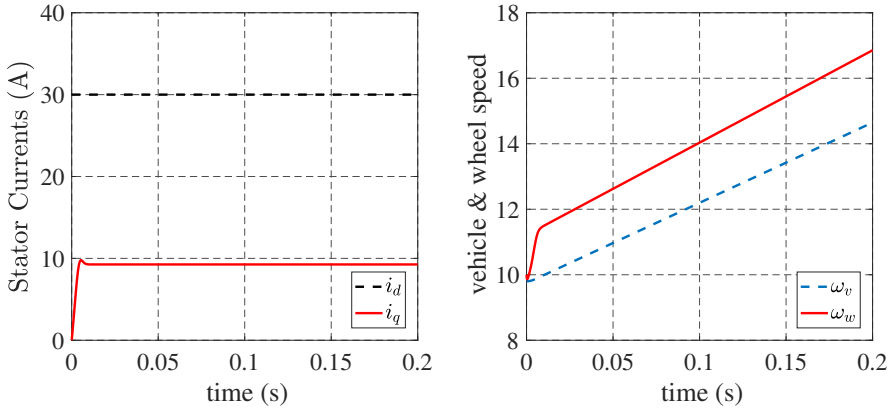

Figure 5.11: Trajectories of stator currents and the vehicle and wheel speeds

reference and ϕ_d is maintained at its reference value. Figure 5.10 shows the response of the control scheme. No overshoot or steady state error is observed. Figure 5.11 shows the stator currents generated by the control laws and the vehicle speeds. The control inputs are free from chattering and are bounded. The fixing of λ to its optimum value limits the acceleration of the vehicle to its maximum achievable value on the wet asphalt surface.

To test the robustness of the control scheme, the values of $\bar{m}$, $\bar{c}_a$, $\bar{f}_r$, $\bar{g}$, and $\bar{\mu}_p$ were reduced by 50%. The results are depicted in Figure 5.12 . The proposed algorithm effectively estimates the new f_a and cancels the nonlinear and uncertain terms of the model to maintain the convergence of the system. The parameter variation does not

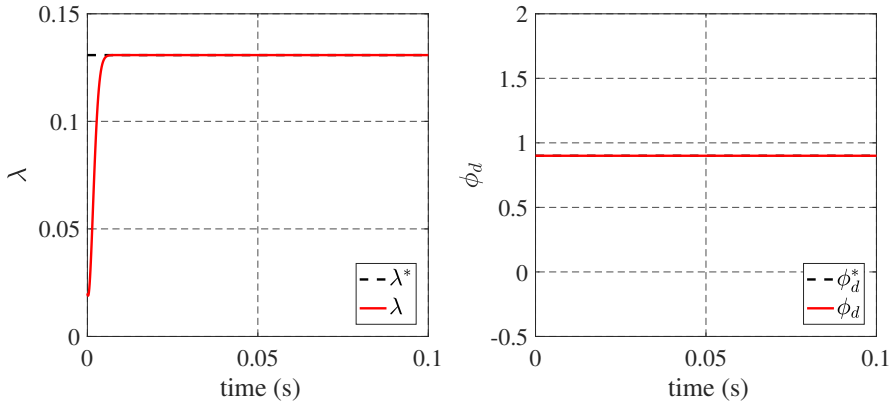

Figure 5.12: Controller response upon 50% parameter variation

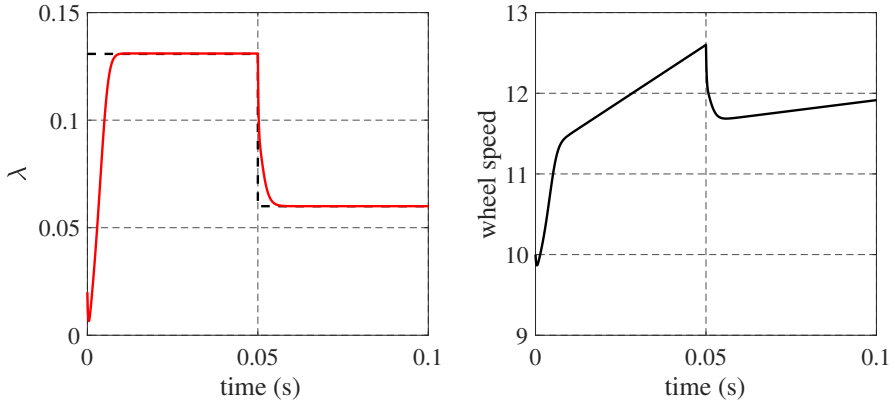

Figure 5.13: Sudden change in the road surface condition

affect the tracking performance of the closed loop system.

It is a common scenario during the driving that the road conditions changes abruptly beneath the vehicle. We assume the the car was moving on the wet asphalt road and after 50ms of acceleration the road condition changes to unpacked snow. The λ^* for the snowfield is 0.06. Figure 5.13 shows the response of the controller upon abrupt change in the road condition. The λ converges to the new reference in 8ms. It can also be seen in figure 5.13 the the wheel acceleration has been limited to a certain value lower than the value of the wet asphalt.

5.7 Summary

In this work, we have proposed the linear active disturbance rejection strategy for robust traction control of induction motor fed electric vehicles. Unlike in previous studies, we have presented the wheel slip ratio model of the car considering the nonlinear dynamics of the actuator, which in our case is induction motor. The presented control technique is based on linear extended state observer which estimates the nonlinear and uncertain part of the model and actively linearizes the system. The observer and control law posses simple structure and does not use the physical parameters of the longitudinal dynamics of the vehicle. This feature makes the technique attractive for practical use. The numerical simulations show the effectiveness of the algorithm. The tracking performance is also not affected by the parameter variation of the system.

CHAPTER 6

CONCLUDING REMARKS

6.1 Findings and Conclusion

In this work, we have investigated the tracking problem of the rotor speed of a squirrel-cage three-phase induction motor. IM is a highly nonlinear, multi-variable and time-varying system. We proposed two new control techniques for the control problem and tested their effectiveness in both numerical simulations and real-time experiments. Moreover, we have also solved the longitudinal traction control for the EVs subject to intrinsic and extrinsic uncertainties.We can draw the following conclusion from this research:

- The two-dimensional control theory is a promising direction to solve the complex nonlinear control problems because it offers the construction of 2-D control laws which are simple and require minimal information about the system dynamics.

- The Inter-sample Iterative Learning Control outperforms the conventional control technique in term of convergence. The settling time for the ISILC is much better than that of the conventional technique.

- The ISILC has a simple and linear control structure with no nonlinear terms for the compensation like the techniques inspired from the Feedback Linearization.
- However, the ISILC is sensitive towards the parameter variation and external disturbances to the system.
- The Active Disturbance Rejection Control is exceptionally robust against the internal and external disturbances because of the active linearization of the system dynamics using the Linear Extended State Observer (LESO).
- The LESO is capable of estimating the system nonlinearities and uncertainties with an acceptable bounded error at steady state. By selecting the high gains, practically the error will be negligible.
- The robust traction control problem for the IM-fed EVs has been solved using the ADRC. The control technique is robust against the variation in the parameters of the EV, i.e., the mass of the car, and also towards the road surface conditions.

6.2 Remarks on Future Research

There are still a lot of avenues to be explored and investigated ahead of this work. The issue of robustness for ISILC can be further investigated to compensate for the external and internal disturbances. Compensation for the load torque is deemed essential for the motor control systems. Furthermore, the estimation of flux and closed loop flux control is ignore in this work. The control schemes can also be investigated with a flux observer, and overall closed-loop performance can be studied. Similarly, the observer-based control for the application of traction control can also be investigated.

APPENDIX

Figure A.1: TI High Voltage Motor Control Kit

Texas Instruments Controller Board

The High Voltage Motor Control and PFC Developer's Kit (TMDSHVMTRPFCKIT) manufactured by Texas Instruments (TI), shown in figure A.1, is used for the real-time implementation of the control algorithms. It consists of the following items:

- High Voltage 3 phase inverter board
- Controllcards
- 15V DC Power Adaptor
- AC power cords and USB Cable

Figure A.2 shows the block diagram of the overall complete hardware setup. It contains four major functional groups: power supply, three phase inverter, instrumentation and digital signal processor (microcontroller). Each of these groups are explained in details in the next sections.

The hardware can be energized by 220V single-phase AC or 380V DC. It is up to the choice of the user. However, it is recommended to use the isolated DC supply for control evaluation, especially when measuring scopes are used. The power supply section generates the DC rail voltage for the three-phase inverter which is controlled through the pulse width modulation (PWM) channels of the DSP processor. The sensing circuitry is used to measure the line/phase currents and voltages of the motor which are fed back to the DSP processor for the closed loop operation. The processor is programmed in C language using Code Composer Studio (IDE) and Digital Motor Control (DMC) Library which is provided by TI. The board also contains power factor correction circuitry. Because it is not in the scope of this thesis, this functional group is bypassed.

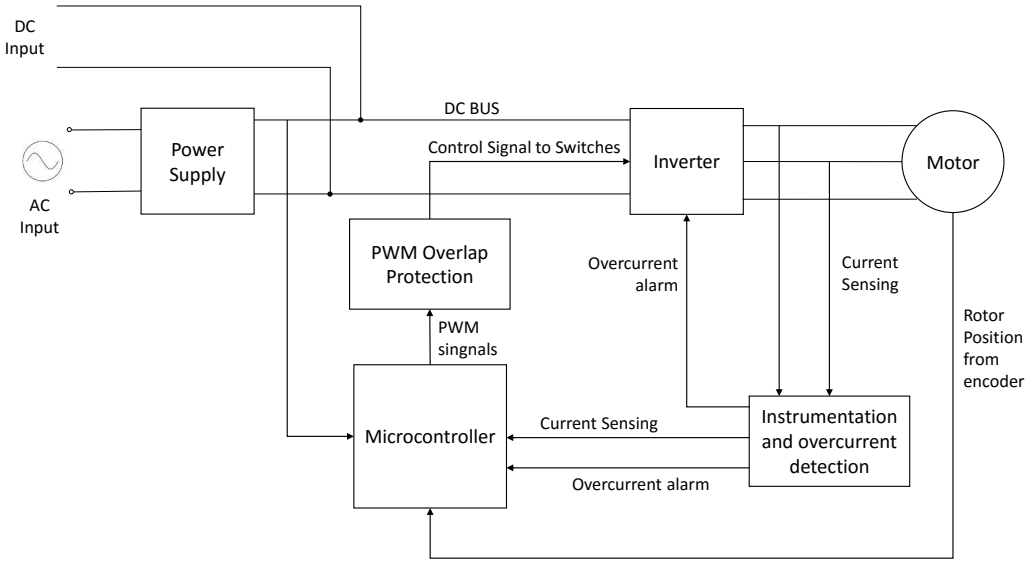

Figure A.2: Block diagram of hardware

Power Supply

High voltage three-phase inverter board, which is the main board of the experiment, is separated into two power domains. The high voltage domain which contains the DC bus which carries the high voltage and power to the inverter, and the low voltage domain which includes the embedded, i.e., controller for the board. The power supply section of the board contains an AC rectifier which can deliver power up to 750W. There are two ways to energize the high voltage domain, either through 220V AC wall socket in which the onboard rectifier is used, or we can directly plug an external DC supply on the DC bus. When evaluating the onboard control signals using oscilloscope, extreme caution need to the exercised. Either use isolated voltage probes when system is energized with AC wall socket or use isolated external DC supply if the isolated probes are not available.

The low voltage domain of the board can be energized in two ways. From onboard AC rectifier, or using an external 15V isolated adaptor. It is recommended to use the external adaptor because the output of the built-in switching supply can carry noise when the motor is running which can corrupt the ADC values of current sensing.

Inverter

The setup uses a voltage source inverter to generate three-phase AC voltage from the DC bus voltage. An intelligent power module PS21765 is used. It is a six switch IGBT based integrated inverter which include gate drive, under voltage, and overcurrent protection circuit. It can handle up to 350V, 20A and can drive a load up to 1.5KW. A proper heat sink is required for safe operation otherwise the component may damage. For more information about the intelligent power module refer to the component's

datasheet [116]. The gating signals of the inverter are connected to the PWM channels of the microcontroller. PWM overlap protection circuit is also employed to prevent triggering both high side and low side switches of the same leg at the same time. It will cause a short circuit.

To prevent the overcurrent damage to the hardware, there is overcurrent trip circuit which latches the overcurrent fault signal to the microcontroller and inverter. The inverter automatically shuts downs the output to prevent any damage. Overcurrent trip point is adjustable and can be adjusted to any desired value using onboard potentiometer VR1 and an appropriate jumper setting J7.

Instrumentation

The experiment uses the shunt resistors to measure the output currents and voltages. The voltage drop across the resistor is directly proportional to the current passing through it which is then sensed by the analog to digital converter (ADC) of the microcontroller. The sampling period is 10KHz, and it is synchronized with the PWM signals to reduce the switching noise in the measurement. The PWM channels are also clocked at 10KHz. The ADC resolution is 12-bits with values ranging from 0-4092. The current and voltage sensing ranges are 0-7A RMS and 0-280V RMS respectively.

Digital Signal Processor

We are using TI's 32-bit F28035 Piccolo microcontroller clocked at 60MHz in this setup. This microcontroller possesses enough computation power to execute complex control algorithms with the right mix of peripherals especially designed for motor control applications. We are using analog to digital converter (ADC), enhanced pulse width mod-

ulation (ePWM) and quadrature encoder pulse (QEP) modules of the microcontroller. Each of these three modules are explained briefly in the subsequent subsections, and hardware resource mapping is provided in table A.1.

Table A.1: Hardware Resource Mapping

Hardware Resource	Signal
PWM-1A	U-phase high side switch
PWM-1B	U-phase low side switch
PWM-2A	V-phase high side switch
PWM-2B	V-phase low side switch
PWM-3A	W-phase high side switch
PWM-3B	W-phase low side switch
ADC-B3, A1	Low side U-phase current sense
ADC-B5, B1	Low side V-phase current sense
ADC-A3, A5	Low side W-phase current sense
ADC-B7	U-phase voltage sense
ADC-B6	V-phase voltage sense
ADC-B4	W-phase voltage sense

ADC Module

This microcontroller posses 16 ADC channels with 12-bit resolution. There are multiple ways to trigger the Start-Of-Conversion (SOC) for each channel. For this setup, we have synchronized the SOC trigger with PWM module, so the both PWM and Sampling frequencies are 10KHz. One can also use software triggers and external interrupts for SOCs.

ePWM Module

F28035 contains seven ePWM modules, and each module provides an A-B pair of channels. So in total, we have 14 programmable PWM channels in this microcontroller. We used three ePWM modules one for each branch of the inverter and six channels in total.

Channel A of each module triggers the high side switch, and the channel B provides the control signal to the corresponding low side switch. A-B pair is configured to generate an alternate waveform to each other with a dead-time of 15 clock cycle between falling edge of one channel and the rising edge of other or vice versa to compensate the delay of on-time and off-time of the switches. All three ePWM modules are synchronized to a single clock to avoid unnecessary delays between the switching sequence among the branches of the inverter. An automatic trip logic is also employed in case the system detects the overcurrent fault. All the PWM channels will go to high impedance state if overcurrent is detected to prevent any damage. We are using symmetric PWM for the drive.

QEP Module

A 2048 PPR quadrature encoder is used on the motor shaft to measure the position and speed of the motor. F28035 microcontroller possesses a dedicated QEP module to read the quadrature pulses and translate it to the position. The position counter has a resolution 0.04°. The counter increments from 0 - 8192 on 0° - 360° rotation. The speed is measured by differentiating the position value.

Induction Motor

The AC induction motor used in this experiment is GE 5K33GN2A manufactured by Marathon Electric. It is a 3 phase, 180W, 220V and 1.3A squirrel cage machine. The parameters of the machine are summarized in Table 3.1. The rotor's position and speed are acquired using 2048-PPR optical encoder, QD200, installed physically on the machine shaft. The real-time data for the analysis is acquired by transmitting the

desired variables to PC over a serial communication link at the rate of 1KHz. The data stream is collected and logged on a PC by using Realterm, a serial terminal software.

REFERENCES

[1] P. Wach, *Dynamics and control of electrical drives.* Springer, Berlin, 2011.

[2] P. C. Krause, O. Wasynczuk, and S. D. Sundhoff, *Analysis of Electric Machinery and Drive Systems*, 2nd ed. John wiley & Sons, INC., 2002.

[3] R. Marino, P. Tomei, and C. M. Verrelli, *Induction motor control design.* Springer, London, 2010.

[4] W. Leonhard, *Control of electrical drives*, 2nd ed. Springer, Berlin, 1996.

[5] S. J. Chapman, *Electric machinery fundamentals*, 4th ed. McGraw-Hill Higher Education, 2005.

[6] A. M. Trzynadlowski, *Control of Induction Motors.* Academic Press, 2001.

[7] A. Munoz-Garcia, T. A. Lipo, and D. W. Novotny, "A new induction motor v/f control method capable of high-performance regulation at low speeds," *IEEE Transactions on Industry Applications*, vol. 34, no. 4, pp. 813–821, Jul 1998.

[8] L. K. Jisha and A. A. P. Thomas, "A comparative study on scalar and vector control of induction motor drives," in *2013 International conference on Circuits, Controls and Communications (CCUBE)*, Dec 2013, pp. 1–5.

[9] G. Kohlrusz and D. Fodor, "Comparison of scalar and vector control strategies of induction motors," *Hungarian Journal of Industral Chemistry Veszprém*, vol. 39, no. 2, pp. 265–270, 2011.

[10] M. Suetake, I. N. da Silva, and A. Goedtel, "Embedded dsp-based compact fuzzy system and its application for induction-motor v/f speed control," *IEEE Transactions on Industrial Electronics*, vol. 58, no. 3, pp. 750–760, March 2011.

[11] R. H. Nelson, T. A. Lipo, and P. C. Krause, "Stability analysis of a symmetrical induction machine," *IEEE Transactions on Power Apparatus and Systems*, vol. PAS-88, no. 11, pp. 1710–1717, Nov 1969.

[12] K. Koga, R. Ueda, and T. Sonoda, "Stability problem in induction motor drive system," in *Conference Record of the 1988 IEEE Industry Applications Society Annual Meeting*, vol. 1, Oct 1988, pp. 129–136.

[13] J.-H. Jung, G.-Y. Jeong, and B.-H. Kwon, "Stability improvement of v/f-controlled induction motor drive systems by a dynamic current compensator," *IEEE Transactions on Industrial Electronics*, vol. 51, no. 4, pp. 930–933, Aug 2004.

[14] X. D. Sun, K. H. Koh, B. G. Yu, and M. Matsui, "Fuzzy-logic-based v/f control of an induction motor for a dc grid power-leveling system using flywheel energy storage equipment," *IEEE Transactions on Industrial Electronics*, vol. 56, no. 8, pp. 3161–3168, Aug 2009.

[15] K. Lee, W. Yao, B. Chen, Z. Lu, A. Yu, and D. Li, "Stability analysis and mitigation of oscillation in an induction machine," *IEEE Transactions on Industry*

Applications, vol. 50, no. 6, pp. 3767–3776, Nov 2014.

[16] J. A. Ali, M. A. Hannan, and A. Mohamed, "Pso algorithm for three phase induction motor drive with svpwm switching and v/f control," in *2014 IEEE International Conference on Power and Energy (PECon)*, Dec 2014, pp. 250–254.

[17] Y. Liu and B. Piepenbreier, "Improvement of dynamic characteristic for v/f controlled induction motor drive system," in *2014 International Symposium on Power Electronics, Electrical Drives, Automation and Motion*, June 2014, pp. 707–712.

[18] R. Ueda, T. Sonoda, M. Ichikawa, and K. Koga, "Stability analysis in induction motor driven by v/f controlled general purpose inverter," in *Conference Record of the 1990 IEEE Industry Applications Society Annual Meeting*, vol. 1, Oct 1990, pp. 365–372.

[19] R. Ueda, T. Sonoda, and S. Takata, "Experimental results and their simplified analysis on instability problems in pwm inverter induction motor drives," *IEEE Transactions on Industry Applications*, vol. 25, no. 1, pp. 86–95, Jan 1989.

[20] Y. K. He and T. A. Lipo, "Saturation effects in the stability analysis of a vsi induction motor drive," in *IPEC*, 1983, pp. 181–192.

[21] Z. Ma, F. Lin, and T. Q. Zheng, "A new stabilizing control method for suppressing oscillations of v/hz controlled pwm inverter-fed induction motors drives," in *2006 37th IEEE Power Electronics Specialists Conference*, June 2006, pp. 1–4.

[22] Z. Ma, T. Zheng, and F. Lin, "Stability improvement of v/hz controlled pwm inverter-fed induction motors drives," in *2006 1ST IEEE Conference on Industrial Electronics and Applications*, May 2006, pp. 1–4.

[23] Y. Q. Xiang, "Instability compensation of v/hz pwm inverter-fed induction motor drives," in *Industry Applications Conference, 1997. Thirty-Second IAS Annual Meeting, IAS '97., Conference Record of the 1997 IEEE*, vol. 1, Oct 1997, pp. 613–620 vol.1.

[24] M. H. V. Reddy and V. Jegathesan, "Open loop v/f control of induction motor based on hybrid pwm with reduced torque ripple," in *2011 International Conference on Emerging Trends in Electrical and Computer Technology*, March 2011, pp. 331–336.

[25] A. Glumineau and J. de Leon Morales, *Sensorless AC Electric Motor Control*. Springer, Switzerland, 2015.

[26] L. Wang, S. Chai, D. Yoo, L. Gan, and N. K, *PID and Predictive Control of Electrical Drives and Power Converters using Matlab/Simulink*, 1^{st} ed. IEEE Wiley, 2015.

[27] L. Zhao, J. Huang, J. Chen, and M. Ye, "A parallel speed and rotor time constant identification scheme for indirect field oriented induction motor drives," *IEEE Transactions on Power Electronics*, vol. 31, no. 9, pp. 6494–6503, Sept 2016.

[28] C. M. Verrelli, A. Savoia, M. Mengoni, R. Marino, P. Tomei, and L. Zarri, "Online identification of winding resistances and load torque in induction machines," *IEEE Transactions on Control Systems Technology*, vol. 22, no. 4, pp. 1629–1637, July 2014.

[29] D. P. Marcetic and S. N. Vukosavic, "Speed-sensorless ac drives with the rotor time constant parameter update," *IEEE Transactions on Industrial Electronics*,

vol. 54, no. 5, pp. 2618–2625, Oct 2007.

[30] L. Zhao, J. Huang, H. Liu, B. Li, and W. Kong, "Second-order sliding-mode observer with online parameter identification for sensorless induction motor drives," *IEEE Transactions on Industrial Electronics*, vol. 61, no. 10, pp. 5280–5289, Oct 2014.

[31] M. Comanescu, "Design and implementation of a highly robust sensorless sliding mode observer for the flux magnitude of the induction motor," *IEEE Transactions on Energy Conversion*, vol. 31, no. 2, pp. 649–657, June 2016.

[32] W. C. A. Pereira, C. M. R. Oliveira, M. P. Santana, T. E. P. Almeida, A. G. Castro, G. T. Paula, and M. L. Aguiar, "Improved sensorless vector control of induction motor using sliding mode observer," *IEEE Latin America Transactions*, vol. 14, no. 7, pp. 3110–3116, July 2016.

[33] M. T. Angulo and R. V. Carrillo-Serrano, "Estimating rotor parameters in induction motors using high-order sliding mode algorithms," *IET Control Theory Applications*, vol. 9, no. 4, pp. 573–578, 2015.

[34] Z. Yin, C. Zhao, J. Liu, and Y. Zhong, "Research on anti-error performance of speed and flux estimator for induction motor using robust reduced-order ekf," *IEEE Transactions on Industrial Informatics*, vol. 9, no. 2, pp. 1037–1046, May 2013.

[35] F. Alonge, F. D'Ippolito, and A. Sferlazza, "Sensorless control of induction-motor drive based on robust kalman filter and adaptive speed estimation," *IEEE Transactions on Industrial Electronics*, vol. 61, no. 3, pp. 1444–1453, March 2014.

[36] K. Ohyama, G. M. Asher, and M. Sumner, "Comparative analysis of experimental performance and stability of sensorless induction motor drives," *IEEE Transactions on Industrial Electronics*, vol. 53, no. 1, pp. 178–186, Feb 2005.

[37] H. Kubota, K. Matsuse, and T. Nakano, "New adaptive flux observer of induction motor for wide speed range motor drives," in *Industrial Electronics Society, 1990. IECON '90., 16th Annual Conference of IEEE*, Nov 1990, pp. 921–926 vol.2.

[38] T. Tuovinen and M. Hinkkanen, "Adaptive full-order observer with high-frequency signal injection for synchronous reluctance motor drives," *IEEE Journal of Emerging and Selected Topics in Power Electronics*, vol. 2, no. 2, pp. 181–189, June 2014.

[39] W. Sun, J. Gao, Y. Yu, G. Wang, and D. Xu, "Robustness improvement of speed estimation in speed-sensorless induction motor drives," *IEEE Transactions on Industry Applications*, vol. 52, no. 3, pp. 2525–2536, May 2016.

[40] P. Vaclavek, P. Blaha, and I. Herman, "Ac drive observability analysis," *IEEE Transactions on Industrial Electronics*, vol. 60, no. 8, pp. 3047–3059, Aug 2013.

[41] J. C. Moreira and T. A. Lipo, "A new method for rotor time constant tuning in indirect field oriented control," in *21st Annual IEEE Conference on Power Electronics Specialists*, 1990, pp. 573–580.

[42] K. Wang, B. Chen, G. Shen, W. Yao, K. Lee, and Z. Lu, "Online updating of rotor time constant based on combined voltage and current mode flux observer for speed-sensorless ac drives," *IEEE Transactions on Industrial Electronics*, vol. 61, no. 9, pp. 4583–4593, Sept 2014.

[43] V. R. Jevremovic, V. Vasic, D. P. Marcetic, and B. Jeftenic, "Speed-sensorless control of induction motor based on reactive power with rotor time constant identification," *IET Electric Power Applications*, vol. 4, no. 6, pp. 462–473, July 2010.

[44] M. Cirrincione, M. Pucci, G. Cirrincione, and G. A. Capolino, "Constrained minimization for parameter estimation of induction motors in saturated and unsaturated conditions," *IEEE Transactions on Industrial Electronics*, vol. 52, no. 5, pp. 1391–1402, Oct 2005.

[45] Y. He, Y. Wang, Y. Feng, and Z. Wang, "Parameter identification of an induction machine at standstill using the vector constructing method," *IEEE Transactions on Power Electronics*, vol. 27, no. 2, pp. 905–915, Feb 2012.

[46] S. Maiti, C. Chakraborty, Y. Hori, and M. C. Ta, "Model reference adaptive controller-based rotor resistance and speed estimation techniques for vector controlled induction motor drive utilizing reactive power," *IEEE Transactions on Industrial Electronics*, vol. 55, no. 2, pp. 594–601, Feb 2008.

[47] S. M. N. Hasan and I. Husain, "A luenberger-sliding mode observer for online parameter estimation and adaptation in high-performance induction motor drives," *IEEE Transactions on Industry Applications*, vol. 45, no. 2, pp. 772–781, March 2009.

[48] F. R. Salmasi, T. A. Najafabadi, and P. J. Maralani, "An adaptive flux observer with online estimation of dc-link voltage and rotor resistance for vsi-based induction motors," *IEEE Transactions on Power Electronics*, vol. 25, no. 5, pp. 1310–1319, May 2010.

[49] R. Marino, S. Peresada, and P. Valigi, "Adaptive input-output linearizing control of induction motors," *IEEE Transactions on Automatic Control*, vol. 38, no. 2, pp. 208–221, Feb 1993.

[50] S. D. Gennaro, J. R. Domnguez, and M. A. Meza, "Sensorless high order sliding mode control of induction motors with core loss," *IEEE Transactions on Industrial Electronics*, vol. 61, no. 6, pp. 2678–2689, June 2014.

[51] Y. H. Hwang, K. K. Park, and H. W. Yang, "Robust adaptive backstepping control for efficiency optimization of induction motors with uncertainties," in *2008 IEEE International Symposium on Industrial Electronics*, June 2008, pp. 878–883.

[52] C.-J. Zhang, "Adaptive induction machine current control using internal model principle," in *Proceedings of the 2004 American Control Conference*, vol. 1, June 2004, pp. 82–83 vol.1.

[53] J. C. Martnez-Ramrez, R. Lescas-Hernandez, J. Linares-Flores, and C. Garca-Rodrguez, "Adaptive nonlinear zero-dynamic tracking controller for the three-phase squirrel-cage induction motor positioning system," in *2016 13th International Conference on Power Electronics (CIEP)*, June 2016, pp. 1–6.

[54] J. Li, H. P. Ren, and Y. R. Zhong, "Robust speed control of induction motor drives using first-order auto-disturbance rejection controllers," *IEEE Transactions on Industry Applications*, vol. 51, no. 1, pp. 712–720, Jan 2015.

[55] S. Drid, M. Tadjine, and M. S. Nait-Said, "Robust backstepping vector control for the doubly fed induction motor," *IET Control Theory Applications*, vol. 1, no. 4, pp. 861–868, July 2007.

[56] J. Han, "From pid to active disturbance rejection control," *IEEE Transactions on Industrial Electronics*, vol. 56, no. 3, pp. 900–906, March 2009.

[57] J. Bai, Y. x. Yin, Z. h. Hao, H. p. Sun, and P. Xin, "Optimum design of auto-disturbance-rejection controller for induction-motor frequency control systems based on variable-metric chaotic strategy," in *2008 IEEE International Conference on Automation and Logistics*, Sept 2008, pp. 891–895.

[58] Y. Mei and L. Huang, "A second-order auto disturbance rejection controller for matrix converter fed induction motor drive," in *6th International Power Electronic Motion Control Conference*, 2009, pp. 1964–1967.

[59] S. Hussain and M. A. Bazaz, "Neural network observer design for sensorless control of induction motor drive," *IFAC-PapersOnLine*, vol. 49, no. 1, pp. 106 – 111, 2016.

[60] P. Brandstetter and M. Kuchar, "Sensorless control of variable speed induction motor drive using {RBF} neural network," *Journal of Applied Logic*, no. November, 2016.

[61] H. Rehman, "Fuzzy logic enhanced robust torque controlled induction motor drive system," *IEE Proceedings - Control Theory and Applications*, vol. 151, no. 6, pp. 754–762, Nov 2004.

[62] B. Jha, M. K. Panda, P. K. Pandey, and L. Pant, "Pso-based online vector controlled induction motor drives," in *2016 International Conference on Electrical, Electronics, and Optimization Techniques (ICEEOT)*, March 2016, pp. 2234–2239.

[63] J. Yu, Y. Ma, H. Yu, and C. Lin, "Adaptive fuzzy dynamic surface control for induction motors with iron losses in electric vehicle drive systems via backstepping," *Information Sciences*, vol. 376, pp. 172 – 189, 2017.

[64] A. Saghafinia, H. W. Ping, M. N. Uddin, and K. S. Gaeid, "Adaptive fuzzy sliding-mode control into chattering-free im drive," *IEEE Transactions on Industry Applications*, vol. 51, no. 1, pp. 692–701, Jan 2015.

[65] O. Cerman, "Fuzzy model reference control with adaptation mechanism," *Expert Systems with Applications*, vol. 40, no. 13, pp. 5181 – 5187, 2013.

[66] R. Shahnazi, H. M. Shanechi, and N. Pariz, "Position control of induction and dc servomotors: A novel adaptive fuzzy pi sliding mode control," *IEEE Transactions on Energy Conversion*, vol. 23, no. 1, pp. 138–147, March 2008.

[67] S. M. Gadoue, D. Giaouris, and J. W. Finch, "Mras sensorless vector control of an induction motor using new sliding-mode and fuzzy-logic adaptation mechanisms," *IEEE Transactions on Energy Conversion*, vol. 25, no. 2, pp. 394–402, June 2010.

[68] F. Barrero, A. Gonzalez, A. Torralba, E. Galvan, and L. G. Franquelo, "Speed control of induction motors using a novel fuzzy sliding-mode structure," *IEEE Transactions on Fuzzy Systems*, vol. 10, no. 3, pp. 375–383, Jun 2002.

[69] C. I. Huang, K. C. Hsu, H. H. Chiang, K. K. Kou, and T. T. Lee, "Adaptive fuzzy sliding-mode control of linear induction motors," in *2012 international conference on advanced mechatronics systems*, 2012, pp. 626–631.

[70] T. Orlowska-Kowalska, M. Dybkowski, and K. Szabat, "Adaptive sliding-mode neuro-fuzzy control of the two-mass induction motor drive without mechanical

sensors," *IEEE Transactions on Industrial Electronics*, vol. 57, no. 2, pp. 553–564, Feb 2010.

[71] S. Masumpoor, H. yaghobi, and M. A. Khanesar, "Adaptive sliding-mode type-2 neuro-fuzzy control of an induction motor," *Expert Systems with Applications*, vol. 42, no. 19, pp. 6635 – 6647, 2015.

[72] X. Wang, Y. Ma, J. Yu, L. Liu, and W. Li, "Fuzzy approximation-based adaptive command filtered control for induction motors," in *2016 Chinese Control and Decision Conference (CCDC)*, May 2016, pp. 922–927.

[73] J. Yu, B. Chen, Y. Ma, and H. Yu, "Robust speed tracking control for the induction motor via adaptive fuzzy backstepping," in *2011 Chinese Control and Decision Conference (CCDC)*, May 2011, pp. 2181–2184.

[74] R.-J. Wai and H.-H. Chang, "Backstepping wavelet neural network control for indirect field-oriented induction motor drive," *IEEE Transactions on Neural Networks*, vol. 15, no. 2, pp. 367–382, March 2004.

[75] C. M. Kwan and F. L. Lewis, "Robust backstepping control of induction motors using neural networks," *IEEE Transactions on Neural Networks*, vol. 11, no. 5, pp. 1178–1187, Sep 2000.

[76] R. J. Wai and J. M. Chang, "Intelligent control of induction servo motor drive via wavelet neural network," *Electric Power Systems Research*, vol. 61, no. 1, p. 6776, 2002.

[77] K. Sedhuraman, S. Himavathi, and A. Muthuramalingam, "Comparison of learning algorithms for neural network based speed estimator in sensorless induction

motor drives," in *IEEE-International Conference On Advances In Engineering, Science And Management (ICAESM -2012)*, March 2012, pp. 196–202.

[78] M. A. Rafiq, N. K. Roy, and B. C. Ghosh, "Three algorithms for learning artificial neural network: A comparison for induction motor flux estimation," in *2009 12th International Conference on Computers and Information Technology*, Dec 2009, pp. 355–360.

[79] M. N. Uddin, Z. R. Huang, and A. B. M. S. Hossain, "Development and implementation of a simplified self-tuned neuro-fuzzy-based im drive," *IEEE Transactions on Industry Applications*, vol. 50, no. 1, pp. 51–59, Jan 2014.

[80] P. D. Wit, R. Ortega, and I. Mareels, "Indirect field oriented control of induction motors is robustly globally stable," in *Proceedings of 1995 34th IEEE Conference on Decision and Control*, vol. 3, Dec 1995, pp. 2139–2144 vol.3.

[81] R. Lessmeier, W. Schumacher, and W. Leonhard, "Microprocessor-controlled ac-servo drives with synchronous or induction motors: Which is preferable?" *IEEE Transactions on Industry Applications*, vol. IA-22, no. 5, pp. 812–819, Sept 1986.

[82] J. Chiasson, *IEEE Press Series on Power Engineering : Modeling and High Performance Control of Electric Machines (1)*. Wiley-IEEE Press, May 2005.

[83] B. Akin and M. Bhardwaj, "Sensored field oriented control of 3-phase induction motors," Texas Instruments, Inc, Tech. Rep. SPRABP8, July 2013.

[84] Z. Gao, "Scaling and bandwidth-parameterization based controller tuning," in *American Control Conference*, vol. 6, June 2003, pp. 4989–4996.

[85] Q. Zheng, L. Q. Gaol, and Z. Gao, "On stability analysis of active disturbance rejection control for nonlinear time-varying plants with unknown dynamics," in *46th IEEE Conference on Decision and Control*, Dec 2007, pp. 3501–3506.

[86] S. Arimoto, S. Kawamura, and F. Miyazaki, "Bettering operation of dynamic systems by learning: A new control theory for servomechanism or mechatronics systems," in *23rd IEEE Conference on Decision and Control*, Dec 1984, pp. 1064–1069.

[87] D. Meng and M. Du, "ILC-motivated formation algorithm for multi-agent systems with communication time-delays," in *2016 35th Chinese Control Conference (CCC)*, July 2016, pp. 3099–3104.

[88] W. Qian, S. K. Panda, and J. X. Xu, "Speed ripple minimization in pm synchronous motor using iterative learning control," *IEEE Transactions on Energy Conversion*, vol. 20, no. 1, pp. 53–61, March 2005.

[89] Q. Miao, H. S. Lo, S. Q. Xie, and H. S. Li, "Iterative learning control method for improving the effectiveness of upper limb rehabilitation," in *23rd International Conference on Mechatronics and Machine Vision in Practice (M2VIP)*, Nov 2016, pp. 1–5.

[90] D. Shen and J. X. Xu, "A novel markov chain based ILC analysis for linear stochastic systems under general data dropouts environments," *IEEE Transactions on Automatic Control*, vol. PP, no. 99, pp. 1–1, 2016.

[91] S. Ibrir and C. Ramlal, "Iterative learning control schemes for a class of nonlinear systems: Theory and real-time implementation," in *12th IEEE International*

Conference on Industrial Informatics (INDIN), July 2014, pp. 338–343.

[92] D. A. Bristow, M. Tharayil, and A. G. Alleyne, "A survey of iterative learning control," *IEEE Control Systems*, vol. 26, no. 3, pp. 96–114, June 2006.

[93] H. S. Ahn, Y. Chen, and K. L. Moore, "Iterative learning control: Brief survey and categorization," *IEEE Transactions on Systems, Man, and Cybernetics, Part C (Applications and Reviews)*, vol. 37, no. 6, pp. 1099–1121, Nov 2007.

[94] J. R. Domínguez, "Discrete-time modeling and control of induction motors by means of variational integrators and sliding modes-part i: Mathematical modeling," *IEEE Transactions on Industrial Electronics*, vol. 62, no. 9, pp. 5393–5401, Sept 2015.

[95] S. Boyd, L. E. Ghaoui, E. Feron, and V. Balakrishnan, *Linear matrix inequality in systems and control theory*, ser. Studies in Applied Mathematics. SIAM, Philadelphia, 1994.

[96] B. Anderson, P. Agathoklis, E. Jury, and M. Mansour, "Stability and the matrix lyapunov equation for discrete 2-dimensional systems," *IEEE Transactions on Circuits and Systems*, vol. 33, no. 3, pp. 261–267, Mar 1986.

[97] "Piccolo microcontrollers," Texas Instruments, Inc, Tech. Rep. SPRS584J, October 2013.

[98] S. Ibrir, "Online exact differentiation and notion of asymptotic algebraic observers," *IEEE Transactions on Automatic Control*, vol. 48, no. 11, pp. 2055–2060, Nov 2003.

[99] ——, "Linear time-derivative trackers," *Automatica*, vol. 40, no. 3, pp. 397 – 405, 2004.

[100] D. A. Crolla and D. Cao, "The impact of hybrid and electric powertrains on vehicle dynamics, control systems and energy regeneration," *Vehicle System Dynamics*, vol. 50, no. sup1, pp. 95–109, 2012.

[101] V. Ivanov, D. Savitski, and B. Shyrokau, "A survey of traction control and antilock braking systems of full electric vehicles with individually controlled electric motors," *IEEE Transactions on Vehicular Technology*, vol. 64, no. 9, pp. 3878–3896, Sept 2015.

[102] J. Deur, D. Pavković, G. Burgio, and D. Hrovat, "A model-based traction control strategy non-reliant on wheel slip information," *Vehicle System Dynamics*, vol. 49, no. 8, pp. 1245–1265, 2011.

[103] Y. Lee and S. H. Zak, "Designing a genetic neural fuzzy antilock-brake-system controller," *IEEE Transactions on Evolutionary Computation*, vol. 6, no. 2, pp. 198–211, Apr 2002.

[104] H. Mirzaeinejad and M. Mirzaei, "A novel method for non-linear control of wheel slip in anti-lock braking systems," *Control Engineering Practice*, vol. 18, no. 8, pp. 918 – 926, 2010.

[105] M. Amodeo, A. Ferrara, R. Terzaghi, and C. Vecchio, "Wheel slip control via second-order sliding-mode generation," *IEEE Transactions on Intelligent Transportation Systems*, vol. 11, no. 1, pp. 122–131, March 2010.

[106] A. E. Hadri, J. Cadiou, K. M'Sirdi, and Y. Delanne, "Wheel-slip regulation based on sliding mode approach," in *SAE Technical Paper*. SAE International, 03 2001.

[107] J. H. Montonen and T. Lindh, "Analysis of sensorless traction control system for electric vehicle," in *16th European Conference on Power Electronics and Applications*, Aug 2014, pp. 1–7.

[108] H. Guo, R. Yu, W. Qiang, and H. Chen, "Optimal slip based traction control for electric vehicles using feedback linearization," in *2014 International Conference on Mechatronics and Control (ICMC)*, July 2014, pp. 1159–1164.

[109] W. Kirchner and S. Southward, "Implementation and verification of adaptive longitudinal traction control," *Vehicle System Dynamics*, vol. 51, no. 11, pp. 1674–1694, 2013.

[110] J. Li-Qiang, L. Mingze, and Y. Weiqiang, "Tire-road friction estimation and traction control strategy for motorized electric vehicle," *PLOS ONE*, vol. 12, no. 6, pp. 1–18, 06 2017.

[111] S. Kuntanapreeda, "Super-twisting sliding-mode traction control of vehicles with tractive force observer," *Control Engineering Practice*, vol. 38, pp. 26 – 36, 2015.

[112] M. Jalali, A. Khajepour, S. ken Chen, and B. Litkouhi, "Integrated stability and traction control for electric vehicles using model predictive control," *Control Engineering Practice*, vol. 54, pp. 256 – 266, 2016.

[113] M. Ehsani, Y. Gao, S. E. Gay, and A. Emadi, *Modern Electric, Hybrid Electric and Fuel Cell Vehicles*. CRC Press, 2005.

[114] C. Unsal and P. Kachroo, "Sliding mode measurement feedback control for antilock braking systems," *IEEE Transactions on Control Systems Technology*, vol. 7, no. 2, pp. 271–281, Mar 1999.

[115] S. Bozhko, S. Dymko, S. Kovbasa, and S. M. Peresada, "Maximum torque-per-amp control for traction im drives: Theory and experimental results," *IEEE Transactions on Industry Applications*, vol. 53, no. 1, pp. 181–193, Jan 2017.

[116] *PS21765 Dual-In-Line Intelligent Power Module*, Powerex, rev. 07/07.

LIST OF PUBLICATIONS

- M. M. Shirazi and S. Ibrir,"Inter-sample Iterative Learning Control for Induction Motor Drives", 43^{rd} Annual Conference of the IEEE Industrial Electronics Society, Oct-Nov, 2017.

- M. M. Shirazi,"Robust traction control for in-wheel electric vehicle stabilization using active disturbance rejection control", 19^{th} International Conference on Industrial Technology, Feb, 2018.

- M. M. Shirazi,"Robust traction control of induction motor fed electric vehicles with intrinsic and extrinsic uncertainties", 19^{th} International Conference on Industrial Technology, Feb, 2018.

Vitae

- Name: Muhammad Mutsaied Shirazi
- Nationality: Pakistan
- Date of Birth: August, 9^{th}, 1990
- Email: *mutsaied.shirazi@gmail.com*
- Permenant Address: Flat: G-6, five star luxury apartment Gulshan Iqbal block 14, Karachi, Pakistan

- Masters of Science in Electrical Engineering, King Fahd University of Petroleum and Minerals, Saudi Arabia
- Bachelors of Electronics Engineering, National University of Sciences and Technology, Pakistan